THESIS

DEVELOPMENT AND CHARACTERIZATION OF SOLID-STATE, INTERNET OF THINGS-BASED PH SENSORS FOR IN-SITU MONITORING OF SOIL AND GROUNDWATER

Submitted by

Charles H. VanTilburg IV

Department of Civil and Environmental Engineering

In partial fulfillment of the requirements

For the Degree of Master of Science

Colorado State University

Fort Collins, Colorado

Fall 2022

Master's Committee:

Advisor: Joseph Scalia

Co-Advisor: Thomas Sale

Jay Ham

ABSTRACT

DEVELOPMENT AND CHARACTERIZATION OF SOLID-STATE, INTERNET OF THINGS-BASED PH SENSORS FOR IN-SITU MONITORING OF SOIL AND GROUNDWATER

Herein I test and examine a new solid state pH sensor design for use in soils and groundwater monitoring. The concept presented here is intended to expand the capabilities for monitoring geochemical parameters in the subsurface by combining a durable, solid-state pH sensor for subsurface deployment with an automated 'internet of things' (IoT) based pH meter that allows the collection of near-real-time continuous data streams for monitoring biogeochemical processes in hydrologic systems. Tests performed in this work were intended to provide a benchmark for further refinement of the design and yielded promising results, including hydrogeologically useful response times (on the order of hours), durability (stresses >1,000 kPa), and reproducible behaviors with multiple sensors. These results support that this technology is promising for future work.

The pH sensor design combines a titanium mixed-metal-oxide electrode (TiMMO), solid epoxy body, and a proton-selective Nafion^{TM} ionomer coating to yield a durable solid-state sensor that is sensitive to aqueous proton activities. As the sensor is exposed to water, the diffusion of aqueous protons through the selective Nafion^{TM} coating causes an increase in voltage on the electrode as compared to a reference electrode. The Nafion^{TM} coating reduces the influence of other ions in the system, creating a proton selective sensor.

Because of the durable solid-state construction, the sensor can likely be deployed in-situ in challenging environments such as in soils where common glass pH sensors are too fragile for use. This unique advantage allows the pursuit of new biogeochemical monitoring strategies that leverage a high volume of discrete in-situ measurements for near-real-time continuous datastreams. This new strategy, powered by IoT systems, can integrate with smart networks of multiple components and generate large amounts of data for use in artificial intelligence and machine learning systems while also providing insight into processes that occur at smaller spatial and temporal scales than those understood with current subsurface monitoring strategies.

pH is a master variable in aqueous and soil chemistry, both an indicator and controller of most chemical reactions and many physical processes that take place in soil and groundwater. pH is important for understanding chemical speciation, mobility, and stability in the soil, while also influencing soil physical properties like soil structure. pH is a parameter of interest to many industries and fields of study including, but not limited to, agriculture, mining, water resources, and engineering.

As this work was intended to be a first approximation for studying this technology, multiple promising results and points of improvement were discovered. This work identifies a clear voltage response by the sensor to pH changes (-29 mV/pH) while also demonstrating the change behavior during stepwise pH changes to be approximately logarithmic (Δ_{volt}=3.85ln[t], where Δ_{volt} is the change in millivolts and t is time in minutes). Furthermore, this work demonstrated that these sensors can be used with an IoT monitoring system in the intended application.

However, more work is needed to remove variability in the data, explore further designs and processes for coating and treating the sensors, analyze the long-term use, drift, and

standardization of the sensors, and employ the data in analytics. Future work should include further lab testing to compare alternative design features and to evaluate stressors such as non-target ions and dehydration. After refinement in the lab, the sensors should be installed in pilot scale studies and in the field to evaluate their performance in real world conditions.

ACKNOWLEDGEMENTS

It has been a long road since the start of this project and my time here at Colorado State University. During the beginning of the COVID-19 pandemic, I embarked on a journey far away from home to an unknown house, school, and state 1,100 miles away. I was greeted with masked faces and people afraid to talk to one another, shake hands, or be inside together.

I came to CSU aiming to broaden my horizons but found that I was on the right path all along—groundwater is my passion. So, I thank my wonderful advisor and friend, Dr. Joe Scalia, for making that clear to me and for leading me down the path that has given me so much enjoyment and reward. Joe changed my life, and I am forever grateful for his guidance. His passion for what he does, welcoming attitude, and impressive work ethic make Joe an example of excellence. In January of 2021, he introduced me to another great friend and mentor, Dr. Tom Sale, who decided I was worth the effort of at least one more project before his retirement. Tom welcomed me into the Center for Contaminant Hydrology, my home for the past 18 months, with a smile on his face and an eagerness to keep changing the world. His passion and optimism make him a joy to be around and an inspiration to keep fighting the good fight. Together, we took on my first trip to Canada, a humbling class from another great mentor, Dr. Jay Ham, and the massive endeavor which has been this research. And of course, we took on some of Fort Collins' breweries.

To everyone at the Center for Contaminant Hydrology, I owe a huge amount of gratitude. Dr. Jens Blotevogel unlocked an understanding of chemistry for me that I'd never had and inspired us to work diligently. Dr. Andrea Hanson-Rhoades humbled me with her skills as a leader and interdisciplinarian in our lab and was always there to give her assistance. Dr. Kayvan

Karimi Askarani, a skilled technologist, taught me so much and rode deep into Wyoming with me to face a nest of wasps. And Dr. Jay Ham taught me the majority of what I know of electronics. Holly Proulx and Andy Quach dedicated significant time to help me with experiments and building equipment late into the night. To my fellow students, especially Christophe, Angelo, Jordan, and Sam, thank you for welcoming me into your lives and enjoying so many great times together. This place wasn't so lonely after all.

I'd also like to thank my colleagues and mentors from the Center for Applied Earth Science and Engineering Research (CAESER) at the University of Memphis and that Civil Engineering Department for engineering a strong foundation for me to build on. The opportunities given to me there were invaluable. Furthermore, I'd like to thank the Chevron Corporation, the University Consortium for Field Focused Groundwater Research, S3NSE Technologies, and Borin Manufacturing Inc. for supporting this research project.

And last, but definitely not least, I want to acknowledge my family, friends, and wonderful girlfriend, Thaiz, back home. Without them, I never would have made it here to start this journey, and I definitely could not have finished it. My family has always been supportive, interested in my life, and gave me the help I needed to succeed. My friends have made life a joy with so many rich experiences. A special thanks goes to my friend, Falcon, who showed me all about Colorado and so much more. Thaiz has been so inspiring throughout this process and has been my rock through it all, even from far away—she knows this work almost as well as I do by now.

Now, it is time to close this chapter and start writing a new one. I'm most excited to see what will fill the next pages, but I know that those mentioned here will continue to be part of them. To all of my colleagues, mentors, sponsors, family, and friends—thank you so much.

PREFACE

As of 2021, the United States Environmental Protection Agency (USEPA) regulates over 86,000 chemicals per the Toxic Substances Control Act and in 2019 (alone) recorded 21,343 facilities releasing or storing 3.43 billion pounds of toxic waste in the environment (USEPA 2021). Notably, only 72.9 million pounds of this waste (2.1%) was disposed in a RCRA Subtitle C hazardous waste landfill (USEPA 2021). Figure 1 shows the annual waste reported to the EPA Toxic Release Inventory by disposal method since 2007. The majority of waste is stored in on-site land disposal facilities, which are commonly landfills with varying regulations for containment. Often, these facilities do not have an adequate liner system, allowing toxic leachate to contaminate the environment. Off-site disposal facilities typically are engineered landfills with containment systems designed to prevent groundwater contamination.

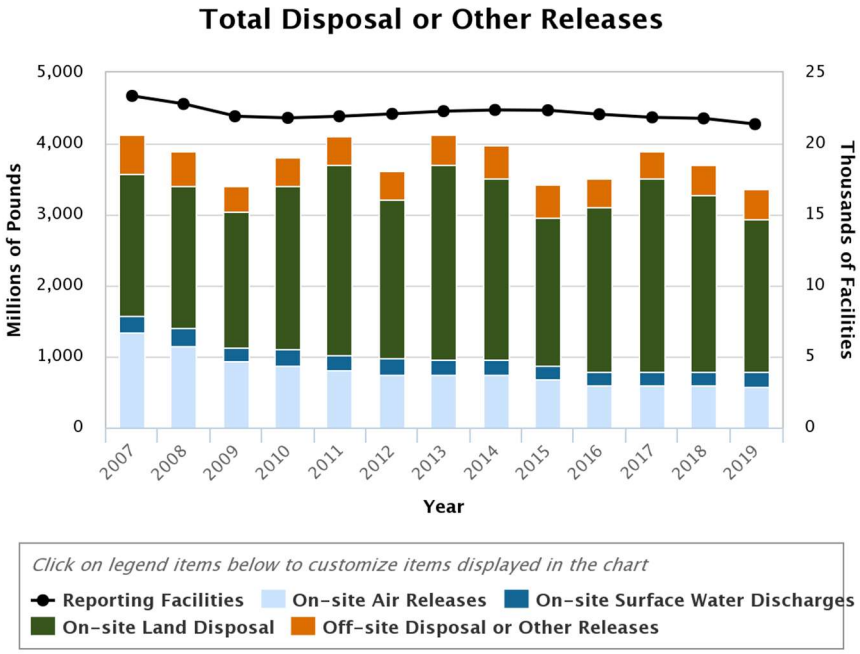

Figure 1. USEPA Toxic Release Inventory Annual Data (from USEPA 2021)

Remediation of the contaminated environment became an industry practice after the passage of the Comprehensive Environmental Response, Compensation, and Liability Act (CERCLA), starting the Superfund program. Initial estimates of the Superfund program's cost and scope were extremely underestimated and misunderstood (National Research Council 2013). The problems were much larger and recalcitrant than originally expected. Kitanidis et al. (2012) conceptualizes the problem well:

> "Original estimates, in 1980, projected an average Superfund cleanup cost of a mere $3.6 million per site and assumed only around 400 sites would require remediation. The DoD's early estimates of the cost to cleanup its contaminated sites were also optimistic. In 1985, the DoD estimated the cleanup of its contaminated sites would cost from $5 billion to $10 billion, assuming 400-800 potential sites. A decade later, after an investment of over $12 billion on environmental restoration, the cost-to-complete estimates had grown to over $20 billion, and the number of sites had increased to over 20,000. By 2007, after spending $20 billion in the previous decade, the estimated cost to address the DoD's known liability for traditional cleanup (not including the munitions response program for unexploded ordnance) was still over $13 billion. Why did we underestimate the cost of cleaning up contaminated sites? All of these assumptions were made with the tacit assumption that existing, off-the-shelf remedial technology was adequate to accomplish the task, that we had the scientific and engineering knowledge and tools to remediate these sites, and that we knew the full scope of chemicals of concern.
>
> However, it was soon and painfully realized that the technology needed to address the more recalcitrant environmental contamination problems, such as fuels and chlorinated solvents in groundwater and dense nonaqueous phase liquids (DNAPLs) in the subsurface, was seriously lacking."

Remediation is not a simple task. As our experience with remediation has evolved, the importance of innovative methods to understand the in-situ transport and fate of contaminants has come into focus. This thesis aims to expand our toolbox, and make subsurface soil and groundwater remediation more effective, with the ultimate goal of making our country and our world a safer, healthier, and more equitable place.

TABLE OF CONTENTS

LIST OF TABLES

LIST OF FIGURES

1. INTRODUCTION

1.1 What is the Project?

Herein I test and examine a new solid state pH sensor design for use in soils and groundwater monitoring. The concept presented here is intended to expand the capabilities for monitoring geochemical parameters in the subsurface by combining a durable, solid-state pH sensor for subsurface deployment with an automated 'internet of things' (IoT) based pH meter that allows the production of near-real-time continuous data streams for monitoring biogeochemical processes in hydrologic systems. Because pH is a master variable in geochemistry, this work has applications in agriculture, mining, water resources, and engineering. Though widely applicable, the main focus herein is on a sensor platform for monitoring contaminated soils and groundwater.

High-resolution spatial and temporal monitoring of subsurface geochemical conditions is needed to pragmatically monitor and remediate contaminated soil and groundwater. Historically, groundwater monitoring has depended on the use of manual sampling from monitoring wells, chemical analysis in off-site labs, subsequent data analysis, and infrequent reporting. This approach consumes significant resources, delays availability of data for decisions, and is constrained by the scarcity of adequately trained and experienced personnel. However, new technologies allow aspects of site monitoring to be automated and improved, reducing the time to make interpretations, and enabling a more complete understanding of dynamic subsurface conditions.

Low-cost, internet of things (IoT) based sensors can be used to monitor in-situ conditions at contaminated sites. These sensors offer the benefits of continuous monitoring in real-time

from the office, home, or field. Because of the low cost of these systems and sensors, they can be deployed in greater numbers enabling high resolution spatial and temporal definition of critical parameters. Current IoT sensors exist for temperature, pressure, soil water content, and oxidation-reduction-potential (ORP). The goal of this work is to add a new tool to Colorado State University's IoT toolbox for soils and groundwater.

1.2 What Problem Does the Project Address?

This work is intended to address the need for low-cost pH monitoring at contaminated sites. Many sites have regulatory requirements for costly monitoring in near perpetuity and operation of remedial actions that may not improve protection of human health and the environment. Better understanding of the geochemistry at a site can lead to better decisions for site managers and regulators to protect the public and environment, while limiting inefficiencies.

1.2.1 Monitoring Subsurface Conditions

1.2.1 (a) Regulatory Standards

The Federal Safe Drinking Water Act (SDWA), passed in 1974, allowed the EPA to regulate contaminants in drinking water. The SDWA was further amended in 1986 to establish Wellhead Protection Zones. The Resource Conservation and Recovery Act (RCRA) of 1976 established monitoring of groundwater contamination around solid waste disposal sites. However, not until the Comprehensive Environmental Response, Compensation, and Liability Act (CERCLA) of 1980 was a more "comprehensive" approach to historical groundwater contamination applied. CERCLA, commonly known as Superfund, regulates 41 categories of hazardous substances consisting of more than 1,600 individual compounds (US Code of Federal Regulations Title 40 § 302.4, USEPA List of Lists). At sites identified in the Superfund National

Priorities List, any one of these contaminants could be regulated and required for removal or remediation upon discovery in the groundwater, soil, or other environmental compartment.

These regulations established requirements for removal, "to the extent practicable," of many contaminants and the attenuation of any persistent contamination that is not practically removable. To establish a basis for location, quantity, movement, and attenuation of contaminants, many sites have installed monitoring well networks. Monitoring well networks are commonplace among contaminated sites, wellhead protection zones, RCRA facilities, and other points of interest to groundwater monitors.

Importantly, environmental regulators and consultants alike typically prescribe the measurement of pH during groundwater monitoring programs on every sampling event. Measuring pH is ingrained in the well purging process, sample preservation protocol, field and lab analytical methods, and quality control of environmental data. This protocol is almost always based on the use of traditional glass pH probes at the ground surface in the hands of field personnel. Furthermore, these same probes are prescribed for use in the surface water outfalls and water treatment systems of almost all industrial facilities.

1.2.1 (b) First Generation (1G) Monitoring Strategies

Sale et al. (2013) notes "Historically we have characterized groundwater contamination by using 'First Generation' (1G) monitoring strategies that rely on conventional groundwater monitoring wells." Monitoring wells are cheaper than taking deep soil samples with drilling equipment and have historically been viewed as a sufficient tool for understanding contaminants in the subsurface.

In some cases, soil or rock core samples are used, but these samples often have three critical limitations: the samples only represent a single point in time and are not readily re-sampleable, pore fluids tend to drain during sampling or interact with the ex-situ environment such that samples are not representative, and pore fluid volumes are too small for most laboratory analytical work. In contrast, monitoring wells only have to be drilled once and can be sampled frequently. The use of soil or rock cores has primarily been to characterize the environment that contaminants exist and flow through (transport) but were neglected as important in the processes of contaminant transformation and storage (fate).

1.2.1 (c) Second Generation (2G) Monitoring Strategies

Over time as more remedial strategies stalled in effectiveness and costs of management rose, many in the contaminant hydrology field identified that 1G approaches to characterization were not sufficient and were leading to bad management decisions. New approaches developed which provide data at a higher resolution with a focus on more continuous data through the subsurface. Techniques like multi-level groundwater samplers, GeoProbe's Hydraulic Profiling Tool, optical screening tools, membrane interface probes, geophysical tools, and chemical tracers were developed and implemented to provide a better understanding of the complexity (heterogeneity) of the subsurface (Sale et al. 2013).

1.2.1 (d) Limitations of Common Monitoring Strategies

Sale et al. (2013) provide reasons for new approaches to monitoring strategies by highlighting the limitations and misconceptions of earlier approaches. In 1G approaches that relied heavily on monitoring wells, almost all focus was given to aqueous phase contamination, neglecting the importance of nonaqueous, vapor, and sorped phases which can have significant contaminant mass and lead to exposure pathways. In addition, monitoring wells produce samples

that are biased heavily toward contamination in the transmissive zones of aquifers and inaccurately depict the mass stored in less transmissive (low-hydraulic conductivity; low k) zones which can lead to rebounding of contaminant concentrations long after source zones are removed. Last, but perhaps most importantly, the samples obtained from these wells are often an average concentration of chemicals across the vertical well screen interval (or more) and do not depict the distribution of mass in the different strata that make up the subsurface environment, which can lead to large inaccuracies in modeling plume behavior (Martin-Hayden and Robbins 1997).

Second generation (2G) strategies greatly improved our understanding of subsurface complexity, but also have room for improvement. Some of these tools are not widely available, and some are cost prohibitive, especially at sites with large extents of contamination. Some tools still lack the quality of data that is needed and require further advancement. Furthermore, these tools require operators and analysts with the advanced skills and experience to properly apply them. The practice of contaminant hydrology needs new tools and strategies that can be employed at low cost and over the long durations during which attenuation or successful remediation programs occur. Perhaps the most innovative and useful solutions employ low-cost monitoring techniques that are continuous in time and do not require personnel in the field to obtain data.

1.2.2 Subsurface Chemistry

1.2.2 (a) Parameters of Interest

Specific contaminant concentrations are often the focus of analysis and may be obtained in multiple phases, depending on the chemical. Chemicals in the subsurface may exist in four

phases: aqueous, gaseous, solid, and non-aqueous phase liquid (NAPL). Herein, I focus only on the aqueous phase.

Despite the target often being concentrations of contaminants of concern, other parameters of interest are geochemical parameters, including pH, pe, and temperature. Geochemical parameters play a significant role in governing attenuation and/or treatment of contaminants. In addition to geochemical parameters, standard water quality parameters often include total dissolved solids (TDS), total organic carbon (TOC), biochemical oxygen demand (BOD), dissolved oxygen (DO), hardness, alkalinity, turbidity, salinity, conductivity, ions like chloride, nitrates, and sulfates, and metals. Knowledge of these parameters can lead to better interpretations and forecasting of the fate of contaminants. Critically, the master variables governing all chemical reactions in soils are pH and pe (Lindsay 1979).

1.2.2 (b) Limitations of Current Understanding

Despite understanding the fundamentals and even elaborate details of chemical processes and pathways for contaminant remediation, there is still large progress to be made in understanding how these reactions take place in the field under dynamic, real-world conditions. Given that sampling in the field is typically performed on a quarterly or less frequent basis, there is often not enough data to understand the temporal complexity of critical processes. As an example, “Manual measurement [of ORP] methods typically make it impractical to capture temporal and/or spatially dynamic redox conditions,” (Sale et al. 2020).

McHugh et al. (2016) explain that doubling the time between sampling events will double the accuracy of estimating attenuation rates. However, they also explain that this is not always practical, because some sampling is intended to evaluate the effectiveness of a remedial strategy within a short time. In one case studied by McConnell et al. (2022), machine learning was

applied to a historical dataset to evaluate forecasting of reductive dechlorination of trichloroethene (TCE) using a permeable reactive barrier (PRB); increasing sampling frequency from a quarterly to a monthly basis was found to significantly improve the accuracy of the forecasting model. Sale et al. (2020), using in-situ sensors, found that ORPs in the vadose zone varied hourly and were closely related to the weather. They were able to identify events of ebullition occurring using these sensors. These examples support that temporally higher resolution datasets of geochemical parameters are required to increase the accuracy of forecasting using machine learning and can give insight into reactions taking place in small time scales. This can allow better understanding of the effectiveness of remedial strategies and decrease the time needed to obtain those conclusions.

1.3 How Does the Work Aim to Solve these Problems?

1.3.1 New Monitoring Strategies

1.3.1 (a) Internet-of-Things and "Big Data"

New developments to monitoring sites should focus on low-cost technology that does not require highly skilled personnel to maintain and operate. To move in this direction, the world is leveraging IoT which is expanding to every corner of our economy. With developments in internet bandwidth and connectivity that have occurred in the past two decades, IoT devices have become reliable and ubiquitous. Especially with the advent of 5G internet technology and edge or cloud computing, IoT devices are thriving. Data is a valuable commodity, and the interconnected mesh of IoT devices allows datasets and systems to integrate, forming seamless, smart networks where real-time data can feedback into systems that automate complex processes and provide information to managers.

Because of the volume of multifaceted data that these systems can provide, artificial intelligence (AI), machine learning (ML), and deep learning (DL) algorithms can be applied, expanding the processing power that humans have access to, revealing new insights that may have been missed. ML and DL are subsets of AI that require large historical datasets to train the model prior to effective forecasting. IoT devices are uniquely advantageous in developing large datasets and AI systems because of their low cost, small size, and diverse loadout of inputs like sensors or feedback data. Furthermore, these datasets and models can be leveraged in easy-to-use dashboards and applications that most stakeholders can become familiar with, with little training.

1.3.1 (b) High-Volume, Spatially Distributed Monitoring Systems

In the world of contaminant hydrology, mining, agriculture, geoscience, water resources, and more, IoT can be leveraged with systems that can monitor sites with higher resolution, real-time datasets at lower cost than traditional sampling and analysis. This will lead to smarter management decisions that reduce costs of operation and improve efficacy of remedial or containment strategies. This work focuses on the development of pH sensors that can be deployed to provide high resolution spatial and temporal pH data.

1.3.2 Developments in Understanding Subsurface Chemistry

Two of the fundamental parameters for hydrogeochemistry are pe and pH. These parameters quantify the activities of electrons and protons, respectively, in an aqueous solution. Despite the long timeframe for many geochemical reactions, “Equilibrium relationships are useful for predicting chemical changes that can and cannot occur,” (Lindsay 1979) which is especially important when dealing with synthetic chemicals introduced to the environment. By monitoring the pe and pH of a system, we can better understand the stage of a reaction relative to equilibrium and which direction the reaction is proceeding based on thermodynamics. With real-

time, in-situ measurements of these governing parameters, site managers can predict with better certainty the fate and transport of contaminants and make better cases for attenuation and/or remediation efficacy, leading to better strategies for achieving closure or redevelopment.

1.4 Objectives

The work described herein has two primary objectives:

1) Develop a robust, low-maintenance, solid-state sensor and IoT-based monitoring system for pH in soil and groundwater;
2) Perform laboratory experiments to document the efficacy of the pH sensor and monitoring system.

2. BACKGROUND

2.1 pH and pe in the Environment

2.1.1 pH

Aqueous chemistry is critical to the functioning of the environment. Water is the catalyst and substrate for many of the geochemical and biological reactions that keep our world in a dynamic state of disequilibrium that allows life to exist and landforms to change. The pH of water in the environment (i.e., the aqueous proton activity) plays a significant role in how reactions occur and which reactions are thermodynamically favored. Some of the most important environmental impacts of pH are on buffering and neutralization, phase transitions, soil behavior (properties), and soil formation (weathering, deposition), and how the living ecosystem responds. pH extremes in the natural environment have been observed from 0.02 to 12.8, and extremes from anthropogenic impact extend from -3.6 to +13.3 (Merino et al. 2019, Czop et al. 2011, Nordstrom et al. 2000). pH is a *master variable* in aqueous chemistry.

2.1.1 (a) Buffering and Neutralization

Changes to pH can occur quickly in pure water, with protons transferring through an aqueous system on the order of milliseconds (Stumm and Morgan 1996, Schwarzenbach et al. 2016). Given that acids and bases are produced readily throughout the environment by atmospheric gases, mineral dissolution, and organic processes, the pH of natural waters can be in constant flux if not for buffering capacity and neutralization reactions. Natural waters, especially groundwater, are often heavily buffered by natural carbonates which are often abundant (in soils and groundwater). Buffering is particularly common for waters that have been exposed to minerals for longer periods of time, i.e., deep groundwater. The aqueous ‘acid neutralizing

capacity' can be approximated by alkalinity, and 'base neutralizing capacity' can be approximated by mineral acidity (Stumm and Morgan 1996).

However, pH changes in natural waters cannot be dismissed. Not all waters are well-buffered, and some waters can be overloaded with chemicals in excess of buffering capacity. Natural systems typically are effective at buffering against natural influences, but anthropogenic influences can overwhelm a system quickly and cause significant pH changes. This is especially easy in highlands with very fresh water and crystalline rock or in areas close to aquifer recharge zones.

2.1.1 (b) Phase Transitioning

When pH changes, there are impacts to reactions and reaction rates. Because many reactions involve proton transfer, the activity of protons in the solution greatly influences the thermodynamic favorability of some reactions. For example, following Lindsay (1979), as acidity increases (decrease in pH), the activity of aqueous Al^{3+} increases.

$$\gamma\text{-}Al(OH)_{3(gibbsite)} + 3H^+ \leftrightarrow Al^{3+}{}_{(aq)} + 3H_2O \qquad \log K° = 8.04 \qquad (1)$$

$$\frac{(Al^{3+})}{(H^+)^3} = 10^{8.04} \qquad (2)$$

$$\log Al^{3+} = 8.04 - 3pH \qquad (3)$$

The Al^{3+} ion is a solute in aqueous solution whereas gibbsite is a crystalline solid. As acidity increases in the water, aluminum is more mobile and available for uptake by organisms like plants, microbes, humans, and livestock. This pH-dependent solubility is also generally true for many other metals such as iron, manganese, zinc, copper, cadmium, lead, mercury, and chromium.

pH-influenced phase changes are not limited to metals; pH-dependent compositional changes also occur with organic compounds. As noted by Schwarzenbach et al. (2016), "The water solubility of the ionic form of an organic acid or base is generally several orders of magnitude higher than the solubility of the neutral species. The total concentration of the compound at saturation is, therefore, strongly pH-dependent."

Solubility is also pH dependent for many inorganic salts, oxides, and hydroxides (Brown et al. 2022). Karst formations are examples of pH-influenced formations where acidic rain accelerates the dissolution of limestone. pH also affects air-water partitioning where the ionized species is typically assumed to not transfer to the gas phase.

Sorption to soils is of prominent importance in subsurface contaminant behavior and is heavily affected by pH where surface charges of soils are determined by pH of the soil pore water (Fetter et al. 2018, Sparks 2003). Hence, pH has significant implications for understanding the source quantity and distribution across various compartments (e.g., sorped, solid, aqueous phase) of a given chemical in the environment.

2.1.1 (c) Soil Behavior

pH in soils is an indicator of the charge state of particles within the soil, especially clays, oxides and hydroxides, and organic matter. At circumneutral and high pH, proton activity is moderate to low in the solution and prompts protons in the hydroxyl groups at the surfaces of particles to disassociate into free solution. This causes a net-negative surface charge, which typically predominates at near neutral pHs. However, in more acidic conditions, net surface charges may become positive (Sharma and Reddy 2004).

The influence of clay particle charge governs properties such as cation/anion exchange capacity, soil fabric formation, and bound-water structure which can influence permeability and shear behavior. Understanding soil fabric and structure, which are often dependent on pH (among other factors), is important for understanding common engineering behaviors like compressibility and collapse, shear strength, hydraulic conductivity, and erosion (Mitchell and Soga 2005).

2.1.1 (d) Ecological Impacts

Living organisms, especially microbes, have significant impacts on geologic development and environmental chemistry (Sparks 2003). The interaction of life and pH is intertwined, with the pH of an environment influencing what life can be sustained and the metabolic processes of organisms influencing the activity of many chemicals, including the hydrogen ion. As noted by Mitchell and Soga (2005): "Biological activity mediates geochemical reactions, causing them to proceed at rates that are sometimes orders of magnitude more rapid than would be predicted solely on the basis of thermochemical reactions involved." The identification and study of extremophiles, their limits, and their capabilities is a vibrant field of science that is relevant for many applications in environmental remediation; one of the most studied conditions for extremophiles is pH, with organisms living in the range of pH -0.06 to 12.5 with some able to withstand at least 6 pH units of variation (Merino et al. 2019).

2.1.2 pe

A second *master variable* in aqueous chemistry is the electron activity, pe. Just as in acid-base reactions where protons hop from molecule to molecule and are not free in solution, free electrons are essentially absent in aqueous solution. Rather, pe is the "tendency of a solution to accept or transfer electrons" (Stumm and Morgan 1996). Most chemical reactions in the

environment involve some electron or proton transfer, and usually both (Schwarzenbach 2016). There are many concepts related to pe that are pertinent to contaminants in the environment including oxidizing or reducing environments, the carbon cycle, and microbially mediated redox reactions.

2.1.2 (a) Oxidizing and Reducing Environments

pe varies in the subsurface. In the vadose zone, oxygen can enter from the atmosphere and flow through the connected pore structures and diffuse into surrounding pore water whereas in the saturated zone, molecular oxygen is almost entirely absent. About the groundwater table, where the two zones meet, oxygen dissolves from the gas phase into the water and extends partially into the saturated zone. Oxygenated water can also seep into the groundwater system from surface water sources such as rivers. The presence of molecular oxygen in the gas or dissolved phase creates an *oxidizing environment* because oxygen readily accepts electrons from other molecules to form water.

Contaminants, as well as geogenic species, further change redox conditions as they migrate through the environment. Because contaminants are often in a liquid or aqueous form and may have source zones with extending plumes, they carry electron acceptors or donors through the environment. Figure 2 shows a contaminant plume associated with an electron-donor-rich source and the developing redox zones (Christensen et al. 2000). Throughout the plume, redox zones develop where they can be characterized by both the presence of oxygen and the oxidation state of other constituents (Fetter et al. 2018). For example, a landfill leachate with significant organic matter will often have an anaerobic, reducing zone closest to the source and an aerobic oxidizing zone on the leading edge with a transition zone between them.

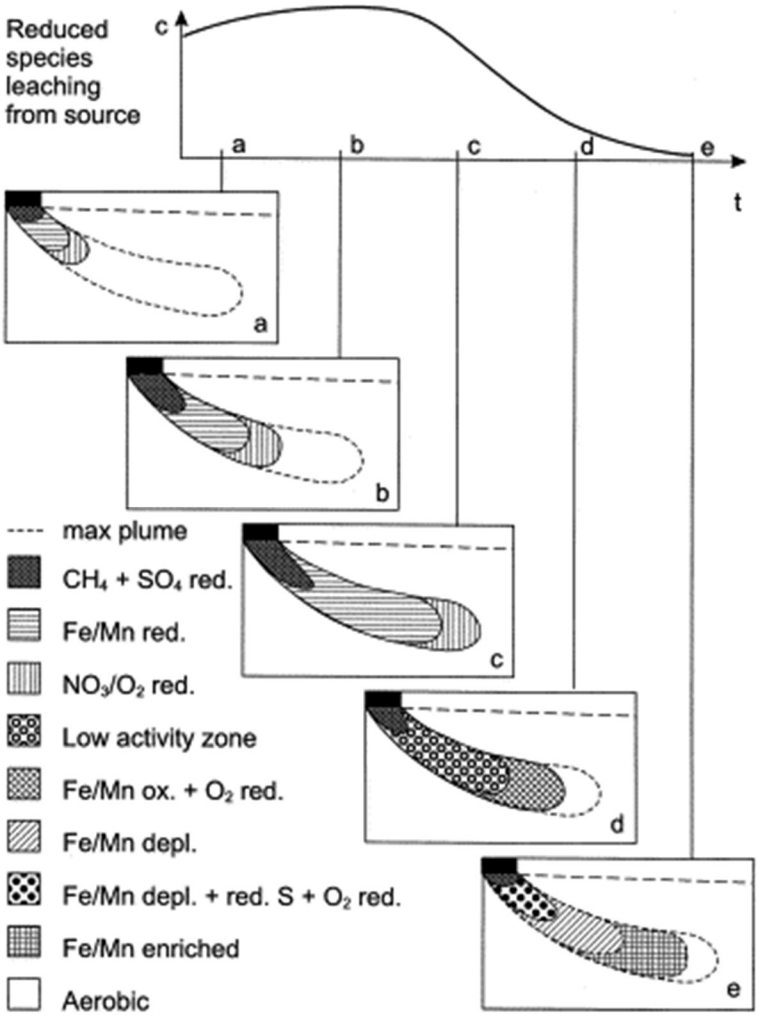

Figure 2. Redox dynamics of an electron-donor-rich contaminant plume with changing redox status across time and space (from Christensen et al. 2000, Fig. 4).

2.1.2 (b) Carbon Cycle

Organic compounds like petroleum hydrocarbons are part of the global carbon cycle, existing as storage vessels for energy cycling through our ecosystems. The hydrocarbons in petroleum reservoirs were produced long ago from photosynthesis of CO_2 and the subsequent accumulation into biomass. These reservoirs, often extracted for reuse as fuel, are in their reduced form and are "highly reactive" when exposed to an aerobic environment; "Their reactivity is both a removal mechanism and an opportunity for causing harm," (Overton et al.

2019). As hydrocarbons (electron donors) move through the environment, they influence the redox zonation and readily degrade into other forms such as carbon dioxide. This happens through inorganic processes such as photooxidation (energy imparted by the sun) and biological processes with microbes such as methanogenesis.

2.1.2 (c) Microbially Mediated Redox

Microbial influence on redox cycles in the environment cannot be overstated. "In environmental systems, [redox reactions] may be controlled by microorganisms that do not participate in the reactions but act as catalysts," (Fetter et al. 2018). Just as animals use oxygen to extract energy from biomass when we eat, microbes can facilitate oxidation of reduced compounds with multiple oxidants (oxygen, nitrate, forms of iron and manganese, etc.). This biologically mediated carbon and energy cycle is both influenced and affected by pe and pH.

2.1.3 pe + pH, the Characteristic Redox Status

Despite pe and pH representing opposite components in the system, they also represent a harmony. Protons and electrons combine to form the building blocks of all things and affect transformation processes. Figure 3 shows the integration of the two concepts where Willard Lindsay (1979) explains that in aqueous systems, the two master variables can be combined into a "convenient single-term expression for defining the redox status," $pe + pH$, where "many redox-associated mineral transformations in soils occur at fixed $pe + pH$ values." Lindsay demonstrated the consistency of pe + pH values for many soils and their constituents. He calls this phenomenon the *characteristic redox status* of a soil.

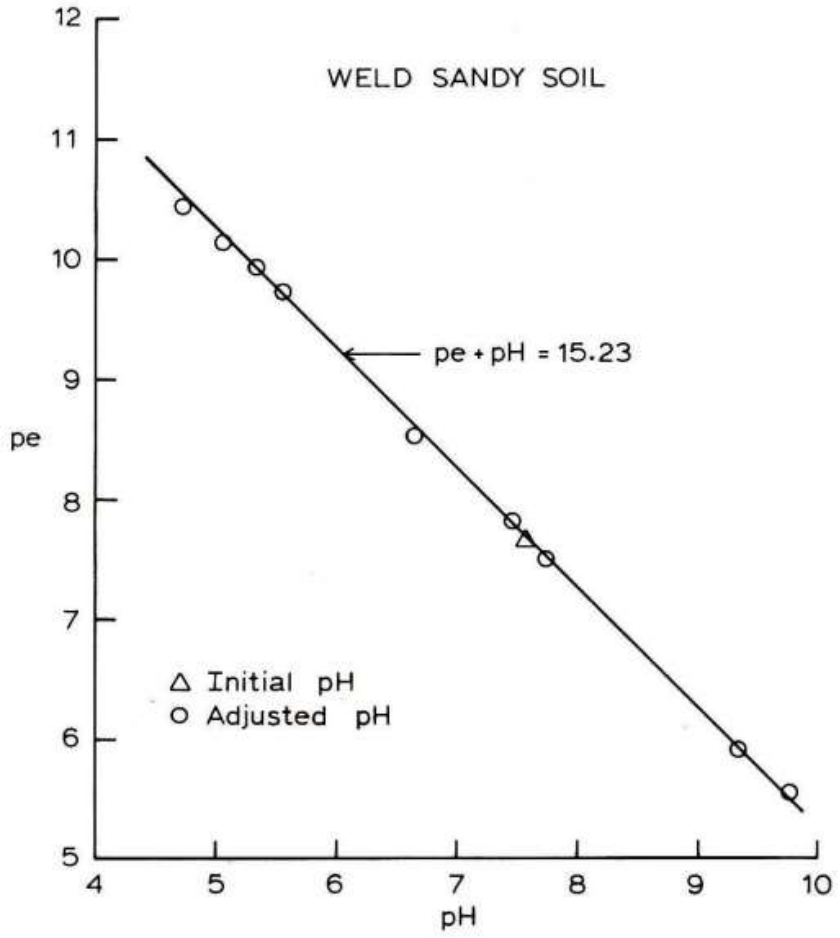

Figure 3. Willard Lindsay's demonstration of a "characteristic redox status" shown in Weld Sandy Soil, influenced by both pe and pH (from Lindsay 1979, Figure 2.2).

2.1.3 (a) Pourbaix Diagrams

Delving into a soil or rock's composition is complex and dynamic through time, especially as pe and pH change. One approach to understanding the transformation of certain compounds as they relate to pe and pH is a Pourbaix diagram, shown in Figure 4, which shows the equilibrium forms of a given element under given element concentrations across the pe and pH spectrum. By applying Lindsay's characteristic redox status approach with a hypothetical soil *pe* + *pH* constant of 12, we can see that some species ($H_3AsO_3^0$, $H_2AsO_3^-$) will not be

thermodynamically favorable in large quantities in this soil. This can be used to determine contaminant behavior in response to remediation methods.

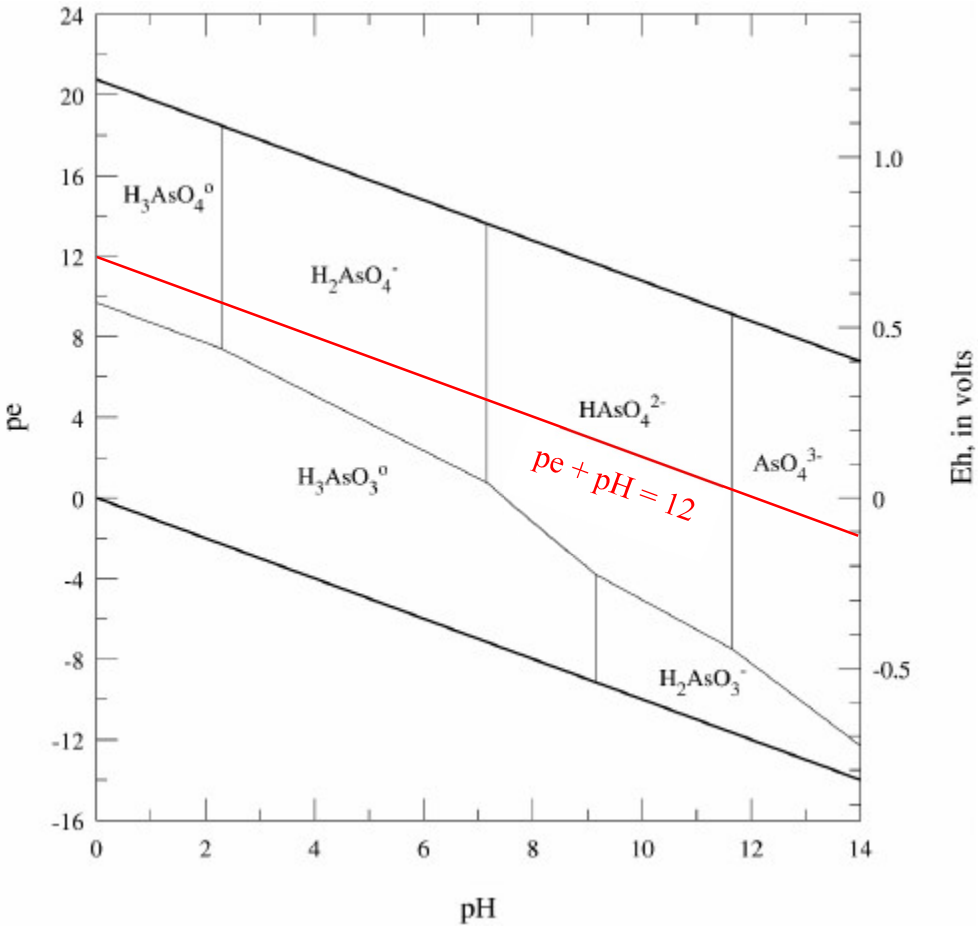

Figure 4. Pourbaix diagram showing predominant aqueous species of arsenic at 25°C, 1 atm. (after Nordstrom et al. 2014, Figure 5) with a hypothetical soil characteristic redox status of (pe + pH = 12).

2.1.3 (b) Deducing Concentrations Given pe and pH

Though measuring pe, pH, and the characteristic redox status do not directly yield chemical concentrations, they may indicate concentrations given other context. For example, if the concentration of a protonated acid species is measured with the pH, the concentration of the ionized species can be determined. If the species are stable in the system and do not readily

degrade, monitoring the pH through time can indicate concentrations of the species, reducing the need to frequently sample concentrations. Critically, a shift in pH will likely cause a shift in pe, allowing determination of redox-related transformations. Complications with this approach are the open systems in the environment where mass and energy can flow into and out of the system, and the kinetics which limit reaction rates, making equilibrium conditions sometimes unrealistic. Most importantly, these two measurements and their combination yield insightful information about the processes taking place which can help to make decisions.

2.2 pH and pe Sensing

Attempts to measure pe and pH should be distinguished from the reality of the pe and pH concepts (Stumm and Morgan 1996). Those concepts, theoretically correct, are difficult to measure and should be taken with context. The measurement of the phenomenon is only as good as the system used to measure, and there is a distinct difference between the thermodynamically derived theoretical voltages produced by a reaction and the measurable response observed at an electrode surface. Thortenson (1984) points out, “the analogy between pe and pH as master variables is generally carried much further than is justified,” explaining that often measured redox potentials do not agree with the verified redox couples from experiments. Perhaps, the issue comes not from the disagreement of apparent redox potentials and the thermodynamics, but rather from the limitations of properly measuring those potentials where the electrode must act as a surrogate electron donor or acceptor. Especially complicating is the ability of the electrode to represent the microbial influences on redox reactions. Despite complications, electrodes can generally produce a reasonable estimation of electron activity in a system with multiple redox couples which can be “very useful in characterizing the oxidation-reduction status of a soil,” (Sparks 2003).

2.2.1 History and Developments

Despite difficulties with measuring redox potentials, sensors for monitoring pH have existed for over a century now and have mostly overcome the challenges. In the early days, pH measurements were also difficult. The first methods for measuring acidity with the standard hydrogen electrode were reported by Böttger in 1897 when he performed a potentiometric acid-base titration (Böttger 1897). Other electrode designs allowed others to do similar work, but the glass electrode developed by Cremer (Cremer 1906) "has been responsible…for the widespread application of pH measurements in the control of industrial and commercial processes," (Bates 1964). Though Cremer was very knowledgeable about electrochemistry and the developments therein (Nernst 1889), he did not see the implications that his work would have when he developed the thin glass electrode for studying biological cell walls (Scholz 2011). Cremer's glass electrode discovery was taken up by the famous Fritz Haber and his graduate student (Haber and Klemensiewicz 1909), who used a glass electrode for measuring pH in analytical chemistry. This electrode is, "doubtlessly the most frequently used analytical [electrode] in laboratories and in industry," (Scholz 2011).

New designs for technology that measures pH are evolving based on modern needs. The main application space that has pushed the forefront of soil pH sensing in the past two decades is precision agriculture, which has led to new forms of ion-selective electrodes (Lemos et al. 2004, Lemos et al. 2007), satellite-based remote sensing integrations (Grunwald et al. 2015, Roelofsen et al. 2015), and proximal sensing technologies (Viacheslav et al. 2002 Veris®, Viscarra Rossel et al. 2017). However, innovation in pH sensing in the environmental and groundwater spaces has not flourished; for that purpose, few new methods have been developed for monitoring pH that challenge the traditional glass pH probe (Maher and Shahriari 1993, Zhang and Angelidaki

2011). Notably, interests have increased more recently regarding new methods for collecting and analyzing soil and groundwater data that can improve spatial and temporal resolution of geochemical parameters (Fan et al. 2022, Sale et al. 2020). Still, new methods and technologies for in-situ monitoring of pH in soil and groundwater are needed.

2.2.2 Standard Glass pH Probe

2.2.2 (a) Conceptual Design

Though pH measurements today are accepted as ubiquitous in all of chemistry, few recognize the limitations and inner workings of the glass pH electrode (Bates 1964). Most glass pH electrodes used today are combination electrodes in which the sensing electrode and the reference electrode are contained in a single housing called the probe. The probe's conceptual design, shown in Figure 5, is centered on comparison of a constant reference electrical potential to a varying sensing electrical potential that is dependent on acid concentration. This comparison of potentials is measured as voltage using a voltmeter which is typically incorporated in a pH meter.

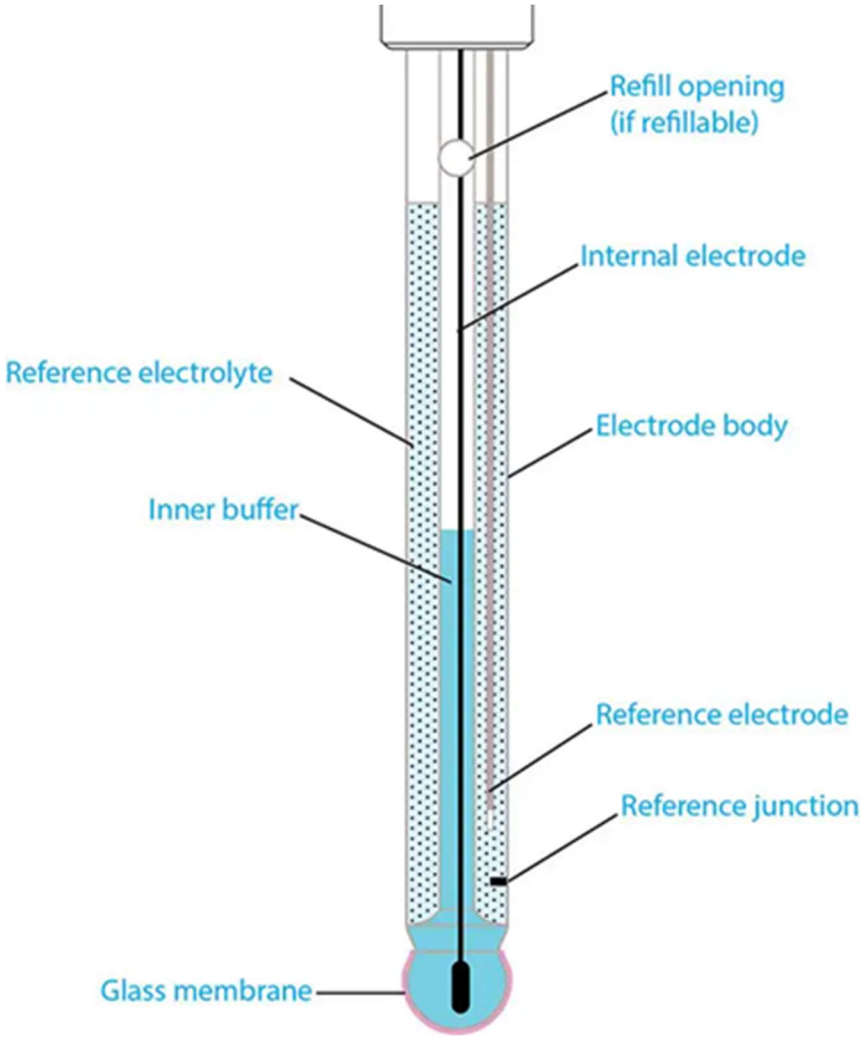

Figure 5. Standard glass pH electrode conceptual design (from Cushman 2021).

The reference electrode is housed in the outermost chamber of the probe which maintains a constant electrical potential. This reference electrode is often a silver-silver chloride (Ag/AgCl) electrode which works by maintaining constant chloride ion (Cl^-) concentration using a saturated potassium chloride (KCl) solution with excess solid potassium chloride present. If electrons flow away from the silver electrode through the lead wire (in this case, connected to the sensing electrode through the voltmeter), the zero-valent silver (Ag^0) substrate will increase oxidation state to plus one (Ag^{+1}). In turn, a chloride ion (Cl^-) in the surrounding solution will bond with

the Ag^{+1} ion, forming silver chloride (AgCl). In response, solid potassium chloride in the chamber will dissociate into potassium (K^+) and chloride (Cl^-) ions, maintaining the chloride concentration and the electrical potential on the electrode. The half reaction for this electrode is shown in Equation 4. The potential on the electrode can be determined using the Nernst equation (Nernst 1889), Equation 5, based on the chloride ion concentration, where (E^0) is the standard reduction potential of the Ag/AgCl electrode, T is the temperature in Kelvin, R is the universal gas constant, F is the Faraday constant, and n is the number of electrons participating, which is 1 in this half reaction.

$$\mathrm{AgCl}_{(s)} + \mathrm{e}^- \leftrightarrow \mathrm{Ag}^0_{(s)} + \mathrm{Cl}^-_{(aq)} \quad (4)$$

$$E_{(\mathrm{Ag/AgCl})} = E^0_{(\mathrm{Ag/AgCl})} - \frac{RT}{nF} \ln[\,\mathrm{Cl}^-_{(aq)}] \quad (5)$$

The innermost chamber of the combination pH probe is filled with a solution of known, constant H^+ activity (often pH 7) surrounding a platinum sensing electrode. This innermost chamber terminates with a thin glass bulb at the tip of the probe. The thin glass bulb is often coated in a special proton-selective gel which aids to reduce the effect of non-target ions. Together, the glass and gel, act as a cation exchange membrane through which an electromotive force can extend (Stumm and Morgan 1996). As protons in the test solution diffuse into or out of the gel membrane and collect on the glass surface (or leave), the charge on the outside of the glass bulb changes, inducing an electromotive force, causing the protons inside the bulb to either collect on or flee the inside of the glass bulb. In response to the redistribution of charged particles in the solution, protons inside of the inner chamber solution will either collect on or flee the platinum electrode's surface, changing the electrical potential on the platinum electrode. For example, if the probe is inserted into an acidic solution, protons in the acid will collect on the

outside of the glass bulb, forcing protons on the inside of the bulb to repel away and collect on the platinum surface. This will increase the *potential* for negatively charged electrons from the reference electrode to move toward the positively charged surface of the platinum sensing electrode (increased voltage).

Finally, the reference electrode chamber must have a porous frit that acts to complete the salt bridge, allowing ions to transfer charge from the inside of the reference electrode chamber to the outside of the sensing bulb, maintaining charge neutrality throughout the system. Using the voltmeter in the pH meter, the voltage between the reference electrode and sensing electrode is read, allowing calculation of the electrode potential at the sensing electrode (Equation 6). The Nernst equation can be applied, shown in Equations 8 and 9, to find the pH of the test solution based on the electrode potential where the standard cell potential, E^0, is based on the Standard Hydrogen Electrode (SHE) which is conventionally given a potential of zero volts. The half reaction for the SHE is given in Equation 7. Equations 10 and 11 show that for a decrease of one pH unit at the standard temperature, the voltage on the electrode will increase by 59 mV.

$$\text{Voltage} - E_{reference} = E_{sensor} \tag{6}$$

$$\mathrm{H^+ + e^- \rightarrow \frac{1}{2} H_{2(g)}} \tag{7}$$

$$E_{sensor} = E^0_{(SHE)} - \frac{RT}{nF} \ln \frac{[\mathrm{H^+_{outside}}]}{[\mathrm{H^+_{inside}}]} \tag{8}$$

$$E_{sensor} = 0 - \frac{RT}{(1)F} \ln \frac{[\mathrm{H^+_{outside}}]}{[\mathrm{H^+_{inside}}]} \tag{9}$$

$$E_{sensor} = \frac{-2.303(R)(298.15\,K)}{(1)F}\log_{10}\frac{[\mathrm{H}^+_{outside}]}{[\mathrm{H}^+_{inside}]} \quad (10)$$

$$-0.059\mathrm{V}(\mathrm{pH}_{outside} - \mathrm{pH}_{inside}) = -0.059\mathrm{V}(-1) = +\mathbf{0.059\ V} \quad (11)$$

2.2.2 (b) Limitations

Though the standard glass pH probe works well and has become a standard piece of equipment in all chemistry labs, has limitations. One limitation of this probe is that the probe is not solid-state; this probe has solution inside that needs to be replaced over time to maintain operation. For our intended application in continuous subsurface deployments, solution cannot be replaced in the probe because the probe will be inaccessible. A second limitation is that the probe must be calibrated through time. Typical glass pH probes must be calibrated approximately once every two weeks, depending on their use. This is also not feasible in our intended application. Most importantly, the glass pH electrode is fragile and cannot withstand deep subsurface deployments.

2.2.2 (c) Alternatives

Because of the fragility and necessity of maintenance, the standard glass pH electrode is not suitable for the intended application in the subsurface. Similarly, standard pe (ORP) electrodes used in the lab are not suitable for field deployments. However, developments made by Sale et al. (2020) show a titanium mixed metal oxide (TiMMO) dimensionally stable anode (DSA) could be used in-situ in the subsurface to monitor ORP in real time. These sensors, still under development, show promise for further applications and are the inspiration for the solid-state pH sensor design explored here.

3. SENSOR AND MONITORING SYSTEM DESIGN

To satisfy Research Objective 1, a pH sensor system was designed, fabricated, and tested. Some parts of the design are novel while others are adopted from previous works (Kinlen et al. 1994, Sale et al. 2020). The system developed can be broken into two main devices: the solid-state pH sensor and the internet-of-things (IoT) based monitoring system. Each device and the associated main parts are described subsequently.

3.1 Solid-State pH Sensor

The main part of this research and central design focus is the solid-state pH sensor. The sensor is a system of three components: a titanium mixed-metal-oxide (TiMMO) wire, a proton-selective Nafion™ membrane, and an insulating body. Each component is summarized in and described in the subsequent sections. The resulting solid-state pH sensor is herein referred to as the TiMMON (Titanium Mixed Metal Oxide Nafion™) electrode.

Table 1. Solid-State pH Sensor Components

Picture	Component	Purpose
	Titanium Mixed-Metal-Oxide (TiMMO) Wire	Dimensionally stable and robust conducting material; structural "back bone" of sensor
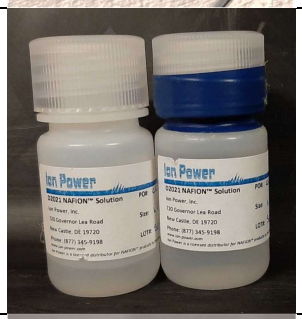	Nafion™ Coating	Proton-selective sulfonic acid polymer membrane (ionomer)
	3M Scotch-Weld Epoxy Potting Compound DP270	Insulates electrical connection and create a durable, solid body
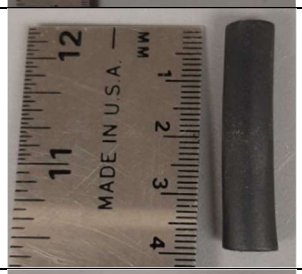	¼" Heat Shrink Tubing	Provides a durable casing for the epoxy potting compound and shrink to push epoxy into gaps
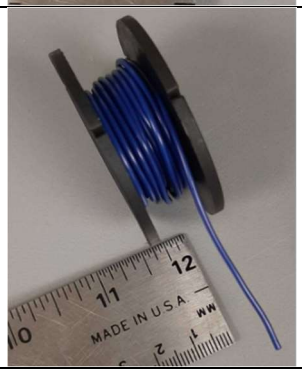	PVC-Insulated Copper Wire	Provides electrical connection from TiMMO wire to the pH meter

3.1.1 Titanium Mixed-Metal-Oxide (TiMMO) Wire

The titanium mixed-metal-oxide electrode, a type of dimensionally stable anode (DSA) was first invented and patented by Henri Bernard Beer in 1965. In the original patent, Beer (1965) states, “The invention consists in an electrode for electrolytic processes comprising a core of a film-forming metal… at least partially covered by a layer… of at least one oxide of a metal of the platinum group.”

The TiMMO electrode used in our design consists of a titanium wire as the film-forming metal and a mixed ruthenium-oxide/iridium-oxide coating acting as the electrolytic catalyst. This material has been proven a suitable electrode for not only electrolytic cells but also cathodic protection (MATCOR 2022) and applications in the subsurface as an electrolytic reactive barrier (Sale and Olson 2010). The TiMMO has been demonstrated to be a suitable material in the previously developed ORP sensors (Sale et al. 2020) with which the pH sensor systems are intended to be compatible.

Consideration was given to different electrode shapes such as the mesh electrode or a flat plate shape, but previous experience showed the mesh electrodes’ sharp edges to be difficult to work with. Our assumption was that surface area would not change the voltage produced in the sensor, so a wire shape of 1 mm diameter and 1 inch length was used. This shape was also conducive to making electrical connections and installing using the single-stick method in bore holes (Karimi Askarani and Sale 2019). Despite being called “wire”, the TiMMO is stiff and does not bend easily.

3.1.2 Nafion™

To mimic the conceptual design of the standard glass pH electrode, a proton-selective membrane was needed to coat the TiMMO wire. A Nafion™ membrane was applied on the

surface of the TiMMO electrode following the design of Kinlen et al. (1994). Kinlen et al. (1994) demonstrated the ability to create a fully solid-state electrode using Nafion^{TM} on an iridium oxide-coated titanium substrate. Nafion^{TM} is an ionomer designed by Walther Grot at the E.I. Dupont company in the 1960s. Nafion^{TM} was the first fluorinated ionomer ever developed and was first adopted as a cation-exchange membrane in fuel-cell applications and a separator in the chlor-alkali process used to produce chlorine gas and sodium hydroxide.

3.1.2 (a) Nafion^{TM} Background

Nafion^{TM} is a copolymer of polyfluorinated sulfonic acid (PFSA) and tetrafluoroethylene (TFE) where the TFE backbone gives the polymer strength and strong chemical and heat resistance, and the sulfonic acid imbues unique chemical properties. Because Nafion^{TM} is a perfluorinated polymer, the body is inert and stable, but the sulfonic acid 'tails' on the attached PFSA chains allow various molecular forms to develop through the manufacturing process. The initial thermoplastic polymer terminates in sulfonyl fluoride (SO_2F^-) groups which are then hydrolyzed with either sodium hydroxide (NaOH) or potassium hydroxide (KOH) in heated tanks. This forms sulfonate groups (SO_3^-) which form ionic bonds with the sodium or potassium to create the neutral salt form of Nafion^{TM}. Then, the neutral form is converted to an acid form by exposure to a strong acid, typically nitric acid (Grot 2011).

Figure 6 shows the general structure of a Nafion^{TM} membrane with water paths carrying positively charged hydronium through the membrane. The black lines represent the branching carbon-fluorine chains from the PTFE backbone and the PFSA. Walther Grot demonstrated in 1964 that Nafion^{TM} could be used to separate ions in solution by allowing some cations (mainly H^+) to flow while restricting the flow of anions (Grot 2011). However, the structure and exact nature of how Nafion^{TM} transports cations has been studied and debated for decades and is still

not fully resolved (Fernandez Bordín et al. 2018). Recent studies show that multiple models of the structure, including the “cluster-channel” model, “core-shell sphere” model, “rod-model”, and “lamellar” model, all “produce appropriate raw descriptions of the membrane structure” (Fernandez Bordín et al. 2018) but are not necessarily general because of changes to the structure due to the chemistry of the solution (Sengupta and Leyulin 2019) or post-synthesis treatments (Grot 2011). Regardless, the models are all similar in that there are apparent pathways for water through the membrane created by the sulfonic acid groups on the tails of the polymer chains. Protons may easily hop to and from water/hydronium molecules through the membrane.

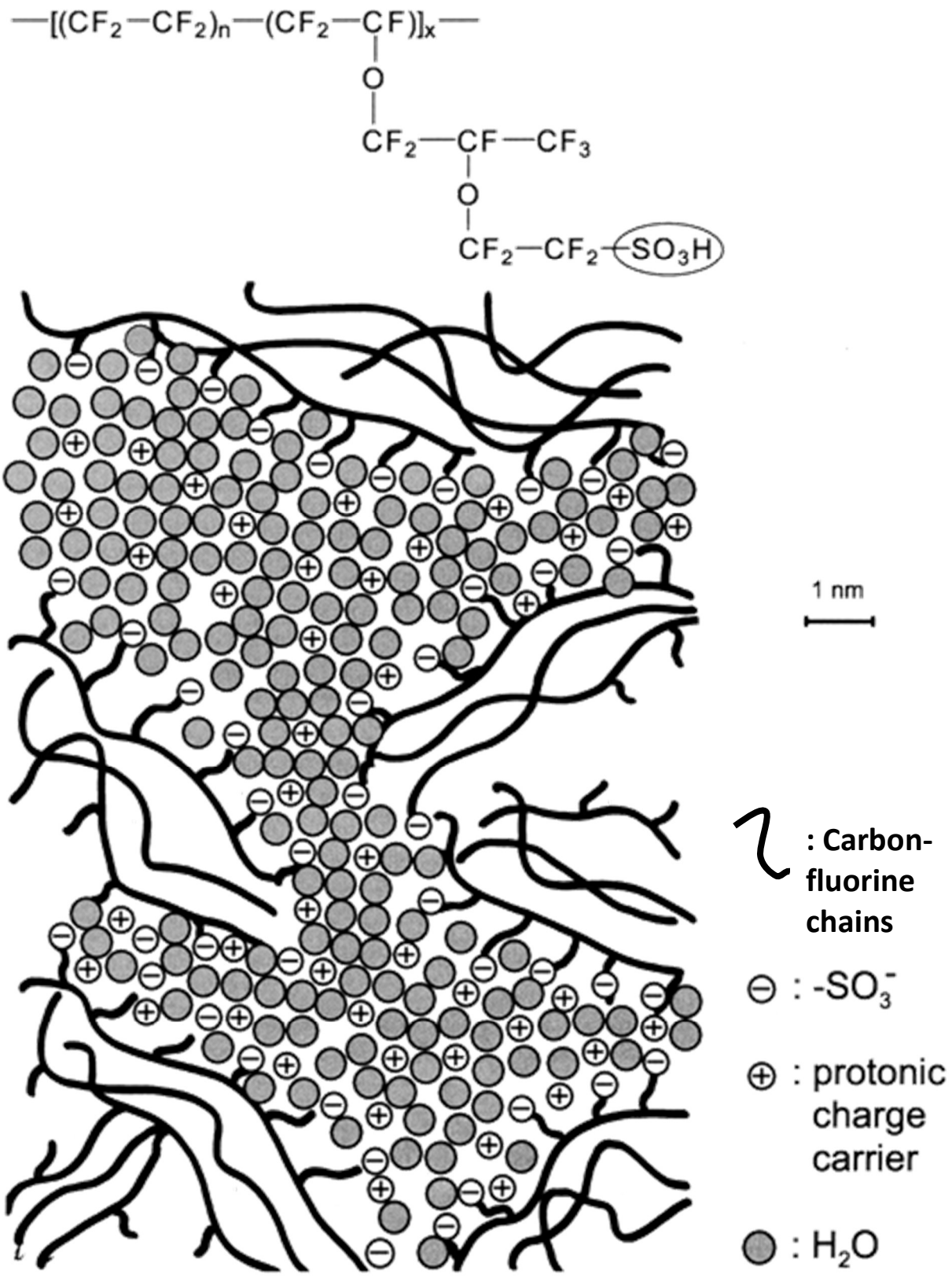

Figure 6. Nafion™ Structural Model (from Kreuer et al. 2004, Figure 6)

3.1.2 (b) Nafion™ Coating

A Nafion™ D2021 dispersion (Ion Power, Inc.), which has a syrupy consistency, can be used to coat the TiMMO electrode through a dipping and annealing process. Following a simple version of the procedure described in Kinlen et al. (1994), half of the TiMMO wire was dipped once into the Nafion™ D2021 dispersion and then hung by one end and allowed to air-dry in a fume hood until the Nafion™ was solid (approximately one hour). Then, the Nafion™-coated TiMMO wires were placed into crucibles filled with sand such that the dry half of the TiMMO was in the sand and the Nafion™ coated half was protruding outward. The crucibles were then moved into an oven and heated from room temperature to 60°C and held at 60°C for 1 hour. After one hour, the temperature was increased to 210°C and held for 30 minutes. Then, the oven was turned off and allowed to slowly cool overnight. After this annealing process, the Nafion™ coating on the sensors resembles a thin, shiny layer of plastic coating half of the TiMMO wire. Some dried droplets of Nafion™ were apparent on the tip of the wire where the viscous dispersion dried before annealing. These dried droplets showed a brownish color after annealing and are brittle. Figure 7 shows the work area inside the fume hood during the coating process.

Figure 7. Coating and drying setup with sensors hanging to dry after being dipped in Nafion™-filled vial.

3.1.3 Insulating Body

After the TiMMO wires were coated in Nafion™ and annealed, the uncoated portion of the wires were connected to a wire lead and insulated, shown in Figure 8. The connection between the wire lead and the TiMMO wire is solely a mechanical connection because solder does not adhere to titanium or the MMO coating. The stripped end of a 20 AWG solid-core copper wire was wrapped tightly around the uncoated half of the TiMMO wire three to four times and then tightly crimped by hand using plyers. After crimping, solder was applied to the wrapped connection to create a larger conductive contact area between the TiMMO and copper wire lead, as well as strengthen the wrapped connection.

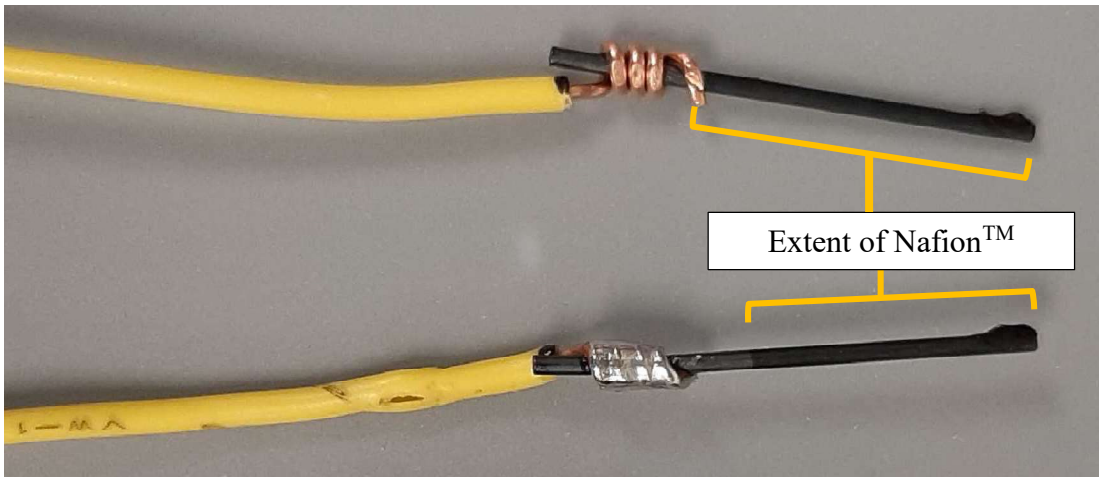

Figure 8. Electrical connection of 20 AWG copper wire to Nafion™-coated TiMMO wire before and after soldering.

After the electrical connection was established, the connection was insulated to prevent corrosion of the copper wire and ensure the test-solution (solution that the sensor is immersed in during operation) did not touch any conductive material. All contact with the test-solution must be through the Nafion™-coated half of the TiMMO to ensure the sensor is only responding to protons through the Nafion™ coating.

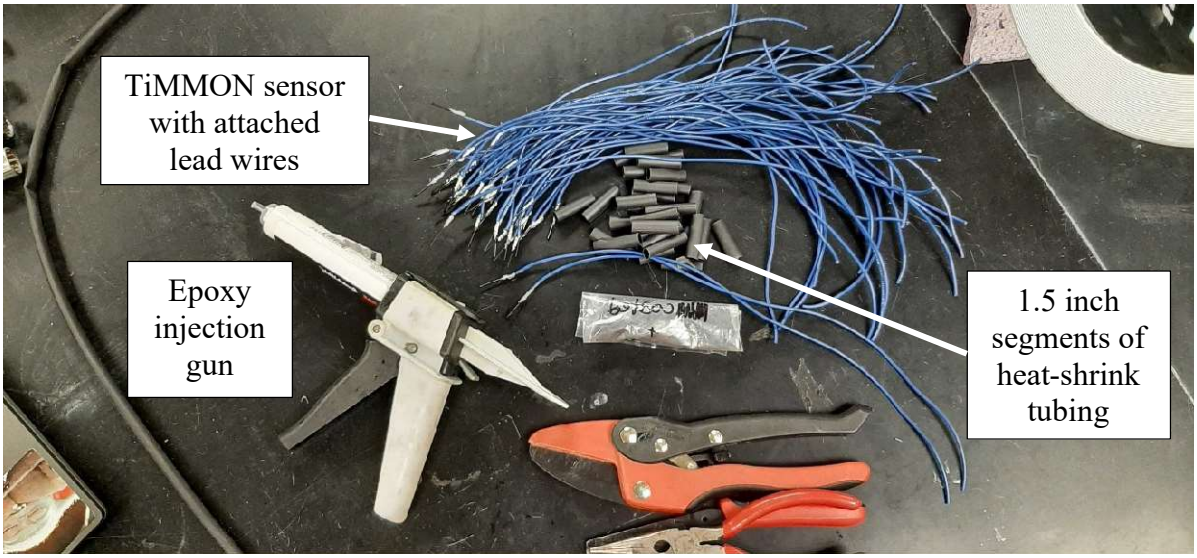

Figure 9. Sensors with electrical connections ready to be insulated and relevant tools.

The insulation of the electrical connection was formed from heat-shrink tubing filled with epoxy, as shown in Figure 10. Generic ¼-inch heat-shrink tubing was cut to 1.5 inch lengths and placed around the electrical connection such that the end of the tubing would extend past the Nafion™ coating and ensure coverage of all un-coated portions of TiMMO wire and the exposed copper wire. The heat-shrink tubing was placed surrounding the exposed conductors, and a syringe tip on an epoxy injection gun was inserted in the open end of the tubing with the tip of the syringe close to the center of the 1.5 inch tubing length. 3M Scotch-Weld Epoxy Potting Compound DP270, a non-conductive, inert, durable epoxy with at least 2,500 psi strength after curing, was used. This epoxy was injected into the space within the heat-shrink tubing to coat the entire electrical connection. After the tubing was filled with epoxy, a heat gun was used to tighten the heat-shrink tubing around the connection and ensure the epoxy was squeezed into all the spaces around the connection. Excess epoxy was wiped away and care was taken to ensure the Nafion™ coating was not covered with epoxy. After tightening the heat-shrink and wiping away excess epoxy, the epoxy was allowed to cure overnight, shown in Figure 10. Figure 11 shows the finished sensors after assembly and insulation as compared to the standard glass pH probe.

Figure 10. Epoxy curing overnight.

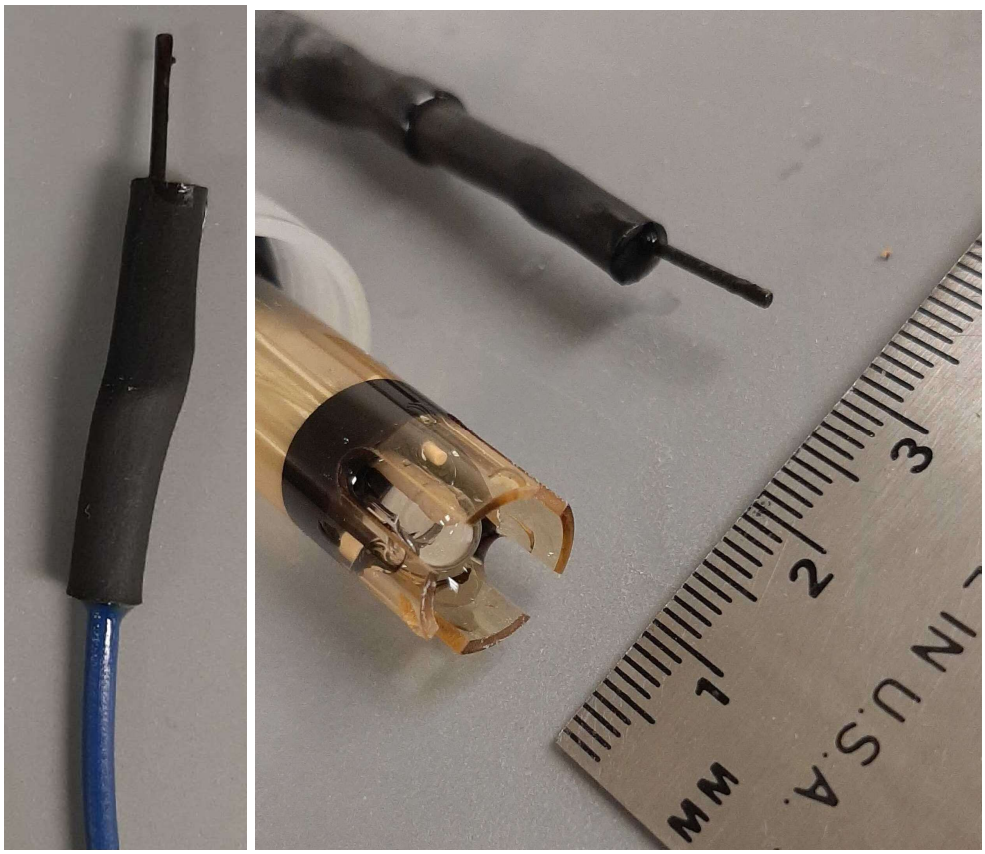

Figure 11. Left: Finished sensor after epoxy body cured; Right: Finished sensor compared to standard glass pH probe.

3.2 Post-Fabrication Sensor Treatment

3.2.1 Treatment Background

After fabrication, sensors must undergo a physicochemical treatment process to ensure an optimally homogeneous structure of the Nafion™ membrane for conducting protons. Kinlen et al. (1994) state "electrodes were boiled in distilled water for 30 min before testing," and that "thermally prepared electrodes exhibit an 'aging' effect, which is attributed to hydration of the oxide surface," but that "the aging process may be accelerated by heating in water at elevated temperature and pressure (160°C, 4000 psi), after which stable potentials are observed," (Kinlen et al. 1994). Preliminary testing indicated that the Nafion™ film required hydration and subsequent maintenance of hydration prior to use.

Grot (2011) states that Nafion™ appears hydrophobic when dry, but upon adsorption of water begins to exhibit hydrophilic properties. The ability to adsorb large amounts of water and polar organic solvents is a dominant property of fluorinated ionomers. "With increasing water or solvent content the dimensions, conductivity, and permeability of the ionomer increases, and the strength and the ability to reject anions decreases," (Grot 2011). The water content of the polymer is controlled by the surrounding water availability, polymer equivalent weight (EW), cations in solution, and pretreatment history. Grot (2011) notes a standard pretreatment for establishing reproducible samples is boiling in water for 30 minutes, but this pretreatment does not completely erase the history of excessive drying.

3.2.2 Sensor Treatment

To identify if an alternative treatment produced a reproducible sensor, fabricated sensors were first boiled or steamed for different durations and the sensor response was recorded. Tests conducted are summarized in Table 2. Two different approaches, steaming and soaking, were

also evaluated. Steaming the sensors for 20 minutes was chosen instead of the boiling described by Kinlen et al. (1994) based on the results presented in Chapter 6.

Table 2. Evaluated Post-Fabrication Treatment Methods

Treatment Method	Duration				
Room Temperature Soaking	3 months				
Boiling	5 minutes	10 minutes	15 minutes	20 minutes	25 minutes
Steaming	5 minutes	10 minutes	15 minutes	20 minutes	25 minutes

After steaming for 20 minutes, sensors were either placed in a test solution or placed in a beaker of room temperature tap water for storage until used for testing which helps to maintain hydration of the Nafion™ membrane.

3.3 Internet-of-Things Based Monitoring System

Another key focus of this research and preliminary design focus was an IoT-based monitoring system. Two versions (V1.0, V1.1) of the IoT based system were explored, consisting of the following components: EzSBC "ESP32 Feather Breakout" based on ESP32 microcontroller, DF Robot "DFR-0316 Fermion" based on MCP3424 analog-to-digital converter, Sparkfun "16-Channel Analog/Digital MUX Breakout" based on CD74HC4067 multiplexer, and the Texas Instruments LMP-7721 precision amplifier. Each hardware component is discussed below and represented in Table 3. More hardware details are attached in Appendix A. Supporting firmware was developed incrementally throughout the design process as described in Section 3.3.4.

Table 3. IoT-Based Monitoring System Hardware Components.

Picture	pH Meter Version(s)	*[Manufacturer]* Component	Purpose
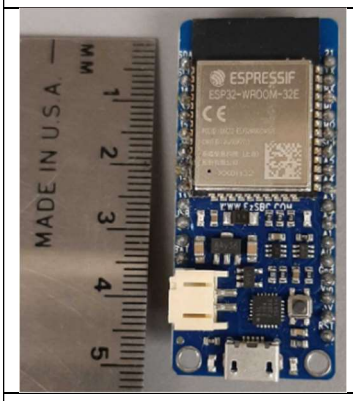	V1.1 and V1.2	[*EzSBC*] "ESP32-based Feather Breakout and Development Board" [*Espressif*] ESP32	Programmable microcontroller unit with built-in Wi-Fi and Bluetooth connectivity that controls and communicates with the other components and sends data to the cloud
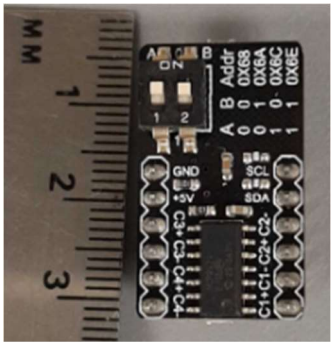	V1.1 and V1.2	[*DF Robot*] "DFR-0316 Fermion" [*Microchip Technology*] MCP3424 18-bit ADC, 4-channel with Programmable Gain Amplifier chip	Converts analog sensor signals to digital signals and sends them to the microcontroller
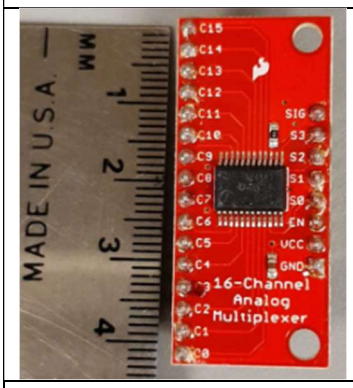	V1.1	[*Sparkfun*] "16 Channel Analog/Digital MUX Breakout" [*Texas Instruments*] CD74HC4067 16-channel multiplexer chip	Takes 16 sensor signal input channels and reduces them to 1 signal output channel
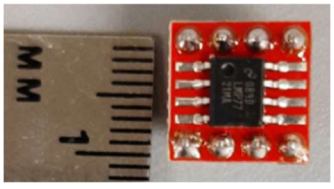	V1.2	[*Texas Instruments*] LMP7721 3-Femptoampere Input Bias Current Precision Amplifier	Operational amplifier that separates ultra-high impedance and low impedance circuit components and maintains a constant voltage

3.3.1 Hardware Components

3.3.1 (a) ESP32-based Feather Breakout and Development Board

The ESP32-based Feather board by EzSBC is the main component for the pH Meter IoT system. This board is a microcontroller using the Espressif ESP32 system-on-a-chip (SOC) and designed in the Adafruit 'Feather' form factor which is easily compatible with any other 'Feather' design. The ESP32 SOC gives the board advantages including built-in Wi-Fi and Bluetooth communications, eight available peripheral communications protocols, numerous analog and digital I/O pins, and low power usage. Though Adafruit makes a Feather board with ESP32, EzSBC made design modifications that reduce the power demand for the board, improve Wi-Fi connectivity, and add user friendly LEDs to indicate status, at a lower price.

3.3.1 (b) DFR-0316 Fermion (ADC)

The DF Robot DFR-0316 Fermion breakout board is a development-friendly board based on the Microchip Technology MCP3424, a delta-sigma analog/digital signal converter with up to 18 bits of resolution (1.56×10^{-5} V), four differential channels, a programmable gain amplifier (PGA) up to x8 gain, and the I^2C communication protocol with four selectable addresses using two switches on the board. This chip has precision and speed much higher than the requirements of this application.

3.3.1 (c) 16 Channel Analog/Digital MUX Breakout

The Sparkfun 16-Channel Analog/Digital MUX Breakout board is a development-friendly multiplexer based on the Texas Instruments CD74HC4067 that allows 16 signal channels to be converted into one signal channel. This can be advantageous in microcontroller circuits because the microcontroller often has a smaller number of sufficient I/O pins than the application requires. The multiplexer can reduce the number of pins required on the

microcontroller board by making the connections on the multiplexer instead. In our application, this allowed up to 16 sensors to connect to the board, allowing for large sample sizes in experiments without a large increase in cost. However, this component did not have sufficient impedance for sensors to be directly connected, causing voltages to drop on the sensors. Inter-channel leakage limited accurate sensor readings. Because of these drawbacks, the MUX was removed from pH Meter V1.1 (described in Sections 3.3.2 and 3.3.3). This reduced the quantity of sensors available to connect from 16 to 4, but largely improved the meter's behavior.

3.3.1 (d) LMP7721 3-Femptoampere Input Bias Current Precision Amplifier (Op-Amp)

The Texas Instruments LMP7721 is a super low input bias current precision amplifier in a small-outline-integrated-circuit (SOIC) package designed for amplifying signals from high impedance (low current) sensing applications. Because pH sensors have very high impedance and are incapable of producing sufficient currents for many analog to digital converters, an amplifier is required to maintain the sensor voltage for measurement. In my application, the LMP7721 is configured as a "buffer" where the amplifier is not intended to increase or invert the voltage on the output, but simply maintain the same voltage on both sides of the amplifier.

3.3.2 pH Meter V1.0

Version 1.0 of the pH Meter Design was developed with the core focus of converting analog voltages produced by the sensor to a digital signal and sending the voltage data to the cloud in a low-cost and user-friendly system. The pH Meter V1.0 was inspired by the previously developed ORP measurement boards by Ham and Ferrie (2019). The main components listed in Table 3 (identified with V1.0) were combined on an Adafruit "Perma-Proto" board to create a prototype which could connect 16 of our solid-state pH sensors and one reference electrode (Borin Manufacturing Stelth 1 HCP Reference Electrode), convert their analog voltages to digital

signals, and then send the signals via Wi-Fi to an internet database and dashboard platform, Ubidots. The main application of this system is in the laboratory with Wi-Fi connectivity to measure the solid-state pH sensors during experiments. Seven of these boards were made, and the board is shown in Figure 12. Appendix A contains details regarding configuration of the design.

These boards successfully measured voltages between each of the 16 sensors and the reference electrode in the ADC. Whenever a sampling interval was completed, the ADC would complete five consecutive conversions for each of the 16 MUX channels and take the median of the middle three conversions to reduce noise. This converted signal, in the digital form, was sent via I^2C communications to the ESP32 where the data was stored momentarily for all 16 channels before being sent via MQTT protocol over Wi-Fi to an internet database and dashboard platform called Ubidots, discussed in Section 3.3.5

Though the voltage was measured and reported without issue, the MUX appears to have interfered with measured sensor voltages, causing them to drop. This effect was identified after consistently seeing voltage drops in measurements, correlation between MUX channels, and studying the ‘impedance’ of the circuit and the sensors, which were incompatible together without design modifications. Because of this, the pH Meter V1.1 was developed.

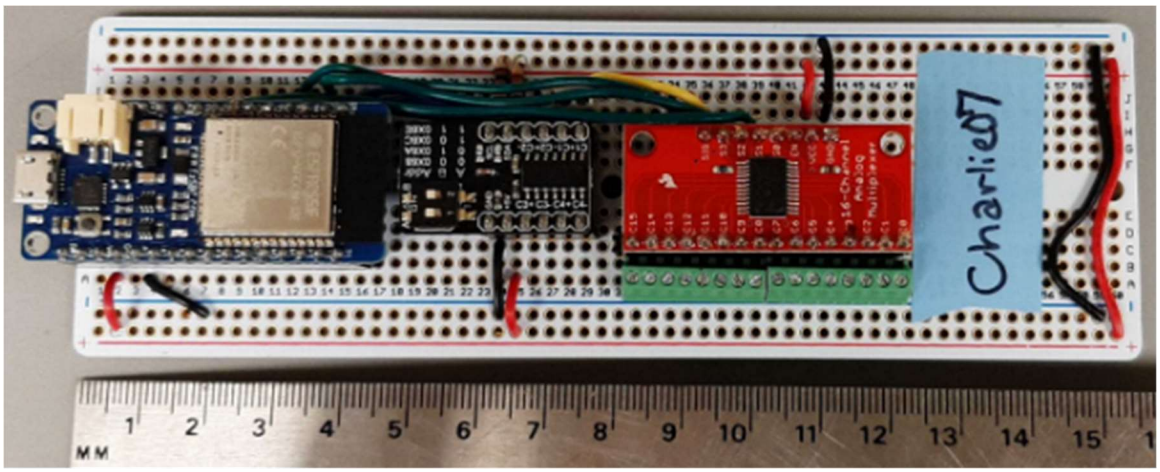

Figure 12. Closeup photograph of pH Meter V1.0.

3.3.3 pH Meter V1.1

pH meter V1.1, shown in Figure 13, was developed to solve some of the apparent issues with V1.0 by improving the compatibility and quality of components but maintaining the same core focus of converting analog voltages produced by the sensor to a digital signal and sending data to the cloud in a low-cost and user-friendly system. Because the 16-channel multiplexer is designed for higher currents (lower impedance) than the pH sensors can supply (high impedance), the multiplexer will drain the voltage on the sensors. This interferes with the sensors' ability to maintain a charge, so the multiplexer was replaced with five LMP7721 precision operational amplifiers (op-amps). These op-amps take a very low input bias current (which the sensors can convey) and input voltage from a sensor or reference electrode and use an outside current source (the circuit power source) to increase amperage on the output line while maintaining the same voltage. This allows low-impedance circuit components the ability to read the voltage without causing a voltage drop on the high impedance components during

measurements. This design showed superior performance over V1.0 with voltages on the sensors stabilizing over time.

The pH Meters were designed and tested on Perma-Proto boards with through-hole mounting, so the LMP7721s (Small Outline Integrated Circuit surface-mount components) were mounted on SOIC-to-DIP (Dual-Inline-Package through-hole components) adaptors. Given this design, guarding of the input lines was not possible and would only be available with a printed circuit board. This would aid in the preservation of the high-impedance input voltage signal from the pH sensors.

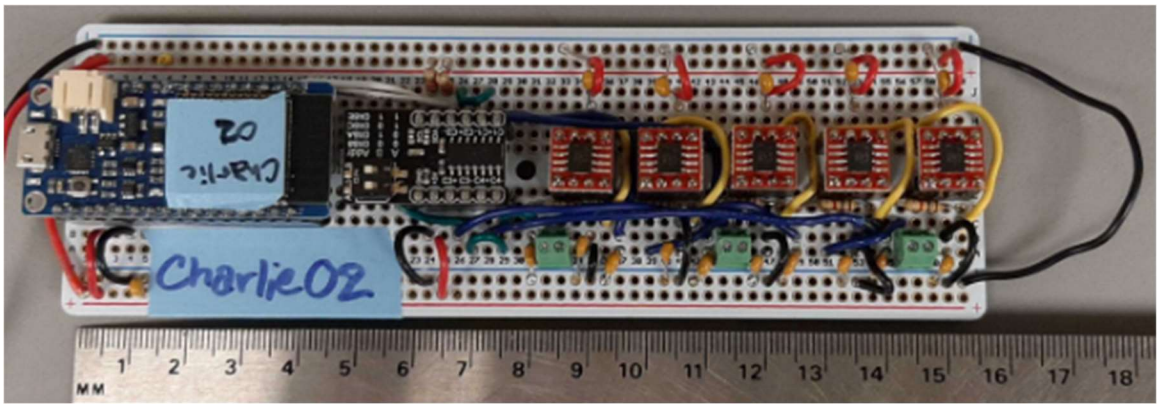

Figure 13. Closeup photograph of the pH Meter V1.1

3.3.4 Firmware

Firmware was another critical piece of the design and was developed incrementally throughout the design process. IoT-based microcontroller systems are versatile and customizable systems with a limited number of designed functions. Even though they are versatile, these systems are computerized hardware devices, not general-purpose computers. They are generally smaller components for input or output in larger general-purpose systems. Because the system is

designed for a specific set of functions, the firmware written is generally written and uploaded via a computer and left to operate the hardware without a significant user interface.

Firmware written for the two pH meter designs was used to:

- Establish interfaces with peripheral devices via USB and Wi-Fi;
- Establish control and communication protocol between primary/secondary (traditionally master/slave) devices;
- Establish memory architecture for data;
- Authenticate the device in secure communications;
- Configure hardware connections and signals;
- Establish timing and settings for functions.

The source code, in plain text, is displayed in Appendix A. Main sections of the code are:

- Introduction;
- Library inclusion;
- Variable definition;
- Instantiation of hardware;
- Auxiliary function definitions for:
    - Connecting to Wi-Fi;
    - Establishing an IP address;
    - Reconnection after loss of connection;
    - Message Queuing Telemetry Transport (MQTT) protocol;
    - Collecting voltage data;
    - Sending data to Ubidots database and dashboard platform;

    - Printing data to USB communication;
- Setup instructions;
- Loop instructions.

Throughout the design and experiment process of this work, firmware was continuously updated to improve device functionality. For example, initial firmware versions did not have the ability to reconnect the device to Wi-Fi upon loss of connection. By the time the experiments using the pH Meter V1.0 were performed, no more changes were made to the firmware. Even after the update to pH Meter V1.1, firmware did not require significant updates, as the functionality of the device remained generally the same and the components of the new design (LMP7721s) did not require firmware.

3.3.5 Ubidots IoT Platform

After the microcontroller system collected the voltage data and stored in internal memory, the data was sent via Wi-Fi internet connection to an online platform, Ubidots. The Center for Contaminant Hydrology maintains an industrial Ubidots account, allowing authenticated IoT devices to send data to the account's database. Ubidots' dashboard service enables users to easily view data from the database in a customizable user interface on any internet-connected PC or mobile device. Ubidots can also send signals to other IoT devices or services, expanding the information and action network. For example, a pH reading could be sent to Ubidots, triggering a pump to turn on and decrease pH by adding acid to the system. The pH sensor then reports to Ubidots again, triggering the pump to turn off when a threshold is met.

4. EXPERIMENT MATERIALS

For the experiments performed as part of this work, multiple chemical solutions, experimental apparatuses, and measuring equipment were used to test the solid-state pH sensor and the IoT-based pH meter. The experimental methods are described in Chapter 5, and the used materials are described herein. Chemical mixtures are calculated in Appendix B.

4.1 Chemicals

The chemicals listed in Table 4 were used for creating stable pH buffer solutions to test the solid-state pH sensor design. Standard buffer solutions were also purchased and are listed in Table 5.

Table 4. House-Made pH Buffer Solution Ingredient List.

Chemical Name	Form	CAS #	% by Mass	Source
Hydrochloric acid	Aqueous	7647-01-0	36.5 - 38.0	EMD Chemicals
Sodium hydroxide	Solid pellet	1310-73-2	>97	Fisher Chemical
Potassium chloride	Solid powder	7447-40-7	99.6	Fisher Chemical
Potassium phosphate monobasic	Solid powder	7778-77-0	>99	Acros Organics
Potassium hydrogen phthalate	Solid powder	877-24-7	99.98	Fisher Chemical
Sodium bicarbonate	Solid powder	144-55-8	>99.7	EMD Chemicals
Borax	Solid powder	1303-96-4	-	20 Mule Team (Home Depot)

Table 5. Purchased Standard pH Buffer Solutions Used in this Study.

Product Name	Form	Catalog #	Source
Buffer Solution pH 4.0	Aqueous	LC122705	LabChem
Buffer Solution pH 7.0	Aqueous	LC123705	LabChem
Buffer Solution pH 10.0	Aqueous	LC125006	LabChem

4.2 Apparatuses

The components listed in Table 6 were used for building the experimental apparatuses used to test the solid-state pH sensors and IoT-based pH meter. Apparatus construction and configuration is detailed in Chapter 5.

Table 6. Apparatus Component List

Apparatus	Component	Manufacturer
Jar with Ports	500 mL glass/plastic jar	Generic
	Plastic lid	Generic
	Teflon tape	Generic
	Electrical tape	Generic
	Rubber stopper	Generic
	Waterproof silicone caulk	GE
	¼" Plastic submersible cord grip (through-hole)	McMaster-Carr
Sensor Bundle	¼" Heat-shrink tubing	Generic
	Waterproof silicone caulk	GE
Reference Electrode	Stelth 1 HCP reference electrode	Borin Manufacturing
	Electrical tape	Generic
Consolidation Oedometer	Consolidation Frame: One-Dimensional Consolidation Incremental Loading Device	ELE International
	Consolidation cell (X mm diameter)	ELE International
	Weights	ELE International

4.3 Measuring Devices

Items listed in Table 7 were used for taking measurements during experiments

Table 7. Measuring Devices List

Device	Attachment	Measurement	Source
Oakton pH 150 Meter	WD-35808-71 All-In-One pH/Temperature Probe, Single Junction, Epoxy Body	pH	Oakton
	WD-59001-75 ORP Electrode	ORP	Oakton
Fluke 189 True RMS Multimeter	Alligator clips	Voltage, resistance, continuity, and capacitance	Fluke
HP 34401A Multimeter	Alligator clips	High impedance voltage	Hewlett & Packard

5. EXPERIMENTAL METHODS

A prototype of the Kinlen et al. (1994) design was made and tested in a pilot experiment, discussed in Section 5.1. This test found the design to be possibly viable, and experiments were designed and completed to evaluate the validity of the solid-state pH sensor for geoenvironmental monitoring.

Experiments were devised to record the response of the sensors to post-fabrication sensor treatments, pH changes, and simulated environmental stresses in the field. Initial experiments were focused on establishing a satisfactory post-fabrication sensor treatment which would be used in all further experiments, discussed in Section 5.2. Next, sensor responses to pH were examined. Sensor response to static pH was recorded using the pH Meter V1.0, discussed in Section 5.3. Simultaneously, the IoT-based monitoring system was being examined for the ability to measure the sensor behavior in this experiment. Additional experiments were also used to test the IoT monitoring system independently as described in Section 5.4. The new V1.1 meter was then used to test sensor behavior in a stepwise pH system, described in Section 5.5. Durability under simulated environmental stresses was tested by applying normal stress to the sensor in a coarse sand material (abrasive) to simulate deep subsurface deployments, as described in Section 5.6.

5.1 Pilot Test

5.1.1 Experimental Design

One TiMMON wire electrode and one non-coated TiMMO wire electrode were placed in solution with voltages compared to an Ag/AgCl reference electrode. Acetic acid was added dropwise to tap water, decreasing the pH over time. Measurements of voltage on the TiMMON

electrode and TiMMO electrode were recorded with time. A standard glass pH probe was used to measure the pH at the same time as the TiMMO and TiMMON voltage measurements. Results are discussed in Section 6.1.

5.1.2 Apparatus Configuration

The pilot test was conducted in an open 500-mL glass beaker containing test solution, shown in Figure 14. A glass burette was held above the beaker with clamps attached to a steel rod lab stand. The beaker was placed atop an electric stirring plate with a stir bar in the solution on a medium setting. Tap water was added to the beaker, filling the beaker halfway. Acetic acid was placed in the burette above the beaker. An Ag/AgCl reference electrode was placed into the solution. TiMMO and TiMMON wire electrodes were taped to the inside of the beaker halfway submerged in the water. The negative lead of a Fluke 189 multimeter was connected to the reference electrode lead with an alligator clip, while the positive lead of the multimeter was connected to the TiMMO or TiMMON electrode when measurements were made.

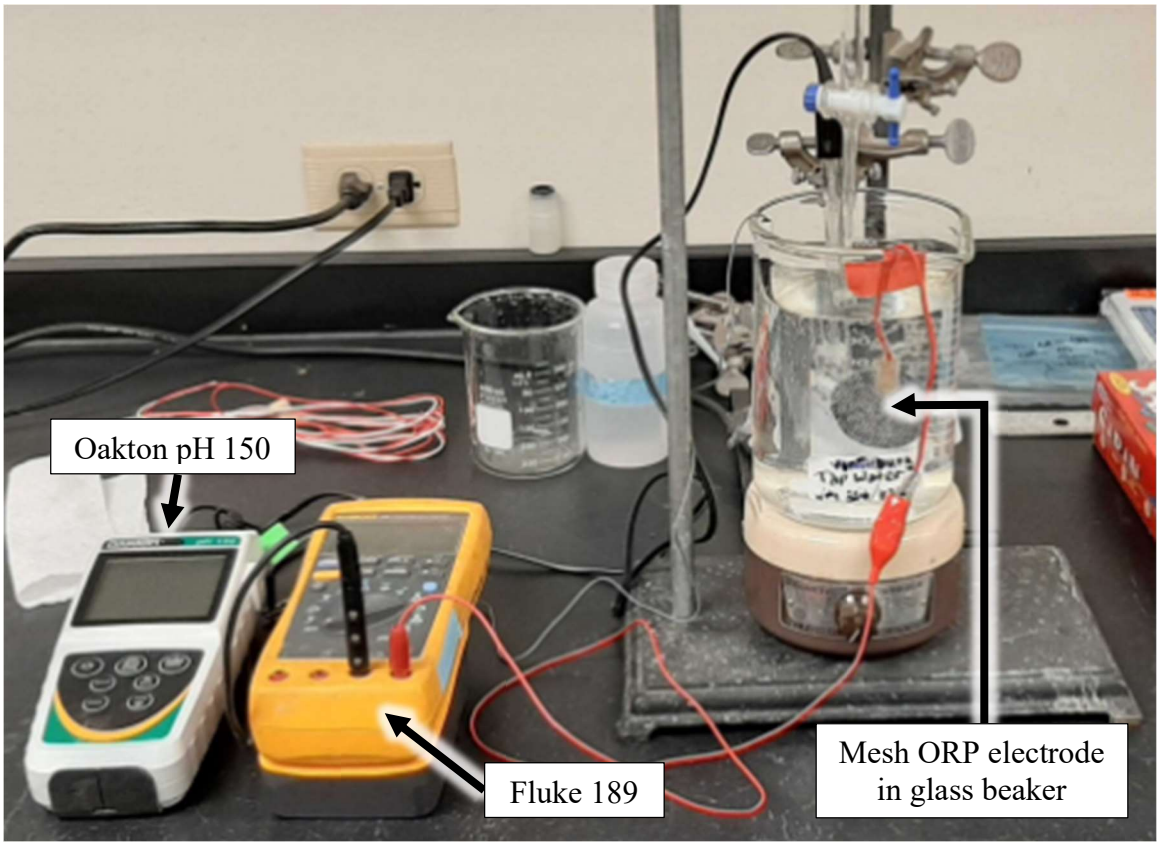

Figure 14. Pilot test setup with mesh ORP electrode (no TiMMON pH electrode shown).

5.1.3 Procedure

1. Initial measurements of pH using the standard glass probe and voltage on the TiMMON electrode were recorded with the time.
2. Acetic acid drops were added to the solution until small (0.05 pH) changes in pH were measured.
3. After five minutes, pH and electrode voltage were recorded again.

These steps were repeated for 35 minutes with samples approximately every 5 minutes. Due to concern about response time in the TiMMON electrodes, the solution was then allowed to

sit for 36 hours. The procedure was then repeated, but with hours between samples instead of minutes. The experiment continued for seven days.

5.2 Evaluation of Post-Fabrication Sensor Treatments

The initial pilot test results showed sensor viability. Thereafter an experiment was setup to study the treatment of the sensors after fabrication which included boiling, steaming, and soaking.

5.2.1 Experimental Design

Sensor voltage responses under three pH conditions (pH 4, 7, and 10) were recorded after a post-fabrication treatment was applied. Eleven groups of five sensors were treated differently prior to testing: one group was soaked in tap water for three months, five groups were boiled to different lengths of time (5, 10, 15, 20, and 25 mins), and five groups were steamed to different lengths of time (5, 10, 15, 20, and 25 mins). Immediately after treatment, the sensors were placed in a plastic baggie until the experiment started the following day. The IoT monitoring system was not yet available when this experiment was performed, so all data was collected manually with a Fluke 189 multimeter. Results are shown and discussed in Chapter 6. A satisfactory treatment should yield sensor groups with low variance and quick convergence to a steady state value.

5.2.2 Apparatus Configuration

5.2.2 (a) Boiling

Boiling of the sensors was performed in an open-top 1 L glass beaker filled approximately two thirds with tap water. The sensors were placed into the beaker such that the TiMMON electrode, epoxy and heatshrink body, and the lower portion of the insulated copper wire were submerged. The beaker was placed atop a hot plate and heated on high throughout the boiling period until the last group of sensors was finished boiling (after 25 minutes).

5.2.2 (b) Steaming

Steaming of the sensors was performed in an open-top, cubic, steel mesh basket that was sealed in plastic wrap, shown in Figure 15. With the "top" noted as the open side of the cubic basket, the sides and top were wrapped with plastic, but the bottom steel mesh surface was left unwrapped such that the basket could be placed atop a boiling beaker and fill with steam. One edge between the top and side of the cube was left unsealed such that the sensors could be placed inside the steam-filled basket.

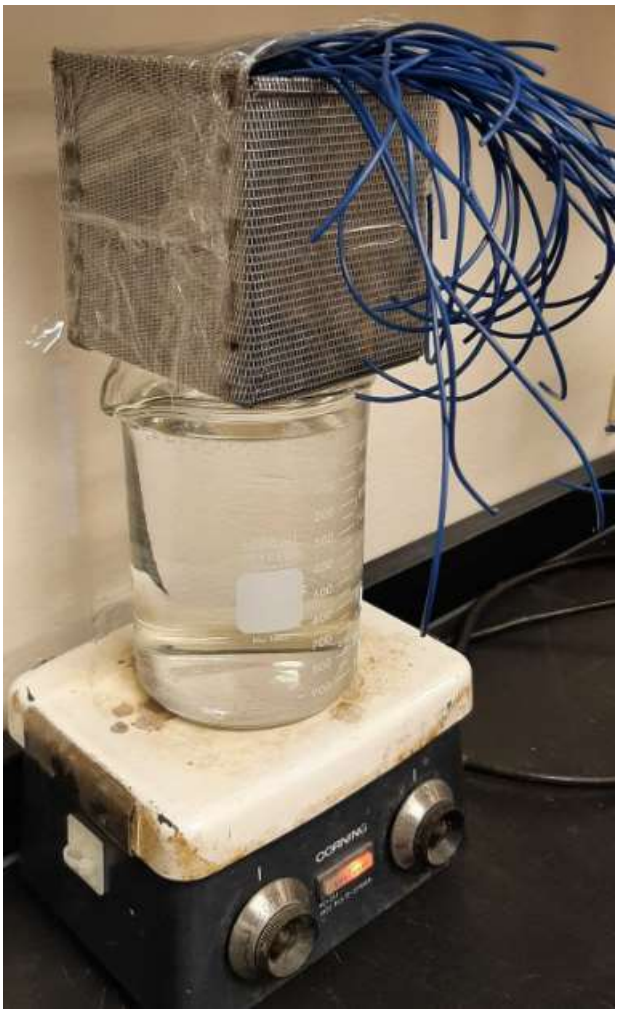

Figure 15. Sensors steaming in a plastic-sealed, steel mesh basket above a beaker of boiling water.

5.2.2 (c) Treatment Evaluation Apparatuses

To evaluate sensor treatments, sensor groups were placed in pH buffer solutions. Groups of sensors were consolidated into bundles of five, shown in Figure 16, using a ¼-inch diameter heat-shrink tube with all five sensor wires pulled through the heat-shrink tube, and the space between wires in the tube was filled with silicone caulk to prevent air flow through the tubing

when sealed into the apparatus test jar. The heat-shrink was then tightened using a heat gun, squeezing the silicone between all the wires.

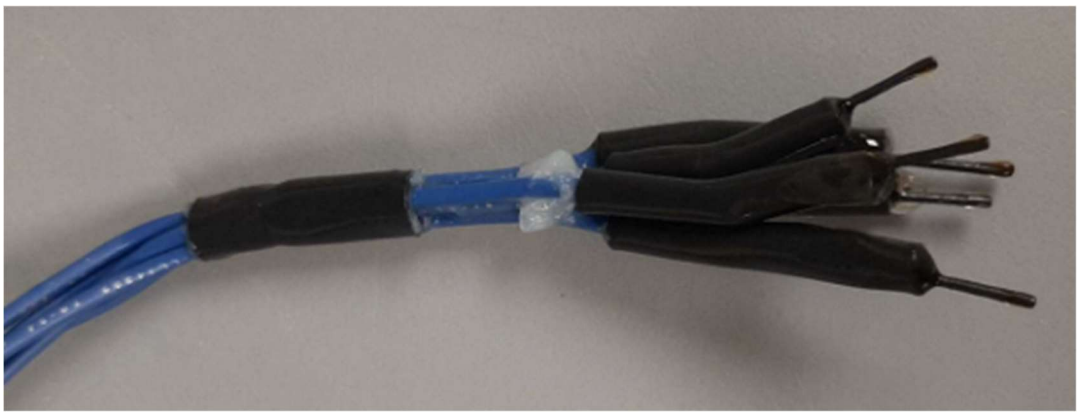

Figure 16. Bundle of five sensors.

Sealed 500-mL glass jars with plastic lids were used for pH testing (Figure 17). Four ¼-inch diameter holes were drilled into the plastic lids to insert three ¼-inch through-hole cord grips and one rubber stopper with the adjustable cord grip tightening seal on the outside of the plastic top. Three sensor bundles were placed through the three cord grips such that the heat shrink placed around the five-sensor bundle was within the cord grip seal. The cord grip was then tightened around the silicone-filled heat shrink bundle such that air could not flow into the jar. The fourth hole in the plastic top was plugged with a rubber stopper, sealing the jar.

A fifth 1.25-inch diameter hole was drilled into the plastic top to insert the Borin Stelth 1 reference electrode (Figure 18). The reference electrode was wrapped with electrical tape to increase girth to snuggly seal into the drilled hole. As the electrical tape is soft and malleable, the tape forms a seal with the plastic hole. Then, a smoothed bead of silicone was placed around the electrical tape and hole to make the penetration airtight. The threads of the jar were sealed with

Teflon tape to improve the cap seal. These seals aid in preventing the exchange of atmospheric air which can change the pH of the test solution over time.

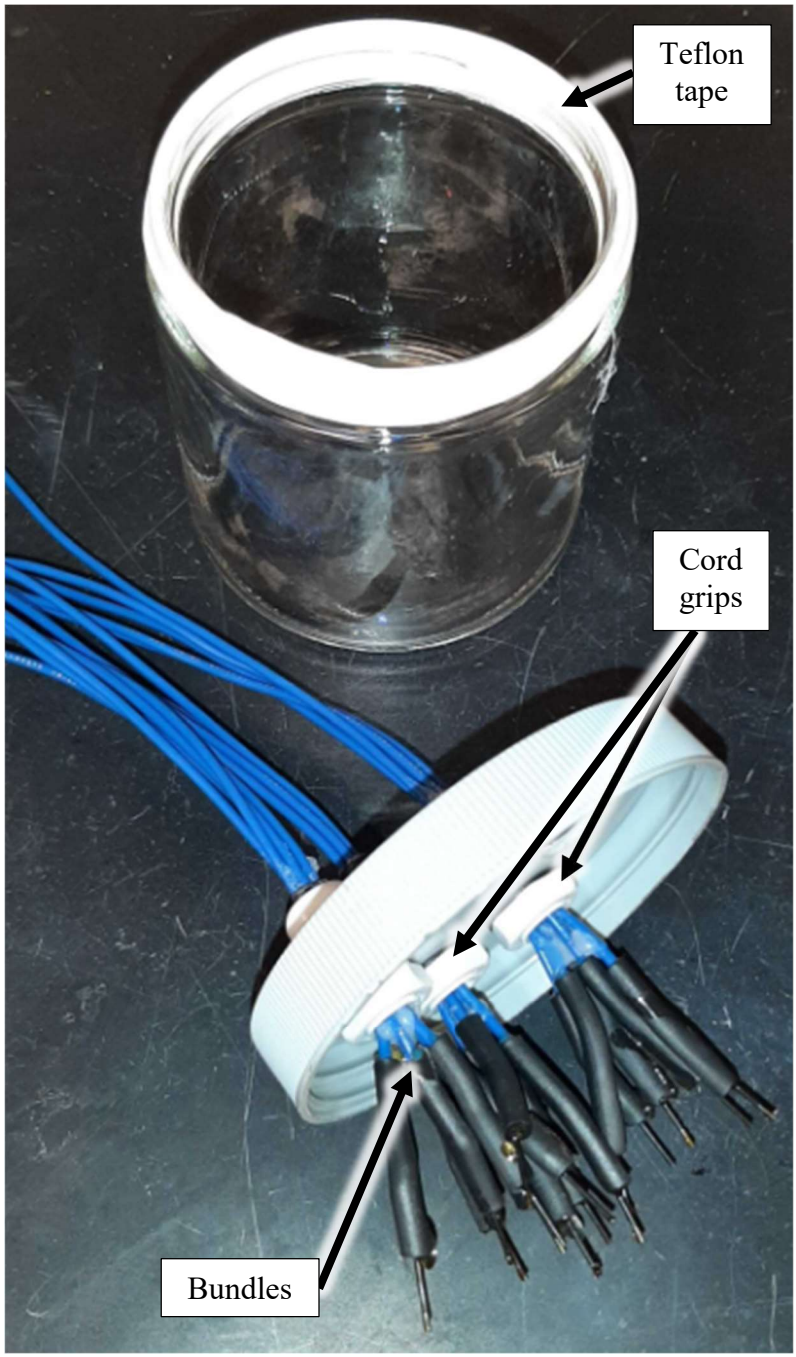

Figure 17. Glass jar apparatus with Teflon tape on threads; plastic lid with three sensor bundles inserted into three cord grips.

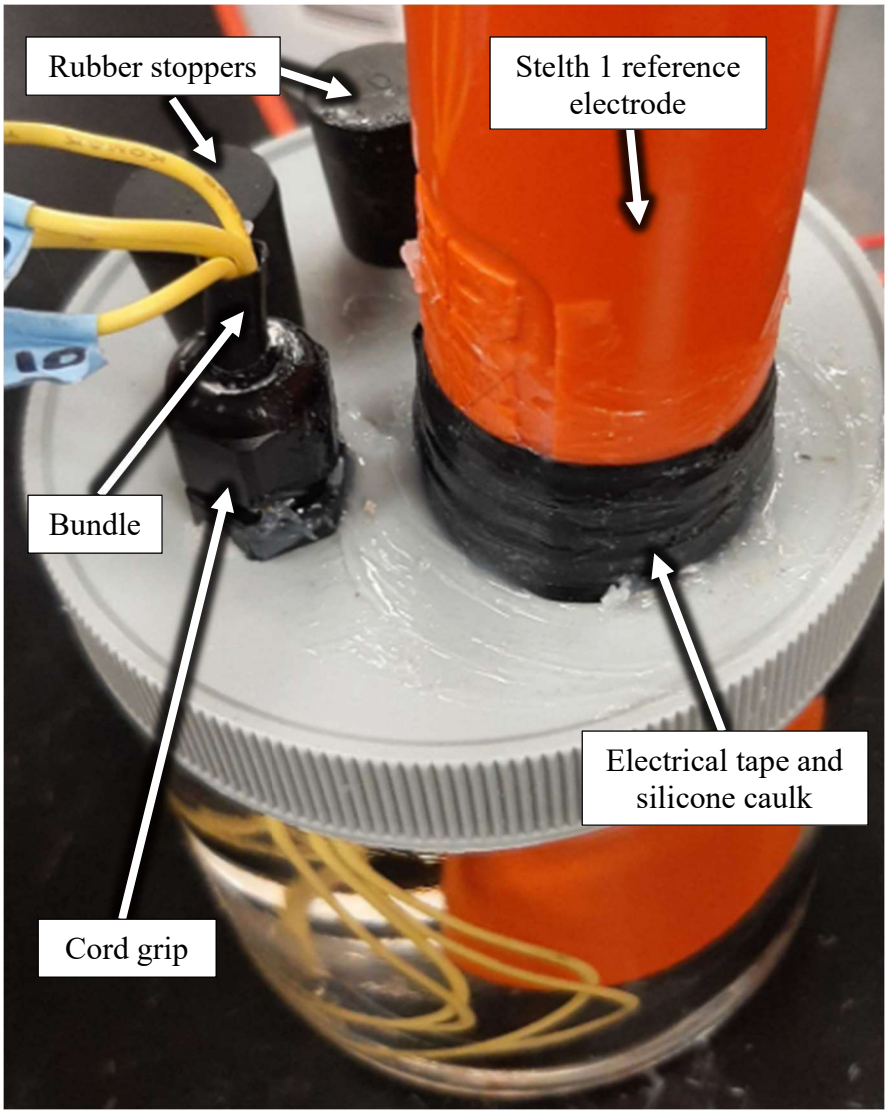

Figure 18. Top view of sensor bundle in cord grip and reference electrode sealed into the lid.

Figure 19 shows the jar apparatuses with sensors during the experiment. After three sensor bundles were placed into the three cord grips, the Stelth 1 reference electrode was inserted into the top, all holes were sealed, the glass jar was filled with a pH buffer solution, and the top cap with the attached electrodes was screwed into place, sealing the jar with the electrodes inside, fully immersed in solution. The lead wires for each electrode were exposed outside of the jar and were connected to the leads of the multimeter where the reference electrode was

connected to the negative multimeter lead and the positive lead connects to the TiMMON sensor leads. Leads were disconnected when not being measured.

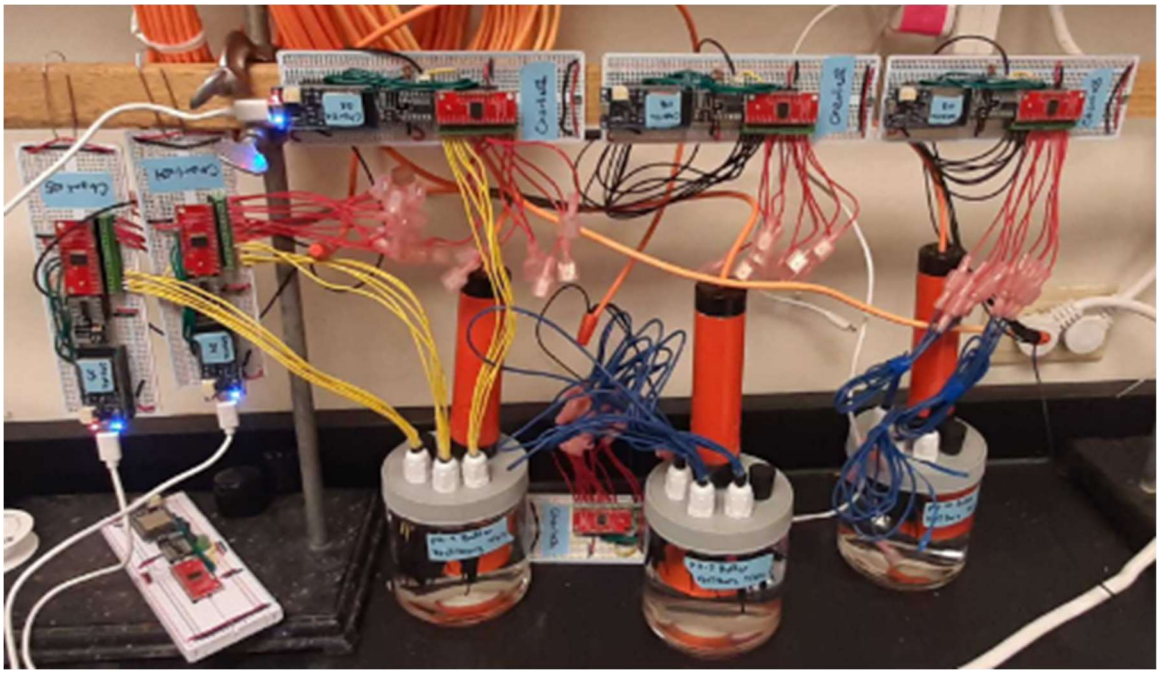

Figure 19. Three jar apparatuses with sensors seen attached to the pH Meter V1.0s.

5.2.3 Procedure

The following procedure was used for testing.

1. After jar assembly, sensors were manually sampled for voltages using the Fluke 189 multimeter. The pH was also measured by removing the rubber stopper from the top and inserting the standard glass pH probe twice weekly.
2. Sensors were then sampled every 15 minutes.
3. After approximately one hour, as the rate of change in readings decreased, sampling was slowed to hourly, and then less frequently given minimal changes in measured voltage. After the second day, readings were taken daily.

4. After 11 days, the sensors were switched from a pH 4 buffer solution to a pH 7 buffer solution. The jars were drained, rinsed, and then refilled with the new solution. Sensors were returned to the jar and immersed, sealing the jar with the top. Sampling steps 1-3 were repeated.
5. After three weeks, the jar was drained, rinsed, and filled with pH 10 solution. Sensors were returned to the jar and immersed, sealing the jar with the top. Sampling steps 1-3 were repeated.
6. After approximately one month, experiments were disassembled.

Timing of samples and switching solutions was in response to observed voltage changes during the experiment. Voltages took longer to approach a steady state in higher pH solutions, hence why the sensors remained in pH 4 for 11 days and in pH 7 for three weeks.

5.3 Sensing in a Static pH System

Similar to the Pilot Tests (Section 5.1), static sensing experiments aimed to characterize the voltage responses of the sensors to varying pH, however, in this experiment the sensors were placed in jars of static pH buffers such that the sensors could equilibrate and show a stable voltage. Buffers of pH 4, 7, and 10 were used, and sensors were measured with the IoT-based pH Meter V1.0 over a period of 26 days.

5.3.1 Experimental Design

Forty-five TiMMON sensors were bundled into nine groups of five. Three groups were placed into three jars and attached to six IoT-based pH Meter V1.0s via the screw terminals on the meter along with the associated Stelth 1 reference electrode. Each jar had 15 sensors attached

to two separate pH meters where one meter was set to a 15-minute reporting interval with ten sensors, and the other meter was set to a 60-minute reporting interval with five sensors.

Fifteen sensors were immersed in a pH 4 solution, 15 sensors were immersed in a pH 7 solution, and 15 sensors were immersed in a pH 10 solution. All jars were left to equilibrate for 26 days. Prior to experiments, sensors were in the same tap water as the initial condition. Results are shown and discussed in Chapter 6. Sensors in a static pH system should approach a steady-state voltage that represents the voltage corresponding to that pH.

5.3.2 Apparatus Configuration

The same apparatus setup from the Evaluation of Post-Fabrication Sensor Treatments (Section 5.2) was used. The apparatus is explained in 5.2.2 (c).

5.3.3 Procedure

1. Sensor bundles of five were passed through cord grips and connected to the plastic jar lid by tightening the cord grips. Reference electrodes were installed
2. The jar was filled with the desired solution.
3. The sensors and reference electrodes were connected to the pH Meter V1.0 via the screw terminals on the IoT meter.
4. The IoT meter was turned on (the IoT meter was programed to send voltage measurements to Ubidots).
5. The sensors were immersed in the solution and the jar lid was sealed.
6. Sensors sat in the sealed jar for 26 days and the IoT meter sampled data for that entire period. Three of the meters took measurements every 15 minutes, and three of the meters took measurements every hour.

5.4 IoT Monitoring System Evaluations

After early data suggested that the IoT-based pH Meter V1.0 was impacting the data and influencing sensor voltages, experiments were performed to determine the extent of effects, if any. The first test was to determine if the time interval between measurements had effects, and the second was to determine if connecting the sensors to the multiplexer yielded different results than connecting directly to the ADC. After these tests showed evidence to redesign the meter, a pilot test of the new pH Meter V1.1 was also performed. Results are shown and discussed in Chapter 6.

5.4.1 Experimental Design

5.4.1 (a) Measurement Time Interval Test

Six sensors were placed in a jar in three groups of two with each group connected to a different pH Meter V1.0 multiplexer via the screw terminals. The first meter was set to a measurement interval of 30 seconds, the second to five minutes, and the third to two hours. The sensors were then cycled between pH 4 and 7 solutions over three months. If the measurement interval has no effect, all sensor groups will respond the same and show parallel trends.

5.4.1 (b) Multiplexer Effects Test

Fifteen sensors were placed into a jar and connected to the same pH Meter V1.0, but only twelve were connected via the screw terminals into the multiplexer. The other three were connected directly to the ADC, bypassing the multiplexer in the circuit. Voltages were measured every two minutes. The sensors were cycled between pH 4, 7, and 10 solutions over 3 months. If the multiplexer has no effect, the sensor groups will respond the same when connected to the multiplexer as when connected to the analog-to-digital converter.

5.4.1 (c) pH Meter V1.1 Pilot Test

A breadboard circuit was setup with the new components, the LMP7721 op-amps, to determine the effect of using the op-amp. Two sensors were hooked directly to the DFR-0316 ADC, bypassing the op-amps, while two other sensors were hooked into the op-amps which feed into the ADC. The data from all four sensors was compared during multiple pH changes from pH 10 to pH 1 with steps of approximately 1 pH unit. The test was performed over approximately one month with pH changes approximately every three days. Voltage measurements were made every five minutes. If the LMP7721 works well, the meter will maintain sensor voltages at their steady-state value.

5.4.2 Apparatus Configuration

The same jar apparatus used in the Static pH testing experiments was used in all IoT monitoring system evaluation experiments. The pilot test of the pH Meter V1.1 was measured with the breadboard circuit shown in Figure 20, although two sensor leads were plugged directly into the ADC as described in the preceding section.

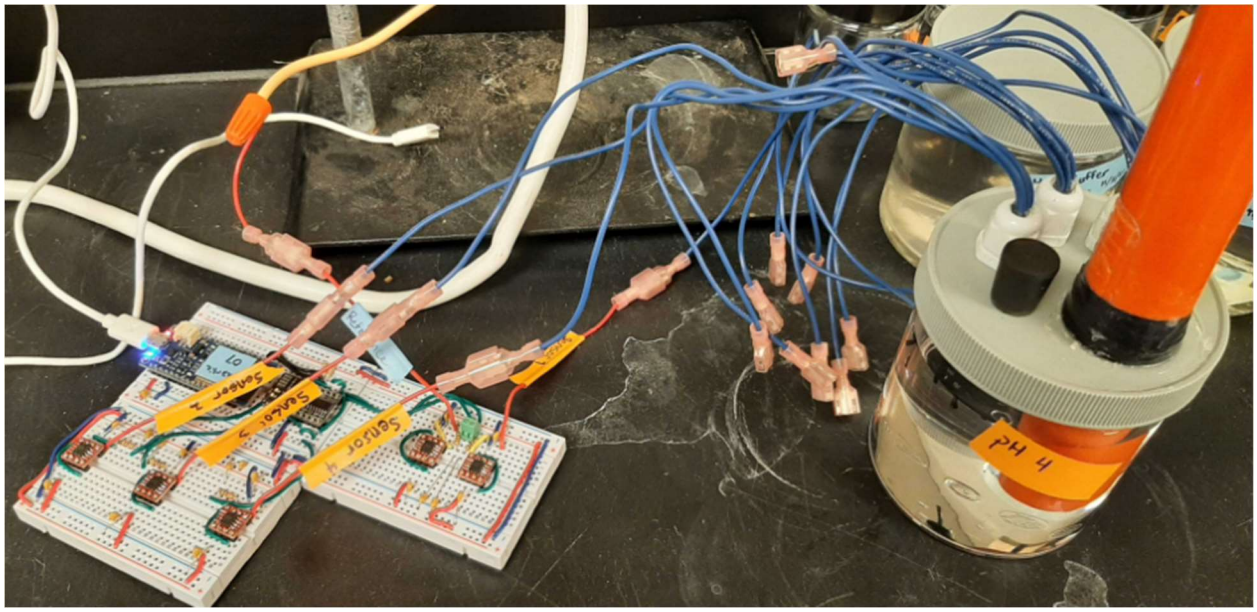

Figure 20. Breadboard circuit design for pilot testing the pH Meter V1.1. The picture here shows all four sensors plugged into the inputs of the LMP7721s.

5.4.3 Procedure

5.4.3 (a) Measurement Time Interval Test

1. Sensor bundles were inserted and sealed into the apparatus cap.
2. Sensors were connected to the three pH Meter V1.0s via screw terminals into the multiplexer.
3. The board was turned on, starting measurements.
4. The sensors were placed into the jar, and the jar was filled with pH 4 solution. Sensors were then sealed in the jar.
5. Changes of the jar solution were performed three time over the first six days, and then the sensors were allowed to remain in the same solution for the remainder of the experiment.

5.4.3 (b) Multiplexer Effects Test

1. Sensor bundles were inserted and sealed into the jar cap.
2. Thirteen sensors were connected to the pH Meter V1.0 via their screw terminals into the multiplexer, and 3 sensors were connected directly to the ADC via other screw terminals on the board.
3. The board was turned on, starting measurements.
4. The sensors were placed into the jar, and the jar was filled with pH 7 solution. Sensors were then sealed in the jar.
5. The jar solution was changed at four points throughout the three-month experiment. Changes were performed approximately every 3 days for the first 12 days, and then the sensors were allowed to remain in the same solution for the remainder of the experiment.

5.4.3 (c) pH Meter V1.1 Pilot Test

1. Sensor bundles were inserted and sealed into the apparatus lid.
2. Four sensors were connected to the pH Meter V1.1 breadboard prototype. Two sensor leads were plugged into the LMP7721 input lines, and 2 sensors were connected directly to the ADC input lines.
3. The board was turned on, starting measurements.
4. The sensors were placed into the jar, and the jar was filled with pH 4 solution. Sensors were then sealed in the jar.
5. The jar solution was changed approximately every three days throughout the month-long experiment.

5.5 Sensing in a Stepwise pH System

Similar to the static buffer test, this set of experiments aimed to characterize sensors responses to pH. However, unlike the static test, these experiments had stepwise changes in pH with abrupt increases or decreases between stable pH phases. Three variants of this experiment were performed with slight changes in the experimental setup and measuring equipment, discussed in Section 5.3.1. The experimental variants one and two were completed using the pH Meter V1.1 due to results from the IoT Monitoring System experiments and observations. However, the third variant used the HP34401A multimeter to measure the sensor voltages. Results from all variants are shown and discussed in Chapter 6.

5.5.1 Experimental Design

5.5.1 (a) First Variant (pH Meter V1.1 Three-Point Calibration)

Twenty sensors were started in pH 7 and repeatedly moved stepwise through pH 4, 7 and 10, and returning to pH 4 while voltages were measured and recorded using the pH Meter V1.1. The repeated pH shifts were intended to provide data in both increasing and decreasing pH conditions, as well as provide multiple observations of the same measurement sequence. By subjecting each sensor to the same pH changes, each sensor could be considered a full dataset rather than having to aggregate all sensor data to represent multiple pHs. All five meters were set to send data on a 5-minute interval. Because the pH Meter V1.1 can only sample four sensors at once, the total sample size was 20 sensors. A successful three-point calibration will yield repeatable voltages for a given pH with appreciable differences between each pH's voltage.

5.5.1 (b) Second Variant (pH Meter V1.1 Wide-Range Test)

The same experiment as the first variant was repeated but instead of only using pH 4, 7, and 10, each sensor was exposed to pH 3 through pH 9 on approximately 1 pH unit intervals.

Instead of using all five pH Meter V1.1s, only three Meter V1.1 were used, reducing the sample size to 12 sensors. A successful test will show unique voltages for each pH with a trend between them.

5.5.1 (c) Third Variant (HP34401A Wide-Range Test)

The third experimental variant was similar to the second variant, but instead of using the pH Meter V1.1, the HP34401A multimeter was used to manually record the data. The pH was changed from pH 10 to pH 3 and then to pH 11 in 1 pH unit intervals. A successful test will show unique voltages for each pH with a trend between them.

5.5.2 Apparatus Configuration

The same jar apparatuses from the Static Buffer tests were used in all three variants of this experiment. Figure 21 shows the apparatuses in use with the sensors connected to the pH Meter V1.1s. Figure A modification made to the setup was the use of simple Faraday cages in the first and second variants of this experiment, as the pH Meter V1.1s showed signs of interference from electromagnetic fields (EMF). Figure 22 and Figure 23 show the Faraday cages, made of steel mesh baskets wrapped in six layers of heavy aluminum foil, and how the apparatuses were placed inside. Figure 24 shows the sensors properly attached to the HP34401A multimeter for measuring the sensor voltage in the final variant of the experiment.

Figure 21. Five jar apparatuses used in the stepwise pH change experiments with sensors seen attached to the pH Meters V1.1s.

Figure 22. Faraday cages used with pH Meter V1.1.

Figure 23. Apparatus and pH Meter V1.1 inside of Faraday cage.

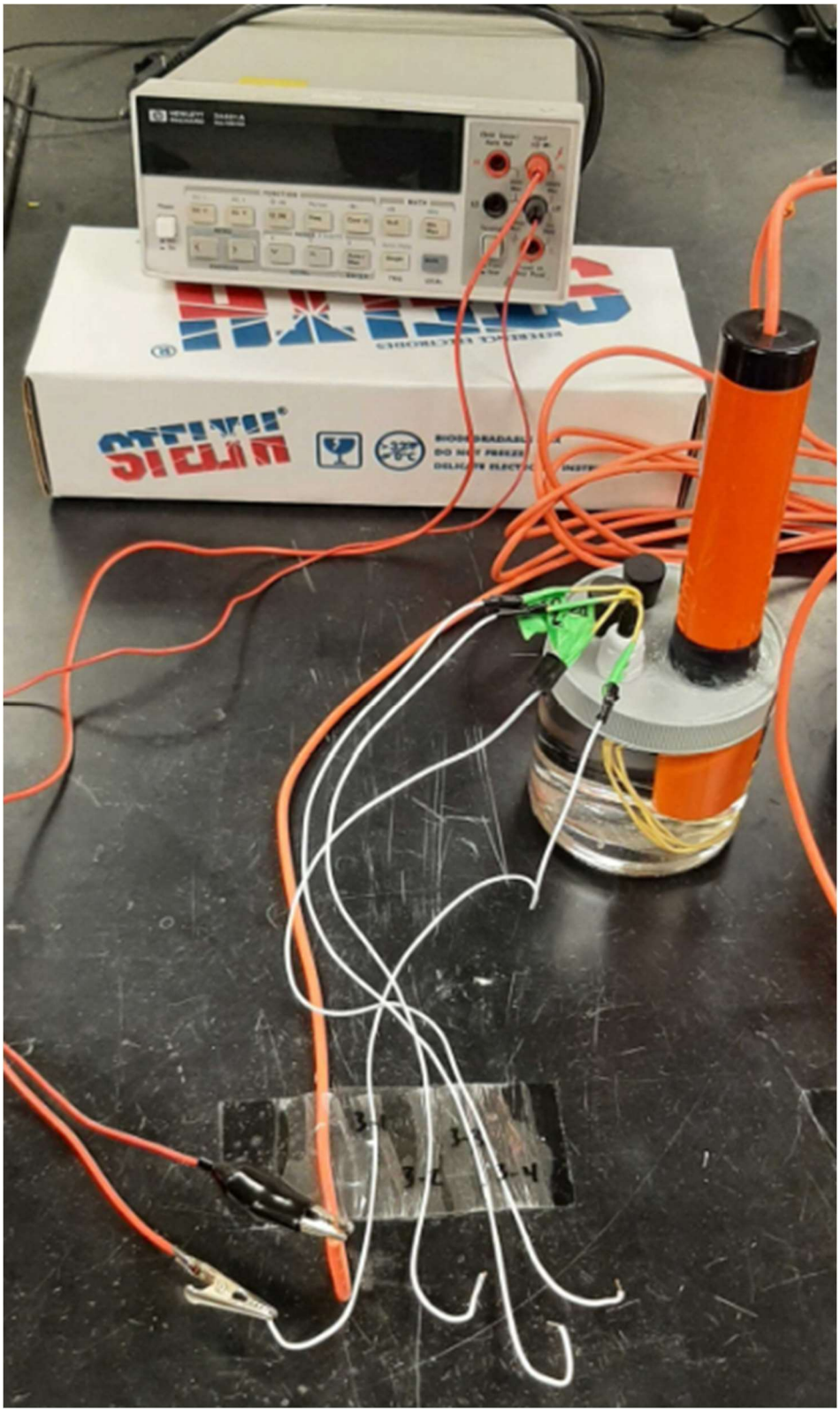

Figure 24. Sensor leads attached to the HP34401A multimeter used in the Third Variant of the Stepwise pH testing.

5.5.3 Procedure

5.5.3 (a) First Variant (pH Meter V1.1 Three-Point Calibration)

The same general procedures as the Static Buffer test were performed for placing the sensors in bundles, inserting the bundles in the jars, and connecting the sensors to the pH Meters. Sensors were moved repeatedly through pH 4, 7, and 10 solutions. The timing for changing the solution is shown in the data charts for this experiment in Chapter 6 and was not consistent throughout the experiment. The changes were not consistent because the aim was to change solutions once voltages appeared in a steady state while simultaneously maximizing the number of cycles throughout the experiment. The entire apparatus and meter were placed inside of the Faraday cage.

5.5.3 (b) Second Variant (pH Meter V1.1 Wide-Range Test)

The same procedure as the first variant was followed, but instead of repeatedly testing the sensors in pH 4, 7, and 10, they were moved stepwise from pH 3 to pH 11 in intervals of approximately 1 pH unit.

5.5.3 (c) Third Variant (HP34401A Wide-Range Test)

The same procedure as the second variant was followed, but instead of using the pH Meter V1.1, the HP34401A was used to manually record data from the sensors where the reference electrode is always connected to the negative multimeter lead and the positive lead connects to the TiMMON sensor leads. Leads were disconnected when not being measured. The pH was first decreased from pH 11 to pH 3, and then reversed back to pH 11 in intervals of approximately 1 pH unit. No faraday cage was required for this experiment because the HP34401A did not show any interference from outside sources.

Prior to measuring the sensor voltages, the settings on the HP34401A were changed such that the multimeter's impedance is set to ">10 GOhm" and the leads on the meter were connected to the correct ports on the front of the meter, shown in Figure 25.

Figure 25. HP34401A Multimeter leads connected to the correct ports for measurement.

5.6 Sensor Durability Testing

5.6.1 Experimental Design

This experiment aimed to simulate the stress of a subsurface deployment of the sensors by placing the sensors in a soil oedometer test cell filled with a coarse angular sand and compressing the sensor(s) and surrounding soil to simulate stresses for five depths (25 ft, 50 ft,

100 ft, 150 ft, and 200 ft). Two sensors were used in each of the first four simulated depths and one sensor was used in the simulated 200 ft depth. The sensor evaluation consisted of measuring a three-point calibration curve with each sensor using pH 4, 7, and 10, then compressing the sensor(s) in the oedometer, and finally repeating the three-point calibration after removal of the sensor from the oedometer. A sensor without damage should show the same calibration after the compression as before.

5.6.2 Apparatus Configuration

The initial three-point calibration was performed in an open-top 500 mL beaker with the sensors and reference electrode placed inside. The cylindrical soil oedometer test cell with a 2.4-inch diameter was placed into the oedometer frame and filled halfway with the coarse sand which was not compacted into the cell. Two sensors were placed into the test cell and laid horizontally with the lead wires allowed to hang out of the edge of the test cell, shown in Figure 26. The cell was then filled to the top with more sand (Figure 27) and covered with the top load plate (Figure 28). The oedometer compresses the specimen by transferring force through the top load platen via a 10:1 moment arm and weights (Figure 29).

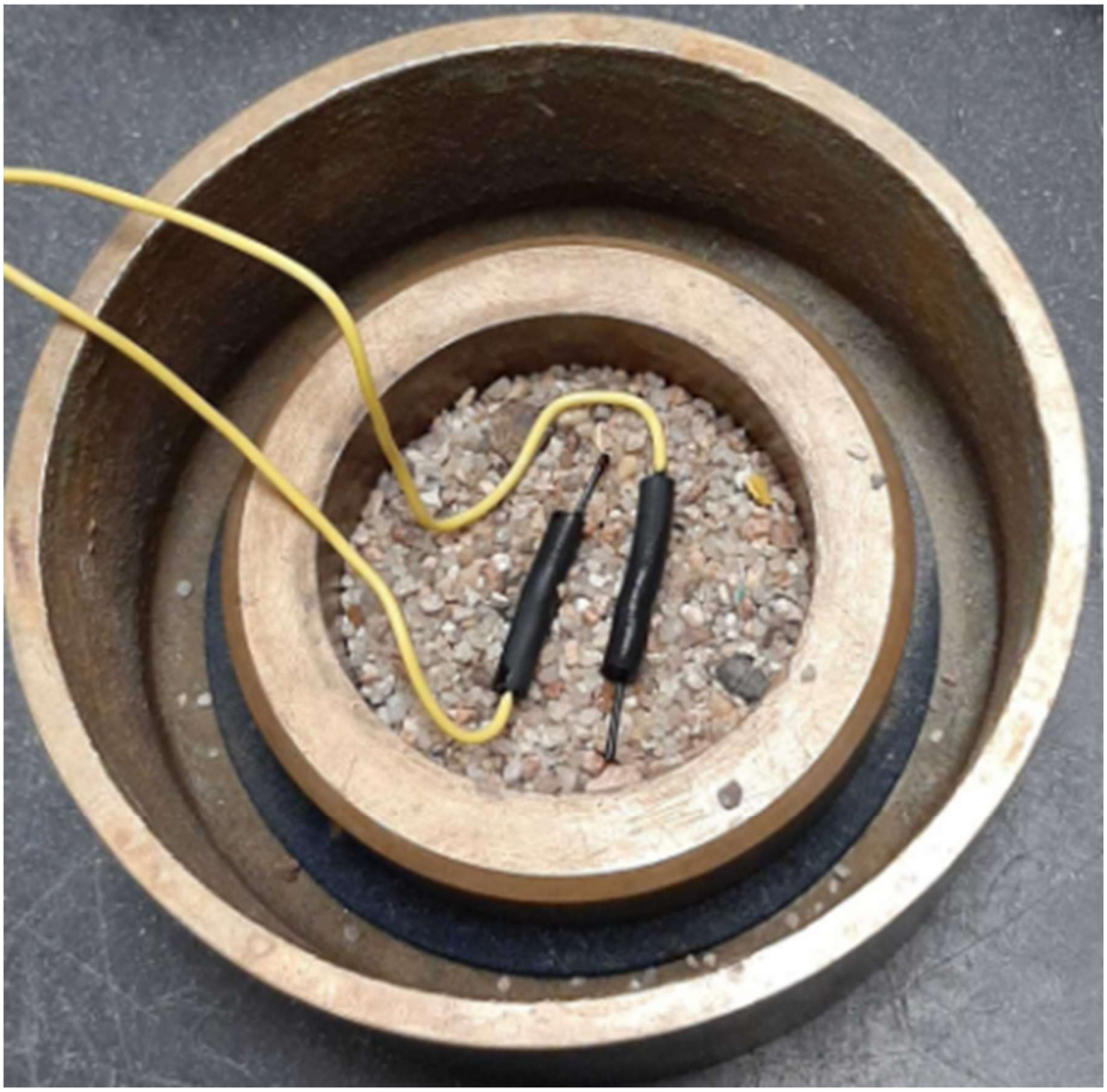

Figure 26. Sensors placed in the soil oedometer test cell half filled with coarse sand.

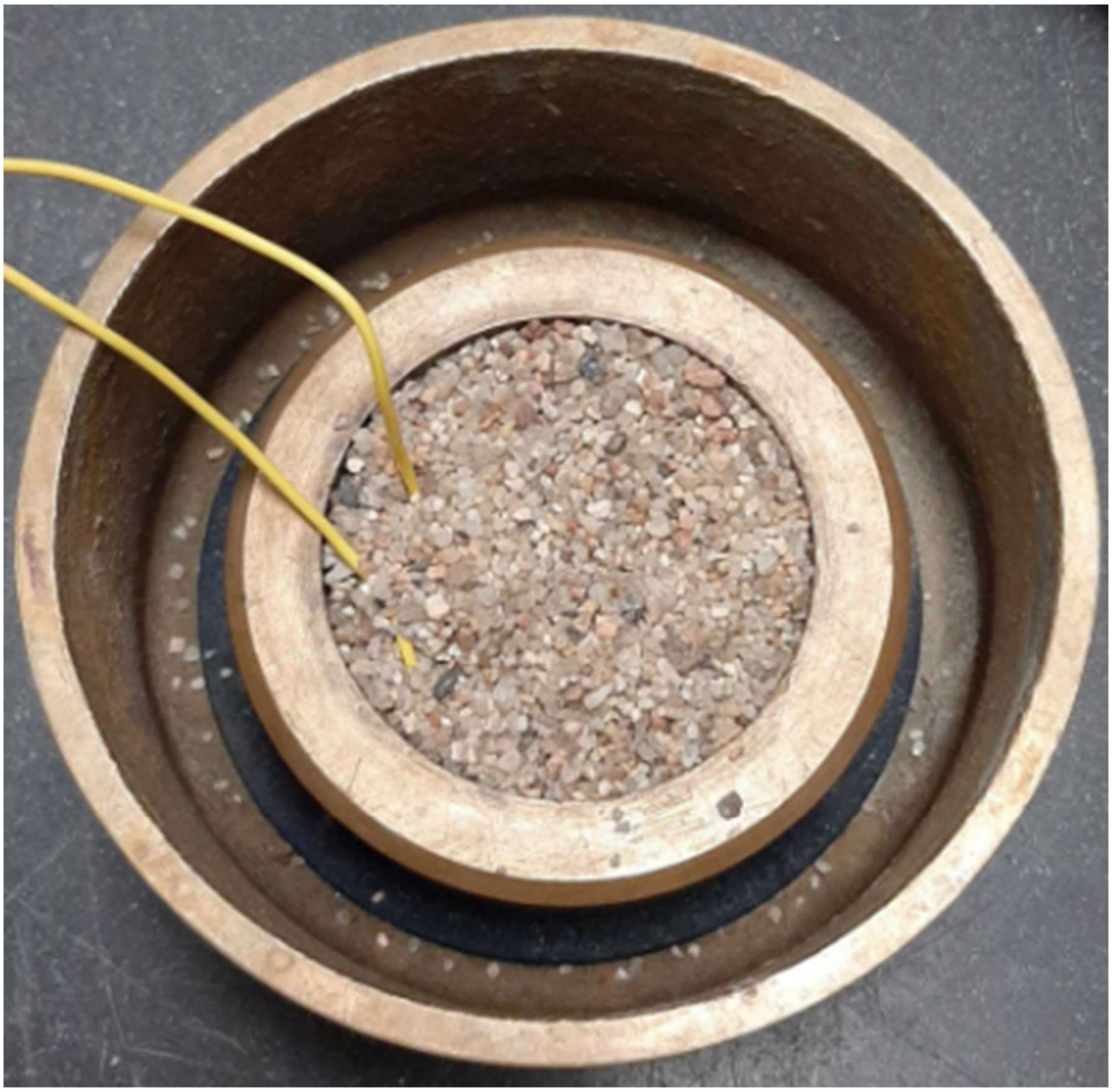

Figure 27. Sensors in the test cell covered with sand before compression.

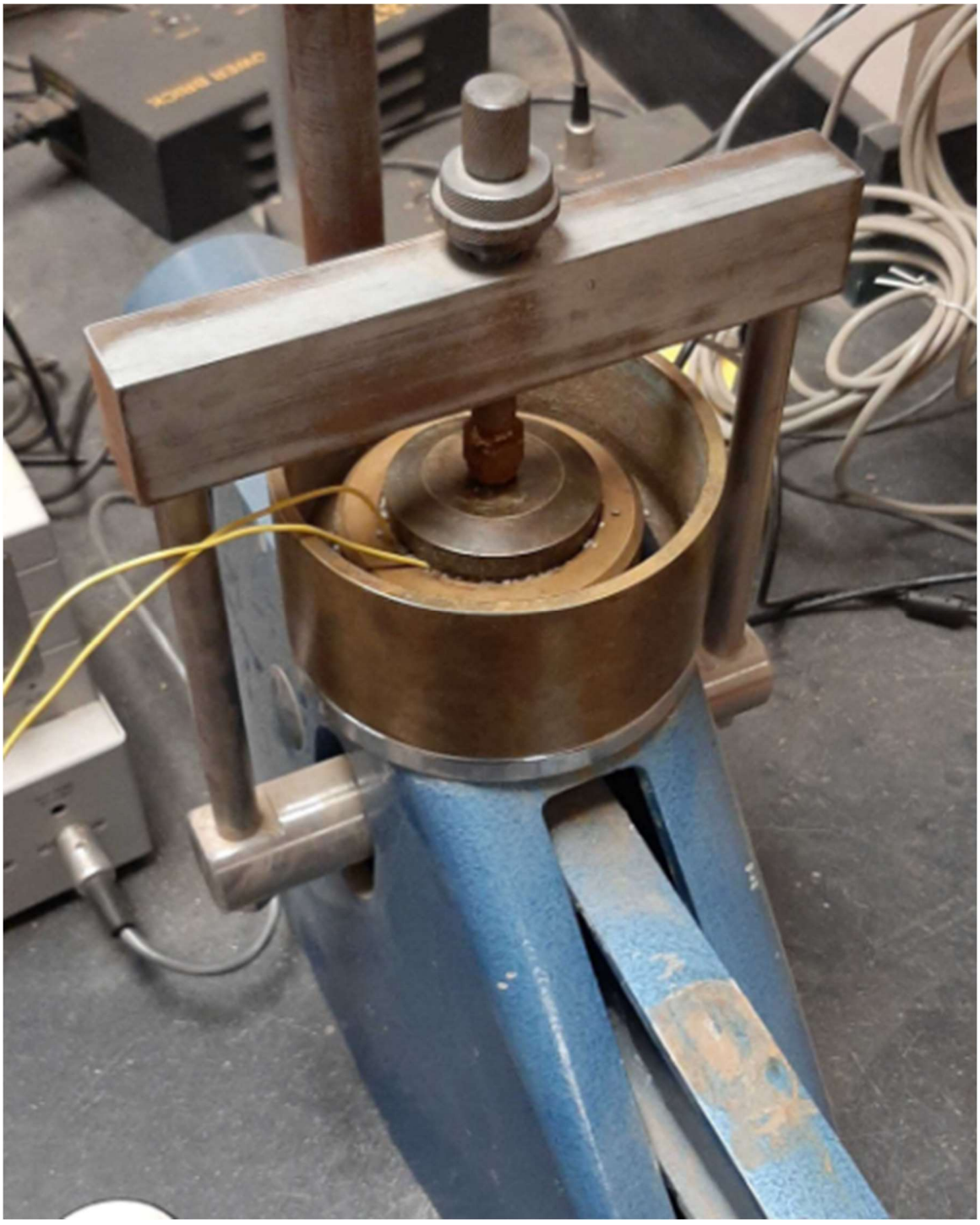

Figure 28. Oedometer test cell placed into the oedometer frame before compression.

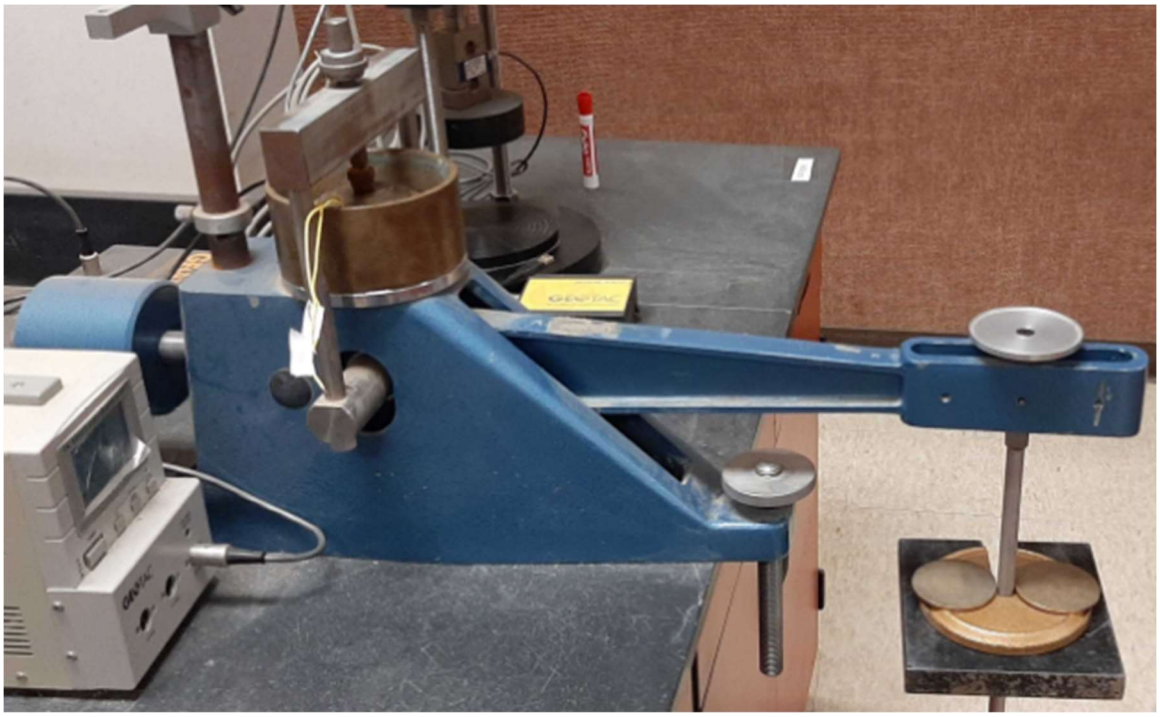

Figure 29. Soil oedometer frame with test cell inside and weights applied to the moment arm.

5.6.3 Procedure

1. Sensors were placed in pH 4 solution and voltages were measured over a period of six hours.
2. Sensors were moved to pH 7 and voltages measured similar to step 1.
3. Sensors were moved to pH 10 and voltages measured similar to step 1.
4. Two sensors were placed in the compression cell as described in Section 5.4.2 and surrounded with coarse sand. The cell was prepared for compression.
5. The oedometer frame was placed on the specimen and the appropriate weight was added to simulate the desired depth (total stress).

6. Weights were left on the specimen until no additional vertical deformation was observed. This typically took less than one minute.
7. Weights were then removed, and the sensors exhumed from the test cell.
8. Sensors were placed back into pH 10 solution.
9. The next set of sensors was then compressed, and steps 1-8 were repeated to varying simulated depths (different total stresses).
10. Finally, steps 1-3 were repeated to get the post-compression three-point calibration curve.

6. RESULTS AND DISCUSSION

The following chapter presents and discusses the results of multiple experiments performed on the solid-state pH sensors and the IoT-based pH meter designed in this work. The design, apparatuses, and procedures for these experiments were described in Chapter 5. The results from each experiment are discussed separately here and then summarized in Chapter 7.

6.1 Pilot Test

The first experiment performed as part of this work was a pilot test to determine if the TiMMON electrode would respond to pH changes with voltage (compared to the reference electrode) changes. A prototype TiMMON electrode was created and tested in a simple experiment described in Section 5.1.

Figure 30 shows the data collected during the pilot experiment. As the pH was changed, potentials on a TiMMON and TiMMO electrode were compared to a Ag/AgCl reference electrode using a Fluke multimeter. Figure 30 shows the TiMMON electrode voltages increasing with a decrease in pH while the TiMMO electrode's voltage decreases with pH decreases. The TiMMON and TiMMO electrodes showed similar responses in opposite directions. Because of these results, further study of the TiMMON electrode was warranted for use in a solid-state pH sensor design. We believe changes in the TiMMO electrode were the results in changes in redox potential across the pH buffer solutions used in the pilot test.

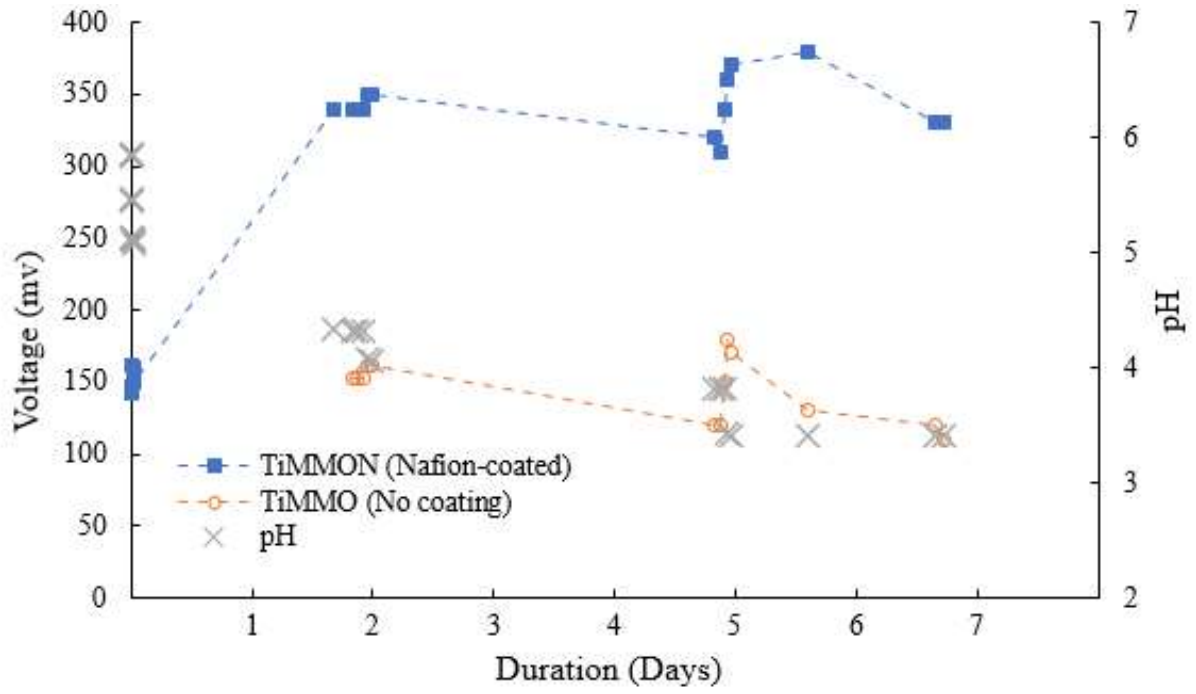

Figure 30. Pilot test showing the TiMMON voltage response to changing pH over time (gray points) is different than the TiMMO voltage response.

6.2 Evaluation of Post-Fabrication Sensor Treatments

The properties of Nafion™ change with the degree of hydration (Grot 2011). The oxide coating on the titanium wire also responds to the degree of hydration (Kinlen et al. 1994). Multiple methods for hydrating Nafion™ coatings exist; three methods of sensor hydration were tested: boiling, steaming, and soaking.

Figure 31 shows the results of sensor hydration by soaking and boiling, and Figure 32 shows the results of sensor hydration by steaming. For optimal performance, sensors groups with smaller intra-group variances (better convergence) and more consistent cross-pH trends are preferred. The boiling and steaming methods were applied for different durations (5, 10, 15, 20, and 25 mins), the influence of the hydration method on the sensor pH-voltage relationship was

observed while sensors were moved through pH 4, 7, and 10. The steamed sensors were not tested in pH 4 solution and were tested for a shorter amount of time. There was not a clear correlation between sensor absolute voltage and hydration method for a given pH solution. However, there were apparent influences of hydration method on the temporal response trends. The main observation was that some groups (soaked, boiled 10 mins, boiled 15 mins, steamed 20 mins, steamed 25 mins) tended to have a quicker convergence and overall trend while others seemed to be more sporadic.

Figure 33 provides a comparison of the 11 treatments by the within-group voltage range. A group with better convergence and trend will show a smaller voltage range more quickly after disturbances and have more consistent voltage over time. As shown in Figure 33, the group soaked for three months converges quickly and tends to maintain a tight voltage range over time. The steamed sensor groups tend to have a lower voltage range than the boiled groups, and four out of the five groups have a lower intra-group voltage range than the soaked group by the end of the experiment.

Based on the results presented in Figure 31 through Figure 33, steaming the sensors for 20 minutes was selected for further testing. The basis for this decision included:

- Consistently low voltage range (variance) throughout the experiment;
- Consistent trend after pH changes;
- No outliers measured during experiment.

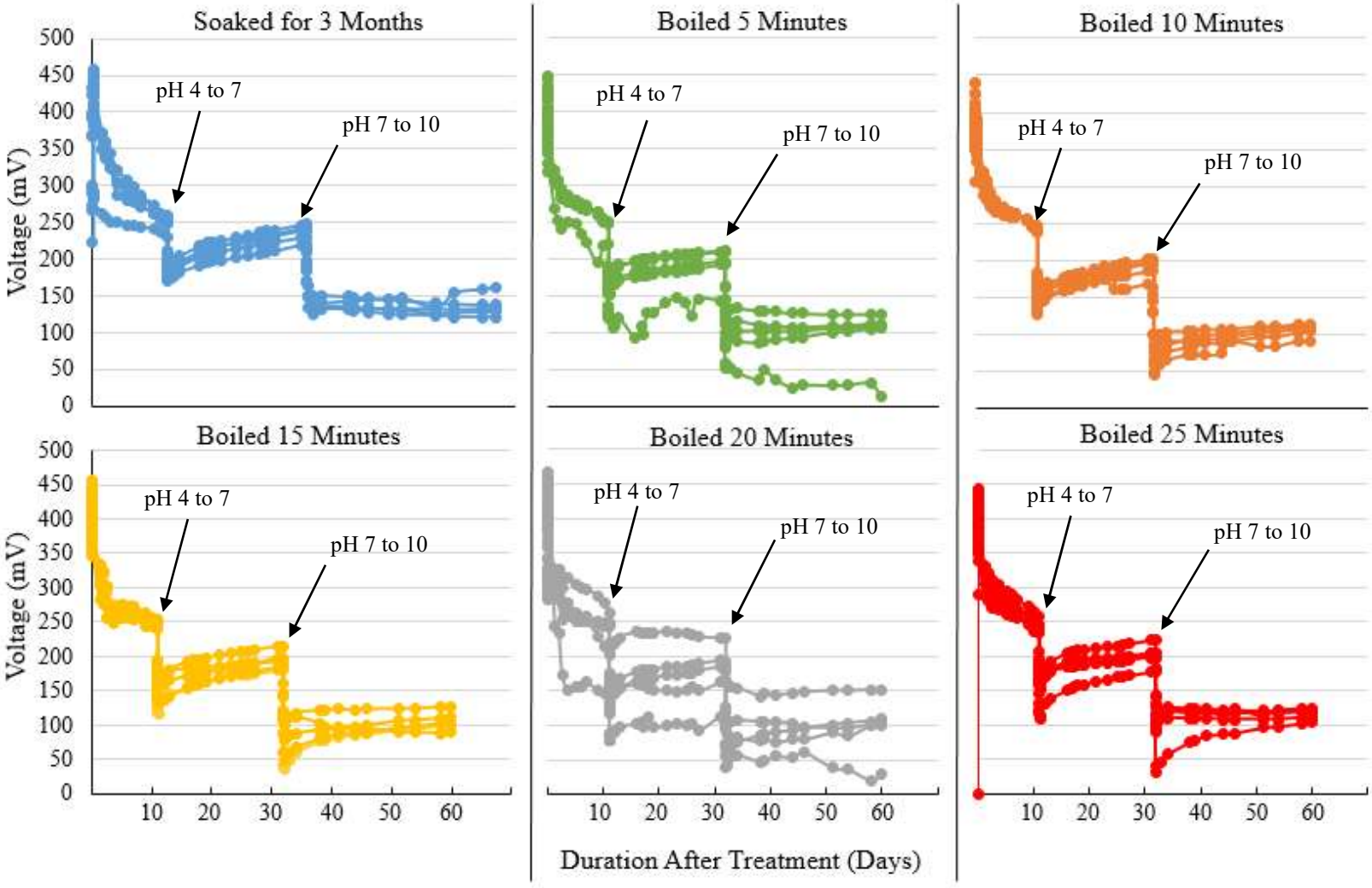

Figure 31. Soaking and boiling treatment responses to pH changes (pH 4, 7, and 10).

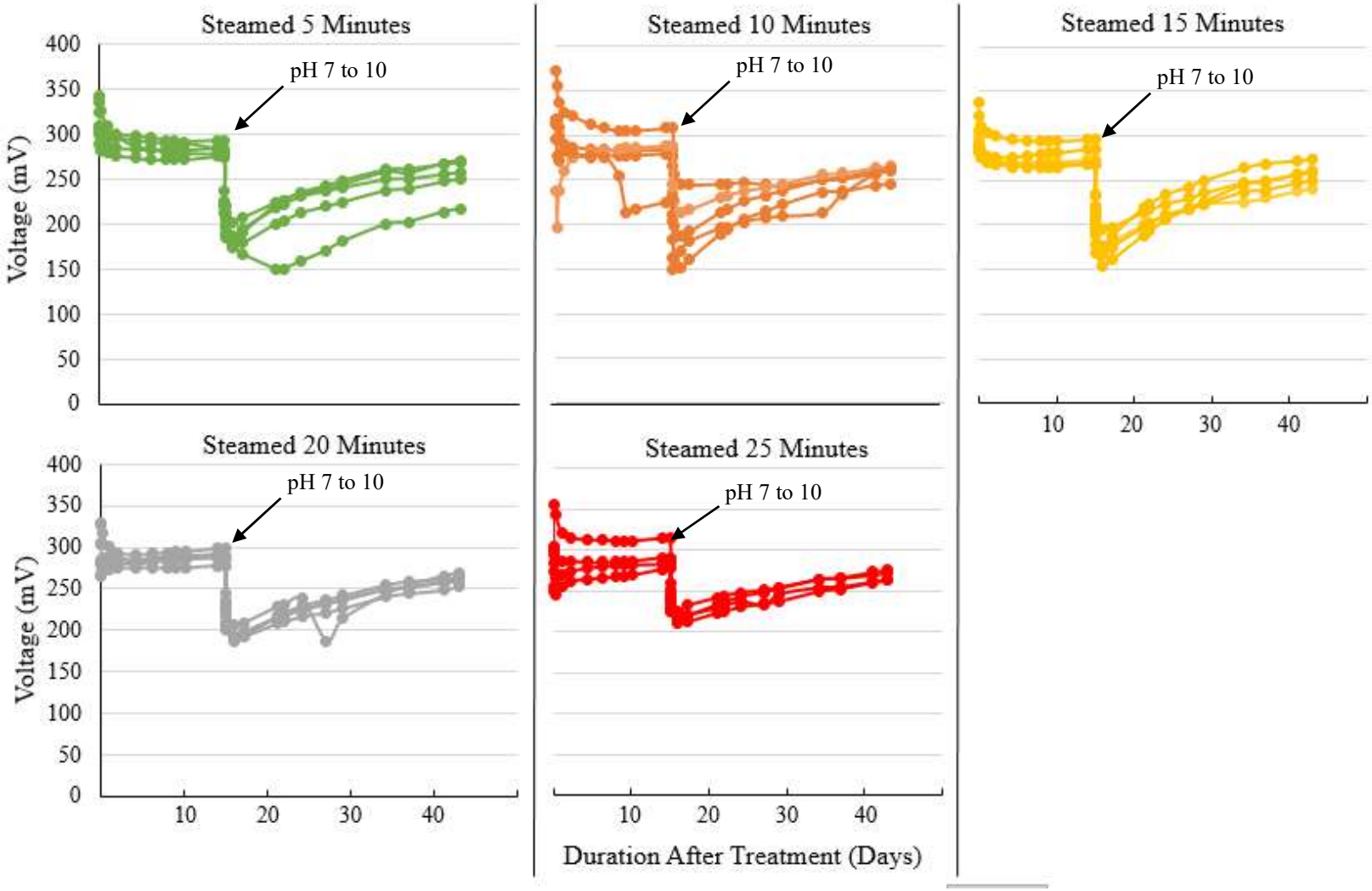

Figure 32. Steaming treatment responses to pH changes (pH 7 and 10).

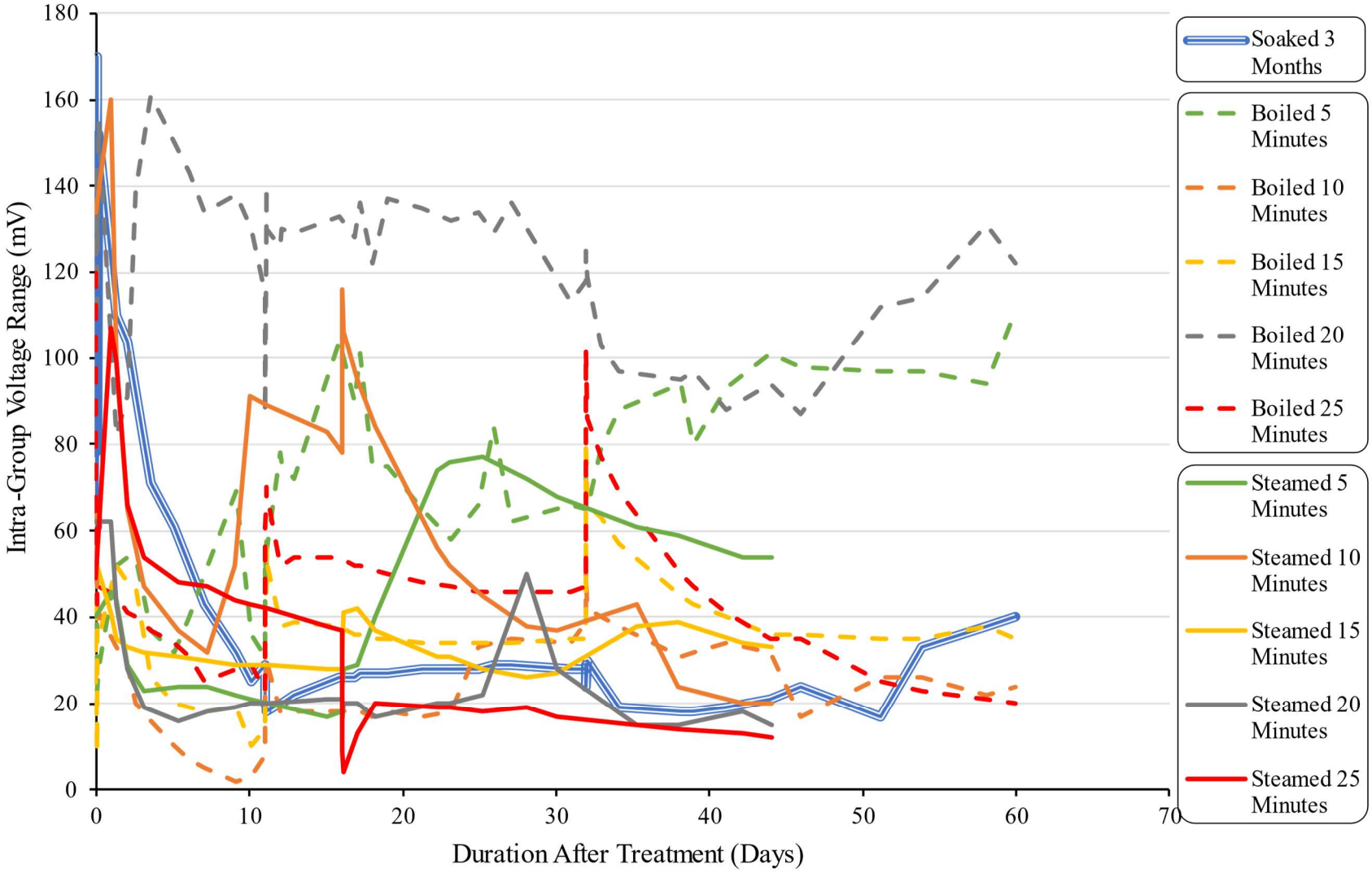

Figure 33. Post-fabrication treatment comparison for convergence.

6.3 Sensing in a Static pH System

To develop a calibration curve (pH-voltage relationship), groups of sensors were placed in static pH buffers and allowed to equilibrate toward an unchanging voltage with time. Three standard pH buffers for pH electrode calibration were used: pH 4, 7, and 10. Sensors were measured using the IoT-based pH Meter V1.0. Fifteen sensors were tested in each pH buffer with five sampled every hour and ten sampled every 15 minutes. Variable sampling intervals were intended to determine if the sampling interval affected the measured pH-voltage relationship.

Figure 34 shows the data collected during the static pH sensing experiment over almost one month. As expected, sensors took time to approach a steady-state voltage, but unexpectedly, there was no apparent absolute voltage for a given pH. This lack of absolute voltage is illustrated by examining the green lines on Figure 34 which represent the sensors in pH 7 solution. One set of green lines is overlapping the orange and red lines (representing pH 4), while the other set of green lines is overlapping the blue lines (representing pH 10). The expectation was that the green lines would be approximately halfway between the lines representing pH 4 and pH 10. Deviation from this predicted behavior indicates that the sensors respond to pH changes but may need to be individually calibrated to provide absolute voltages (and pH measurements). However, the lines representing the pH 4 and pH 10 solutions do show distinct differences in voltage. Because of the questions left after this experiment about calibration and timing, this experiment was not used to create a calibration curve.

The second observation in the static pH sensing experiment relates to sampling interval; in Figure 34 the lighter lines are sampled four times as frequently as the darker lines. The hypothesis was that if sampling interval impacted the data by “draining” the voltage on the sensors sampled more frequently, the lighter and darker lines would show distinctly different

curvature and trend. However, this difference is not observed; the groups sampled less frequently did show consistently higher voltages than those sampled every 15 minutes, but the slopes of these groups were almost identical, meaning the sensors were responding in the same way regardless of sampling interval. Only the curvature at the beginning of the series appears to differ slightly; the orange and cyan lines have a steeper initial curve than their red and blue counterparts.

To further explore sampling interval effects, the sensors in the pH 7 solution, represented by the green lines, were swapped during testing such that the sensors that were initially sampling every hour were then sampled every 15 minutes, and vice versa. The hypothesis was that the two groups would switch places on the chart. However, the observation was that the sensors (approximately) maintained the trend observed before the switch. This further illustrated that sampling interval did not affect sensor behavior for this experimental setup.

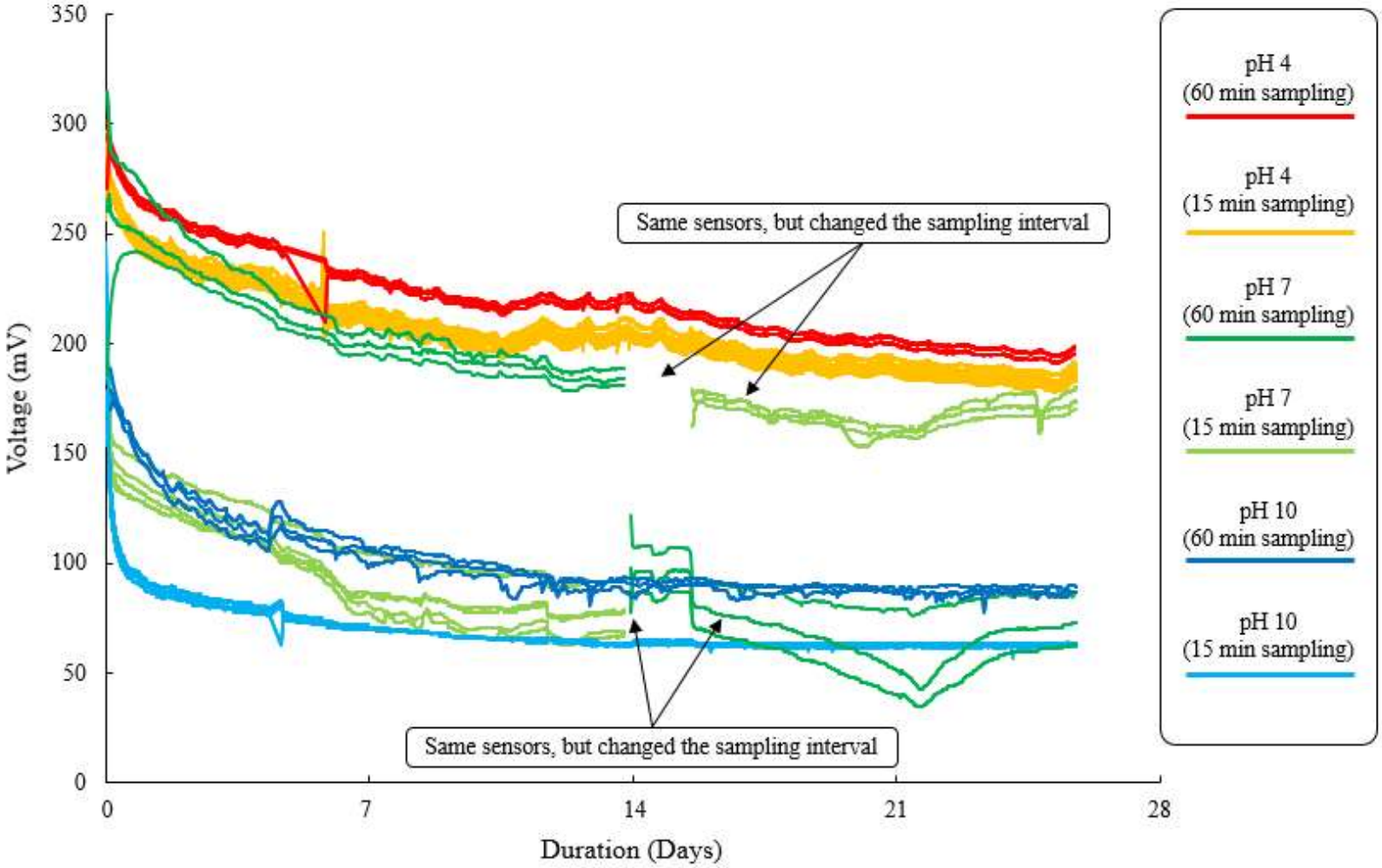

Figure 34. Sensor equilibration in a static pH using different sampling intervals.

6.4 IoT Monitoring System Evaluations

Because of the unexplained behaviors in the static pH buffer experiment and other preliminary data measured prior, questions were raised about the ability of the pH Meter V1.0 to accurately measure and report the sensor voltage responses. Two experiments were performed to test the pH Meter V1.0, these experiments are described in this section.

6.4.1 Measurement Time Interval Test

Three groups of sensors were placed in the same solution but connected to three different pH Meter V1.0s with different sampling intervals (30 sec, 5 min, and 2 hr). These intervals had larger differences in sampling intervals than the intervals in the static buffer test (15 min and 1 hr) which was intended to show more drastic differences in behavior if the sampling interval influenced the sensor voltage responses. The test solution was then changed to different pHs such that multiple voltage changes could be observed.

Figure 35 shows the results from measurement time interval tests with each group color-coded representing a different sampling interval. Despite voltage offsets between groups, there was no apparent difference in behavior related to the sampling interval, and there was no trend observed as the sampling interval decreased. This suggests that differences in absolute voltages may be related to the meter that the sensors are connected to, but not the interval at which sampling is conducted.

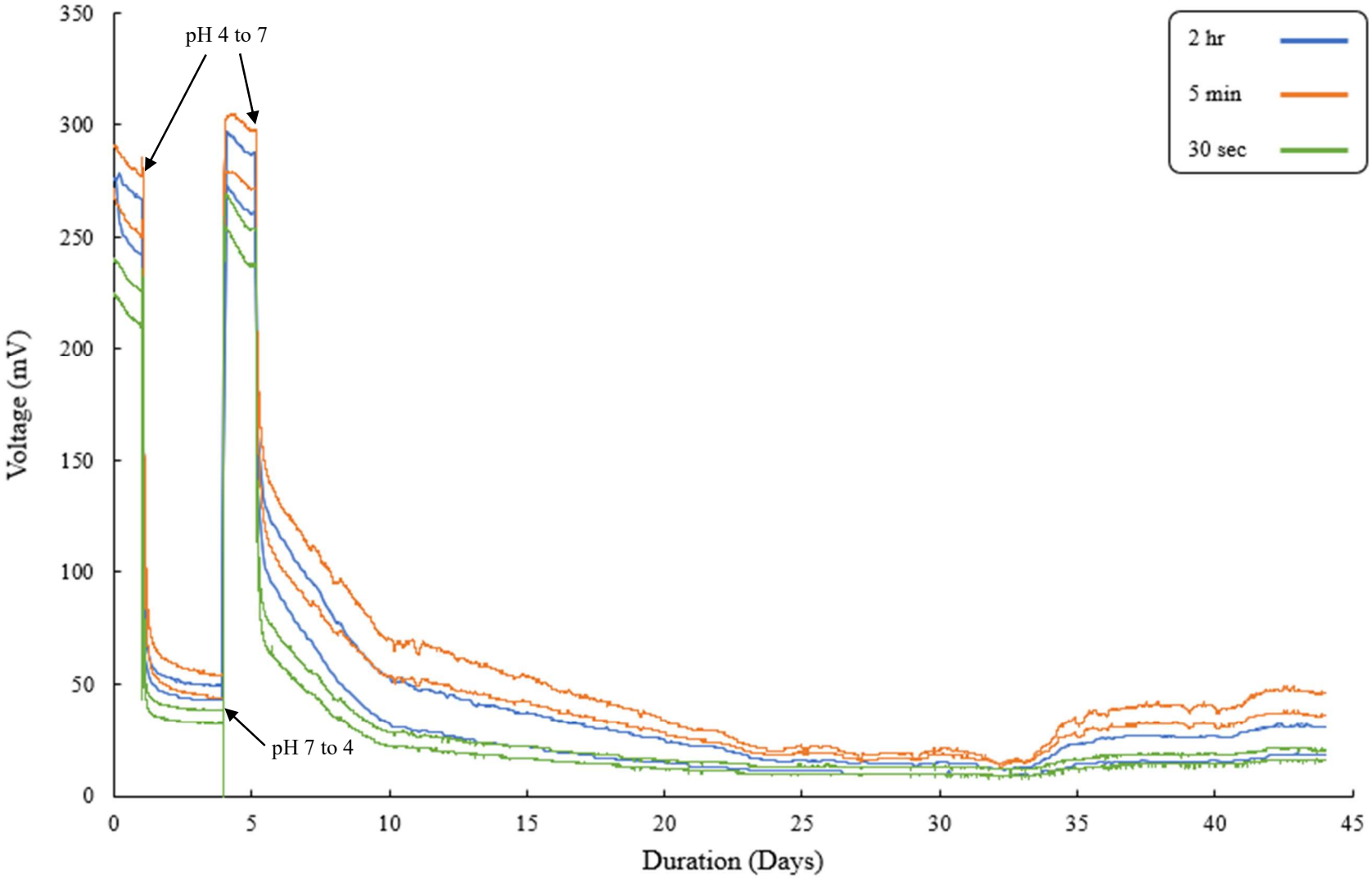

Figure 35. Measurement time interval experiment data showing data from sensor groups measured at different intervals.

6.4.2 Multiplexer Effects Test

Based on previous experience with 16-channel multiplexer (MUX) and the MCP3424 analog-to-digital converter (ADC), questions were raised about the influence of the MUX on the measured voltages. Anecdotal evidence during preliminary tests showed some channels on the MUX having influence over other channels and the potential for voltages to change as signals pass through the MUX. Furthermore, the multiplexer is not an absolutely critical piece of the pH Meter design, as the only purpose is to increase the number of sensors attached to the board.

Sensor voltages, shown in Figure 36, were tested when connected to the MUX versus when connected directly to the ADC. The data shows a clear offset between groups meaning the multiplexer does affect the sensor voltages. Because of this, the pH Meter was redesigned, removing the multiplexer from the circuit.

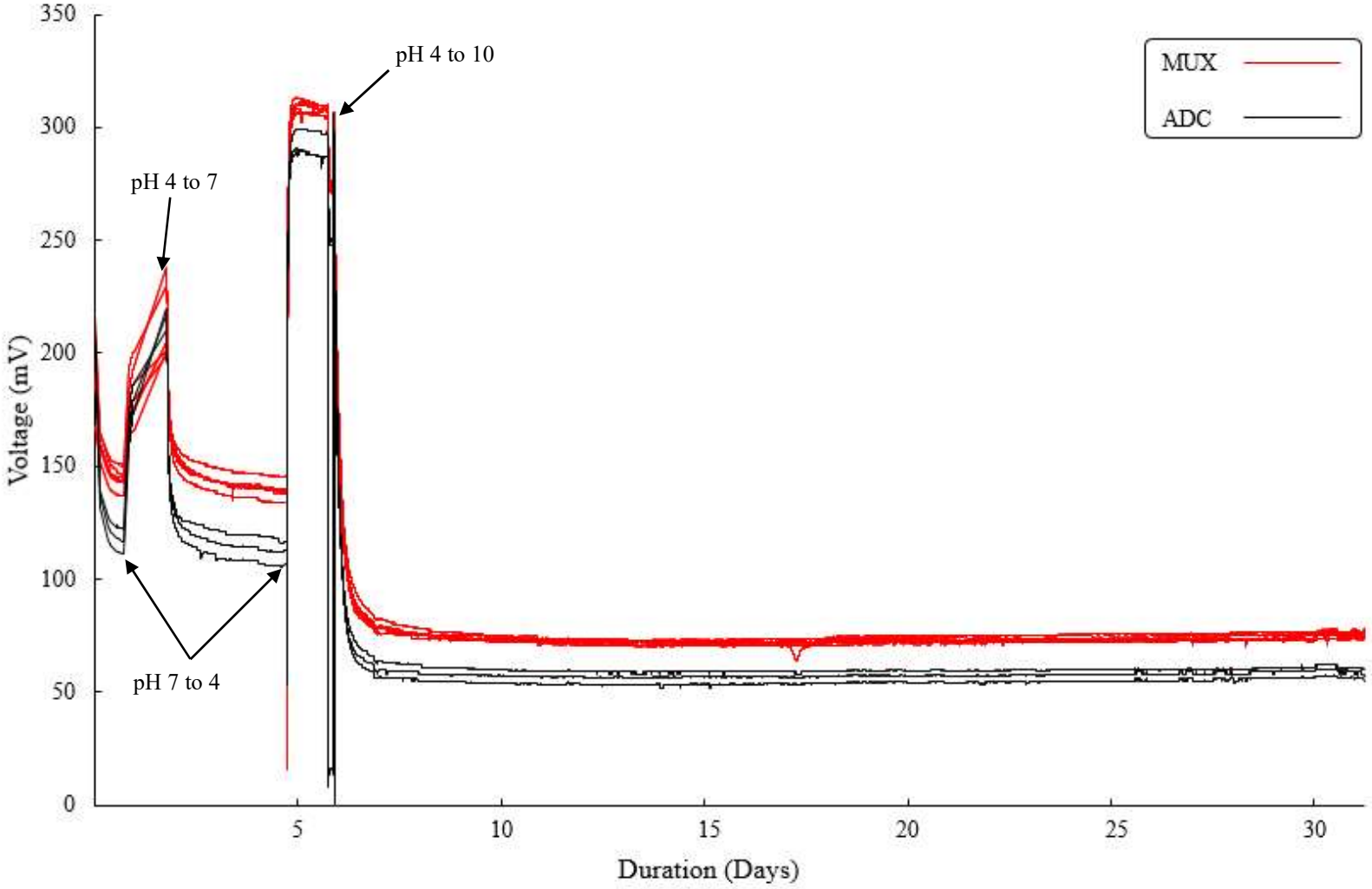

Figure 36. Multiplexer effects test data showing an offset between sensors connected directly to the ADC and those connected to the MUX.

6.4.3 pH Meter V1.1 Pilot Test

The redesigned pH Meter, termed the pH Meter V1.1, is described in Chapter 3. Figure 37 shows the results of a pilot test that was performed on the breadboard circuit of this meter before proceeding to make soldered prototypes. The data shows a significant improvement in voltage responses to pH in the sensors connected to the LMP7721 op-amps (blue) over those connected directly to the ADC (orange), indicating these components are beneficial in the measuring circuit. The sensors connected to the op-amps show less volatility than the sensors connected directly to the ADC. While the directly connected sensors generally show a quick and sustained response to pH changes, the sensors connected to the op-amps show a more pronounced and consistent response. Most importantly, the sensors connected to the op-amps show responses that are repeatable, meaning that sensor voltages can be interpreted and related to pH. For example, when the pH was changed from 4 to 10 and then back to 4, the voltage on the sensors was almost the same. The sensors were then moved to pH 1 and then back to 4, repeating almost the same voltage again. By contrast, sensors without the op-amps showed less repeatable voltages.

Though the new design showed improvement, the responses were not optimal. For example, the last switch shows a change from pH 4 to 5, but the sensor voltages increased where the sensor responses were expected to decrease. More experiments and development must be made to ensure a reliable pH Meter design can accurately measure the sensor voltages.

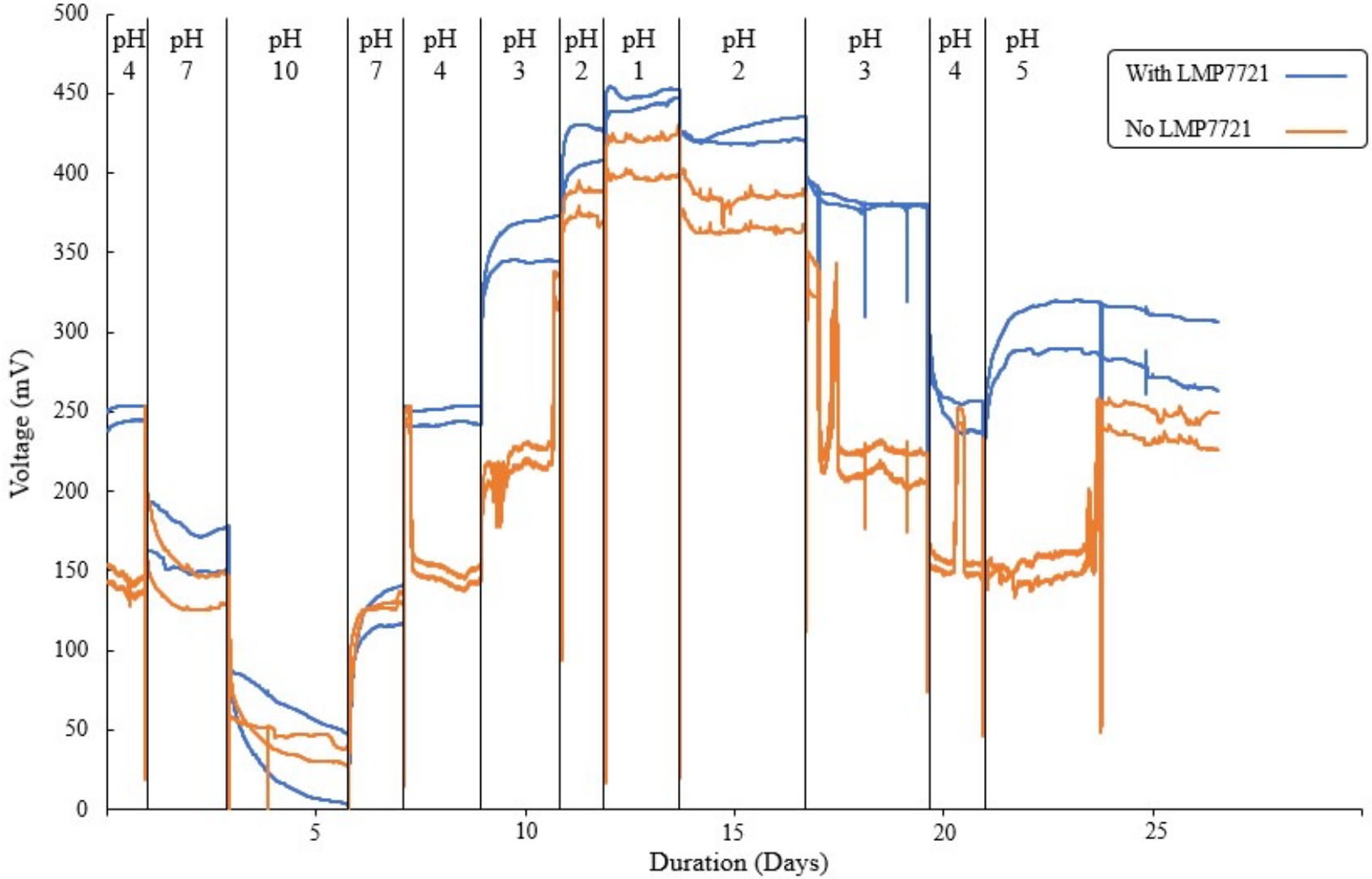

Figure 37. pH Meter V1.1 pilot test data showing significant improvements with the LMP7721 op-amp as compared to connecting sensors directly to the ADC.

6.5 Sensing in a Stepwise pH System

Stepwise pH-solution tests were performed to evaluate sensor behavior in a static (but varying) pH system to identify steady-state voltages for each pH, the change behavior of the sensor during abrupt pH changes, and sensor behavior across multiple pH values over a wide range. Three variants of the experiment (described in Chapter 5) were performed, as discussed subsequently. Figure 38 shows the resulting pH-voltage relationships demonstrated with multiple experiments, with the Third Variant experiment using the HP34401A multimeter producing the best results.

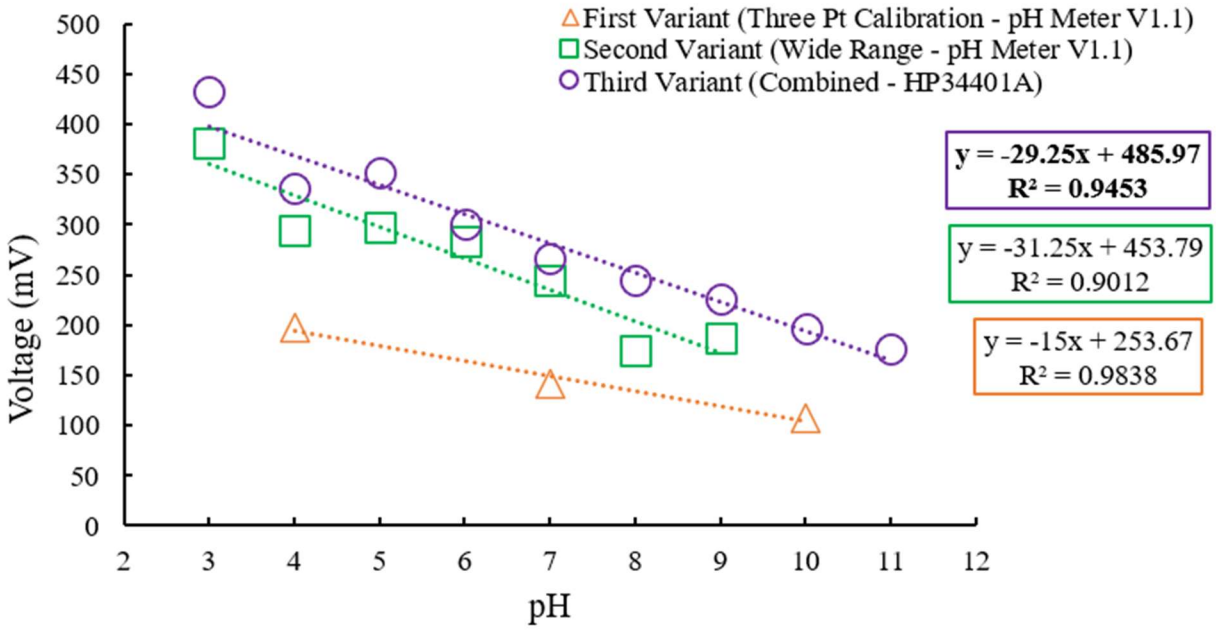

Figure 38. Results of multiple stepwise pH experiments using different measuring equipment.

6.5.1 First Variant (pH Meter V1.1 Three-Point Calibration)

The first variant of this experiment was intended to provide a mid-range pH calibration curve where the sensors were exposed to pH 4, 7, and 10 repeatedly to obtain multiple

measurements. pH was changed in an increasing and decreasing trends to help determine if the voltages are repeatable in the same pH regardless of prior exposure. In this experiment, sensors were exposed to pH 4 stages four times, pH 7 stages five times, and pH 10 stages three times. The sensors were connected to the pH Meter V1.1 via the screw terminals connecting to the LMP7721 op-amps.

Figure 39 shows the sensor voltage progression, and is color coded by the pH of the solution at a given time. Because the sensors take time to achieve a steady-state voltage in a given pH, the calibration was performed by taking samples of the "tails" of each stage of the experiment—the last hour of each stage. These tails consist of 12 measurements on each sensor (12 five-minute interval measurements over a one-hour period) and are shown in Figure 40. Figure 41 shows a violin plot of the distribution of voltages on the tails shown in Figure 40, as well as the mean of those voltages, marked with an "X". Mean and median voltages are tabulated in Table 8. Analysis output from R can be found in Appendix C.

There is a strong trend in the data where voltages decrease with an increase in pH. Sensor voltages have an asymptotic approach toward steady-state values for a given pH, which is suspected to represent the diffusion of positively charged protons into or out of the Nafion™ membrane on the electrode. However, whether the voltages recorded in the tails of each stage represent the steady-state voltage for a given pH is unclear. There was not enough time to allow sensors to equilibrate longer in each stage (graduation termination criteria), and priority was given to having at least three samples of data for each pH. The calibration curve from this experiment is shown for comparison with other curves in Figure 38.

Table 8. Voltage Response Data Summary for the Three-Point Calibration Experiment Performed with the pH Meter V1.1

pH	Mean Voltage (mV)	Standard Error of Mean (mV)	Median (mV)
4	197	1.54	183
7	142	0.54	141
10	107	0.93	108

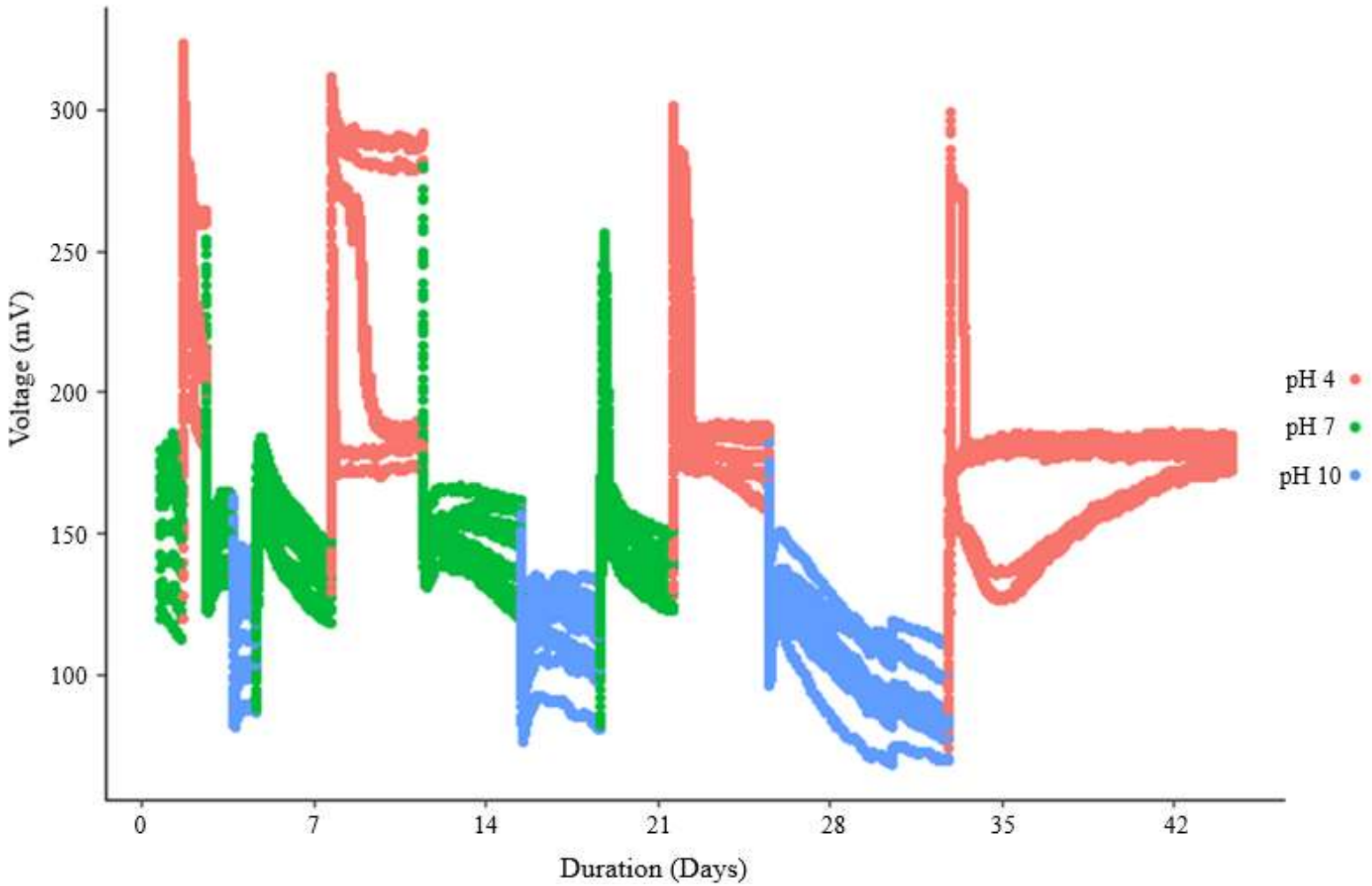

Figure 39. Voltage responses of 12 sensors to iterative three-point calibration sequence test measured with pH Meter V1.1 with each pH stage color-coded.

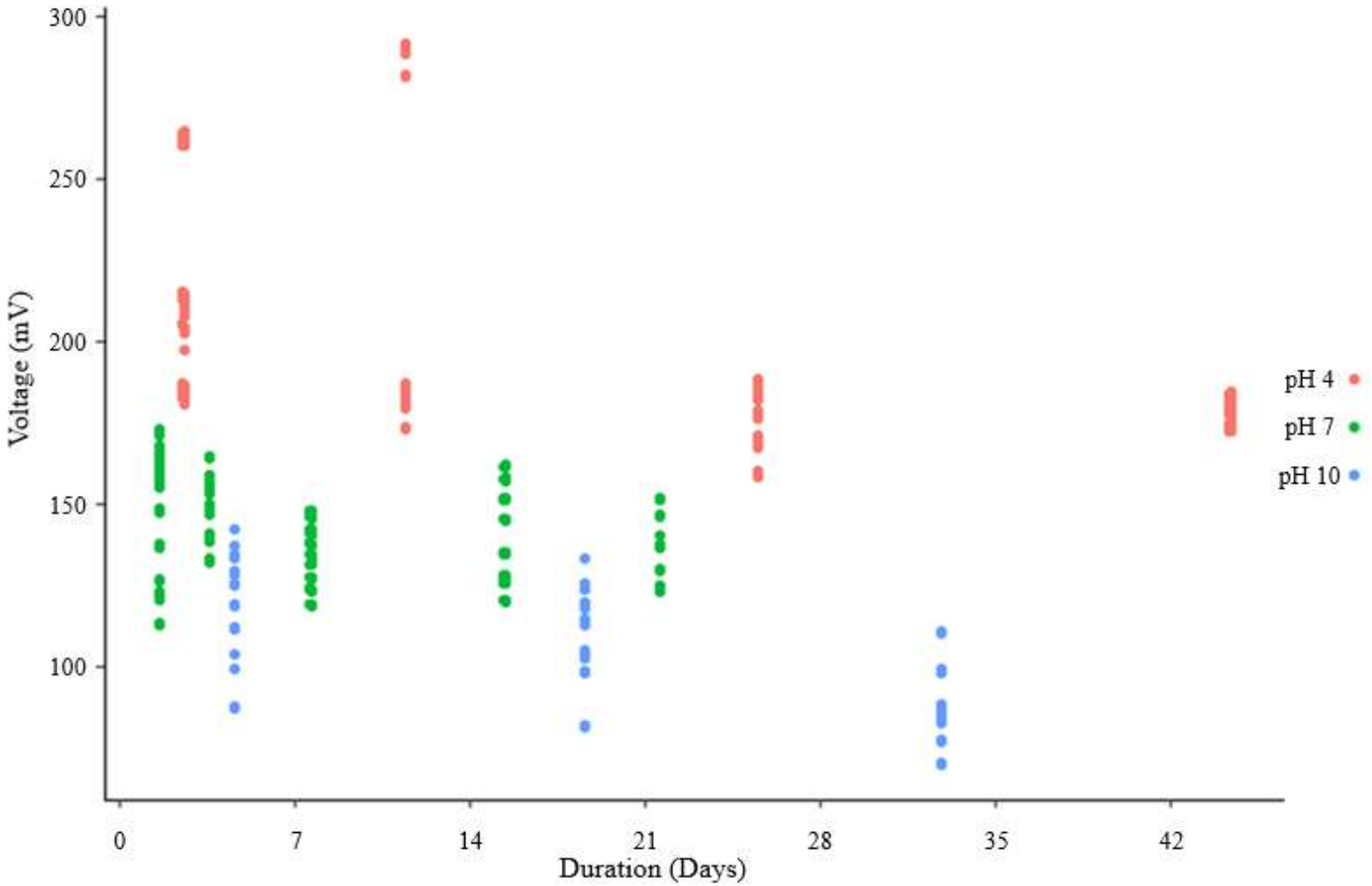

Figure 40. "Tails" of voltage responses of 12 sensors to iterative three-point calibration sequence test measured with pH Meter V1.1 with each pH stage color-coded.

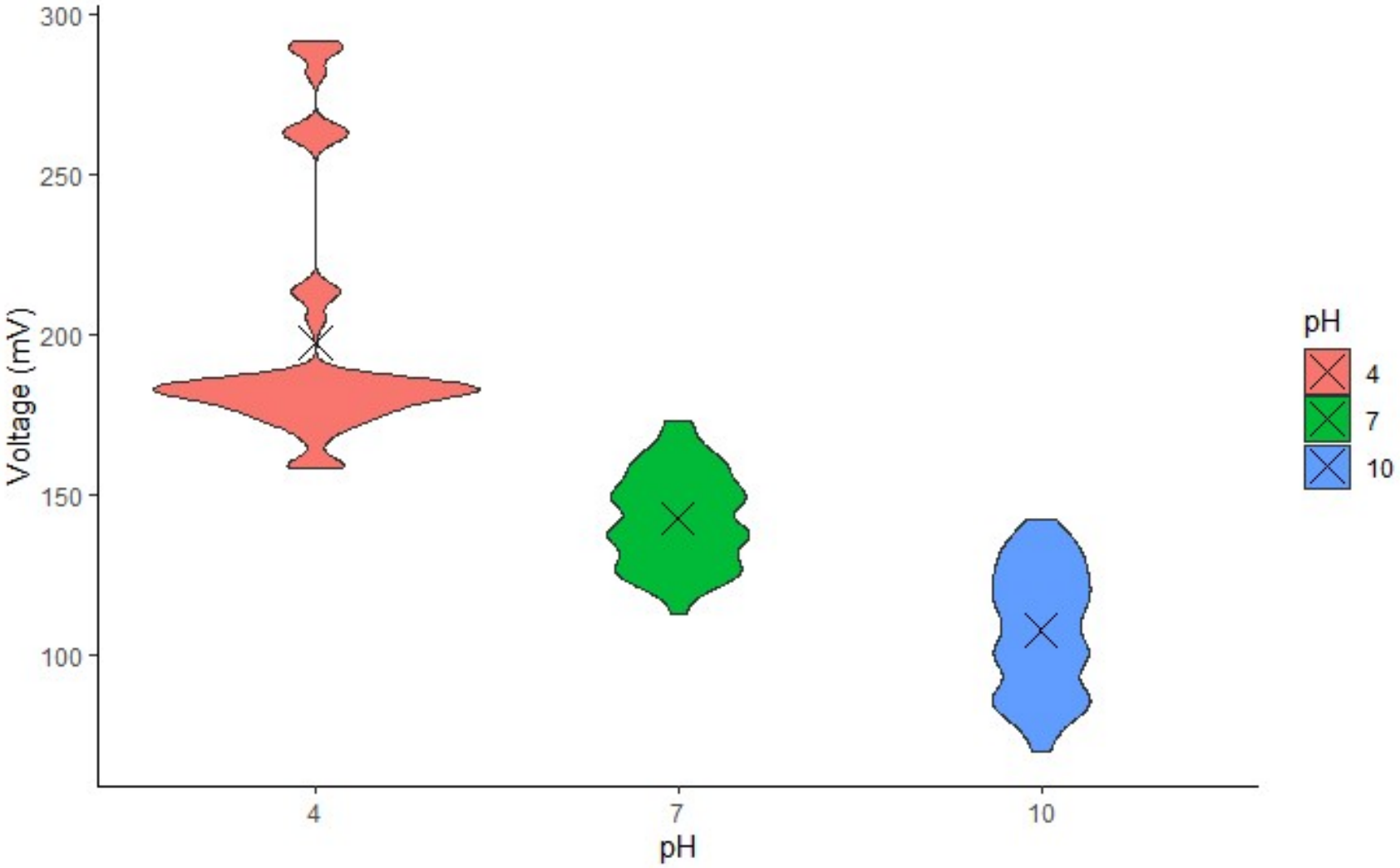

Figure 41. Violin plot of "tails" of voltage responses of 12 sensors to iterative three-point calibration sequence test measured with pH Meter V1.1 with each pH stage color-coded and each pH mean voltage marked with "X."

6.5.2 Second Variant (pH Meter V1.1 Wide-Range Test)

After the first experimental variant was used to measure a calibration curve with the three standard pH buffer calibration solutions, an experiment with a higher resolution and wider range of pH steps was performed (pH 3 to 12). Though these more extreme pH values are less common in natural systems, pH extremes are especially relevant to anthropogenically impacted systems and have been observed in some natural systems (discussed in Chapter 2). There is value in understanding the sensor response to these extremes and any limiting conditions for future applications.

Figure 42 shows the progression of pH and ORP throughout the experiment measured at the beginning and end of each stage. pH was controlled prior to sensor exposure, but ORP was not controlled.

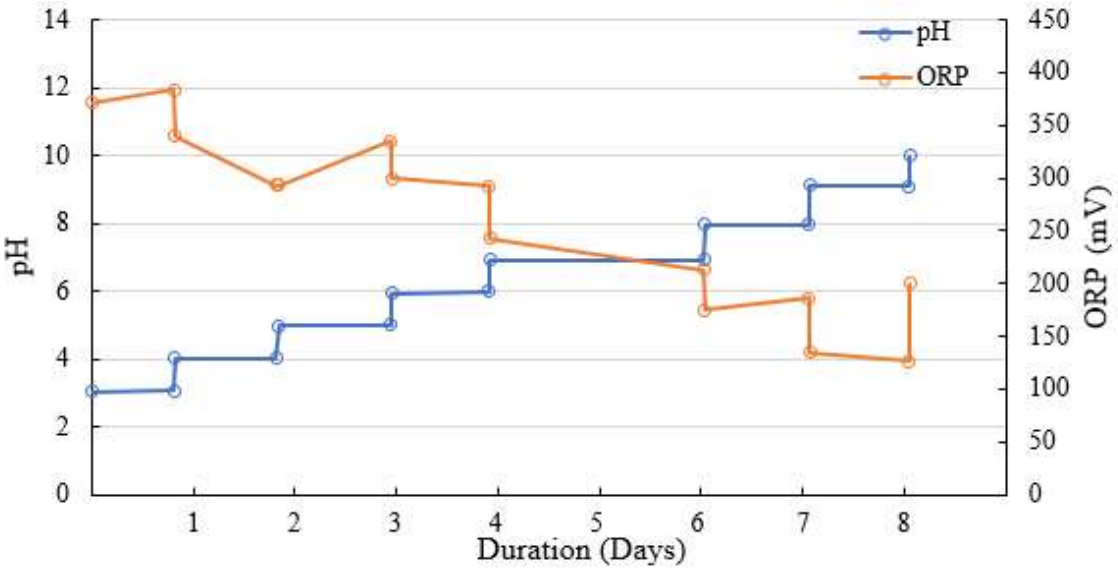

Figure 42. pH and ORP of pH buffer solutions used in stepwise wide-range pH test measured with pH Meter V1.1.

Figure 43 shows the sensor voltage response progression throughout the experiment with a 1-hour rolling mean applied to the voltage measurements. This rolling mean was used to reduce noise in the data. Each stage of the experiment is color-coded by the pH of the test solution at a given time. Despite having the same experimental setup as the first variant of the stepwise pH experiment, the sensor responses were different. No asymptotic behavior is evident in the data, and no steady-state voltage is apparent. This experiment took place approximately one week after the first variant in the same location and used the same measuring system (pH Meter V1.1), pH buffer, reference electrodes, and jar apparatuses. The reason that this data shows different behavior compared to all the other experiments is unknown. My hypothesis is that the pH Meter was receiving interference from an outside source related to electromagnetic fields (EMF). The location where the experiments were performed is in the basement of the Engineering Research Center on the CSU Foothills Campus where numerous pieces of large electrical equipment are used. Because the pH Meter V1.1 construction on Perma-Proto boards with no shielding or anti-EMF design incorporated, these boards are especially susceptible to interference. Furthermore, the LMP7721 op-amps have an extremely low input-bias current on the order of femptoamps which may be easily disturbed by an EMF.

The basis of the EMF-interference hypothesis is observations made during the first tests of the pH Meter V1.1 where all meters showed background signals that were correlated. Two of the five pH Meter V1.1s were not used because they showed increased interference from unknown sources. For example, when all five meters were in the same location and attached to different power sources, if one meter was turned on or off, the other four meters showed changes in their measurement signals. This indicated that unintended signals were produced by the meters when they were operating. Despite this anecdotal evidence, no experiment was performed to

measure this phenomenon. Instead, meters and their respective jar-apparatuses were placed inside of Faraday cages. This showed improvement in reducing the background signals but did not alleviate apparent background signal effects entirely.

Despite these various issues in the experiment, the data still shows a trend of decreasing voltage with increasing pH. Figure 44 shows violin plots of the sensor voltage at each pH, as well as the mean marked with "X." Because of the highly variable voltages throughout the stage, and no trend toward an asymptote, the data analyzed was not reduced to the "tails" similar to the first variant of this experiment. Instead, all the measurements in each stage were analyzed. The calibration curve from this experiment is shown for comparison with other curves in Chapter 7 and values are tabulated in Table 9. The analysis output from R is in Appendix C.

Table 9. Voltage Response Data Summary for the Wide pH Range Experiment Performed with the pH Meter V1.1

pH	Mean (mV)	Standard Error of Mean (mV)	Median (mV)
3	381	0.29	381
4	295	0.42	292
5	298	0.59	296
6	283	0.50	276
7	245	0.39	240
8	175	0.55	166
9	187	0.69	179

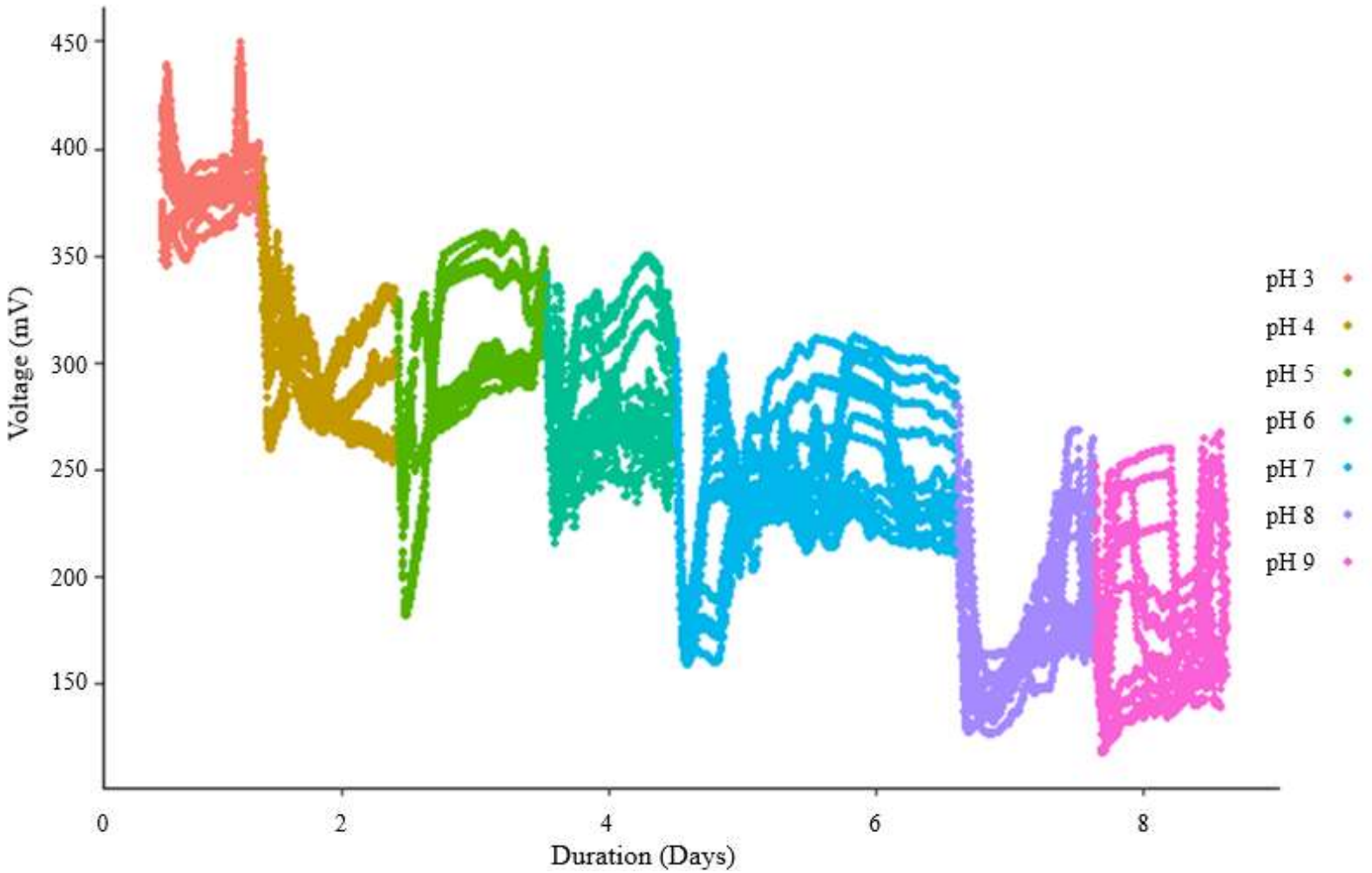

Figure 43. Smoothed 1-hr rolling mean voltage responses of 12 sensors to stepwise wide-range pH test measured on pH Meter V1.1 with each pH stage color-coded.

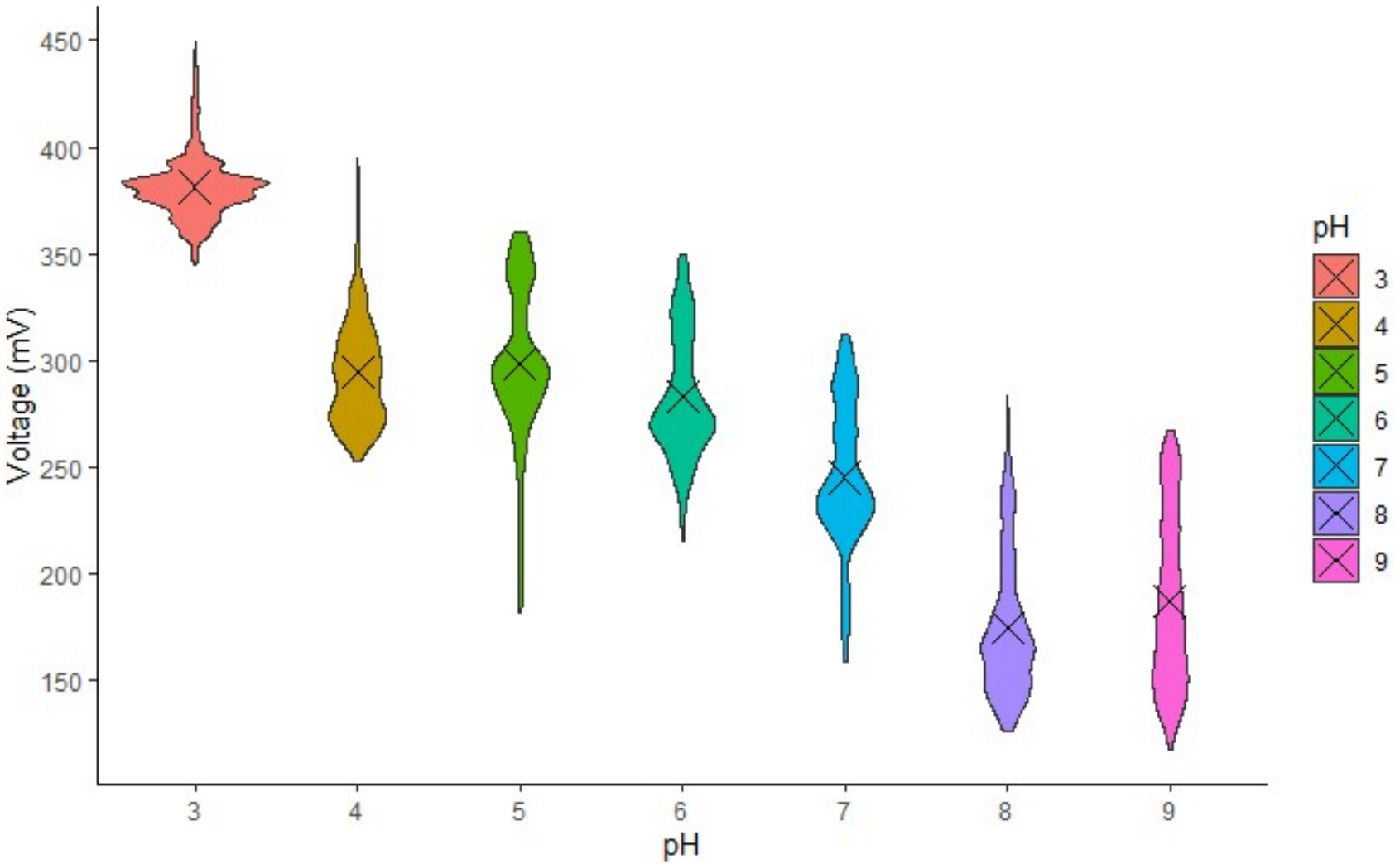

Figure 44. Violin plot (distribution) of smoothed voltage responses of 12 sensors during stepwise wide-range pH test measured on the pH Meter V1.1 with each pH's mean voltage marked with "X."

6.5.3 Third Variant (HP34401A Wide-Range Test)

The third variant of the stepwise pH experiment aimed to remove the issues associated with the pH Meter V1.1 by measuring sensor voltages manually using the HP34401A. The experiment showed significant improvements in data collected with no evidence of background signals. This is interpreted to confirm that the background signals seen in prior tests were associated with the pH meter and not the sensors. Because of the successful measurements in this variant of the experiment, this experiment was carried out over the largest pH range (pH 3 to 11) and time with the experiment first progressing with decreasing pH and then reversing with increasing pH.

Figure 45 shows the 12 sensor voltages during the experiment as well as the pH during each stage. All 12 sensors showed similar voltage responses to each pH change. They typically showed the same trends but exhibited an offset in their absolute voltages, similar to the data from the Static pH experiment and the pH Meter V1.1 pilot test. Agreeing with the other experiments, sensors' voltages tend to increase with a pH decrease. Figure 46 shows the average sensor voltage of each measurement during the experiment with the standard deviation of each measurement. The general trend shows that standard deviations (variability between sensors) decreased with more acidic conditions. This suggests the sensors may be more accurate in generally acidic environments.

Because of the evident asymptotic approach toward a steady-state voltage, this data was again analyzed using the "tails" of each stage. However, because of the manual data measurements, less data was available. Because of this, data was not analyzed by the last hour of measurements; rather, data were analyzed using all data collected after three hours elapsed since

the pH change. This aimed to ensure that the analyzed data was representing the steady-state voltage and not the changes in voltage after a pH change.

Figure 47 shows the tails of the data that were analyzed. Data was also separated into two groups: increasing pH and decreasing pH. This separation allowed analysis of the voltage responses to show if a hysteresis effect is evident in the steady-state voltages. Figure 48 and Figure 49 show the data separated into the increasing and decreasing pH groups. Figure 50 shows violin plots of the voltage distribution for each pH and the mean voltage for each pH represented by an "X." The voltage response curve for the full data, the increasing pH data, and the decreasing pH data, are shown in Figure 51. Values are tabulated in Table 10, and the analysis output from R is in Appendix C.

Table 10. Voltage Response Data Summary for the Wide pH Range Experiment Performed with the HP34401A Multimeter.

pH	Increasing pH			Decreasing pH			All Combined		
	Mean (mV)	Standard Error of Mean (mV)	Median (mV)	Mean (mV)	Standard Error of Mean (mV)	Median (mV)	Mean (mV)	Standard Error of Mean (mV)	Median (mV)
3	433	1.10	434	433	1.10	434	433	1.10	434
4	337	0.54	340	333	0.58	333	340	0.55	337
5	352	0.92	352	352	1.27	351	351	1.30	351
6	300	2.68	287	311	2.23	310	292	3.73	300
7	266	2.92	250	284	2.94	280	257	3.44	265
8	244	2.16	239	253	2.50	250	238	2.95	245
9	226	2.15	236	222	2.57	223	237	3.00	227
10	196	2.91	198	194	5.15	196	198	3.46	197
11	177	4.93	176	N/A	N/A	N/A	177	4.93	176

The sensor response to abrupt pH changes (steps) was analyzed to determine sensor response times and behavior. Because the entire dataset did not show easily identifiable behavior in response to pH changes, only the first five changes were analyzed. These five changes (pH 10

to 9, 9 to 8, 8 to 7, 7 to 6, and 6 to 5) showed similar behavior that looks to be logarithmic in nature and agrees with the asymptotic approaches seen in other data. Figure 52 shows the five analyzed pH steps.

To analyze changes, the average voltage for all 12 sensors was regressed using a logarithmic equation with the best coefficient of determination (R^2). Figure 53 shows the logarithmic regressions for each of the five steps color-coded to represent each change. A sixth regression, shown in black, was performed using all five of the steps overlain to represent a general behavior.

Figure 54 shows the same analysis, but with the X-axis, representing time since the pH change, in log scale. Two outlier data points were removed from the regression analysis, as they did not to represent the general behavior of the response to pH changes. Based on the regression of all the data, shown in black, the sensors will generally increase 40 mV per 1-pH unit change. Though this was not realized in any of the collected data, this change in voltage may be realized given enough time to achieve full equilibration. This may be false if the sensor behavior ceases to follow a logarithmic function. If the logarithmic function approximates the sensor behavior well past the step-change in pH, they will reach 75% of steady-state voltage within 9 hours, 80% within 16 hours, 90% within 44 hours, 95% within 75 hours, and 99% within 113 hours. Though this is not necessarily a true representation of the sensor limitations, this allows a reasonable estimate of time-resolution to be determined.

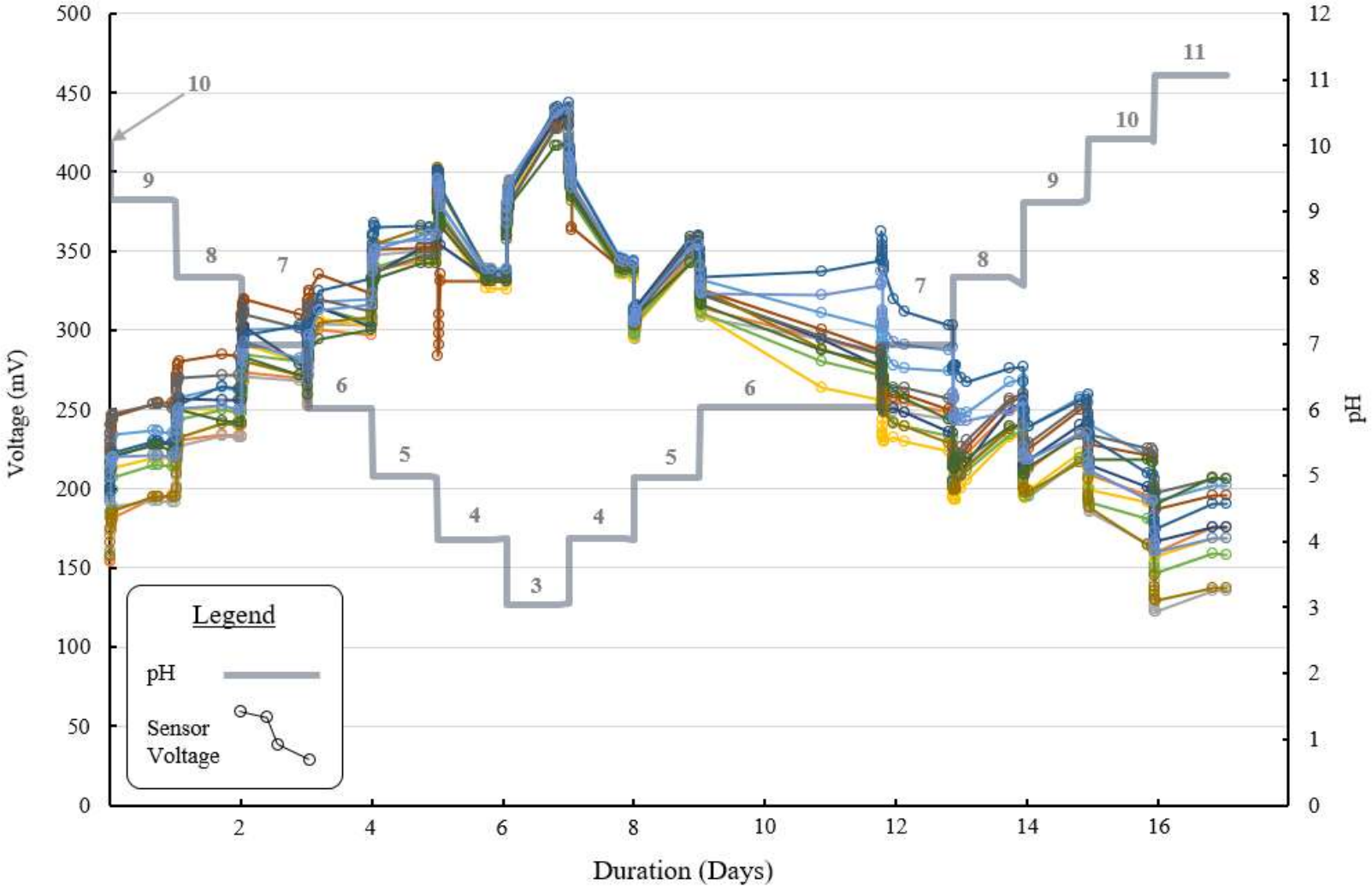

Figure 45. Twelve sensor responses to the stepwise wide-range pH test measured with HP34401A multimeter. pH stages and changes are reflected by the gray line and the axis on the right.

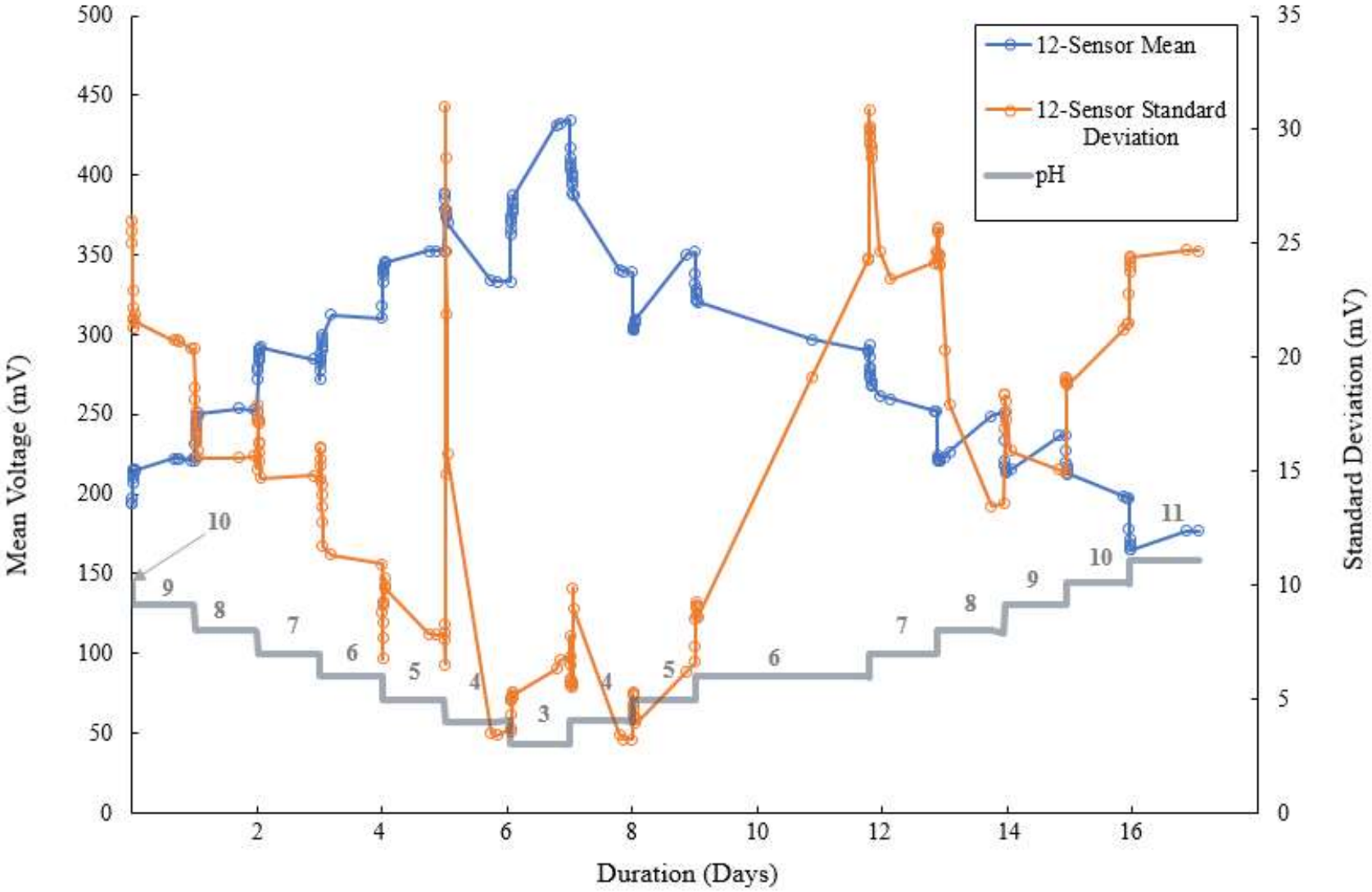

Figure 46. Twelve sensor response statistics through the stepwise wide-range pH test measured with HP34401A multimeter. pH stages and changes are reflected by the gray line and the axis on the right.

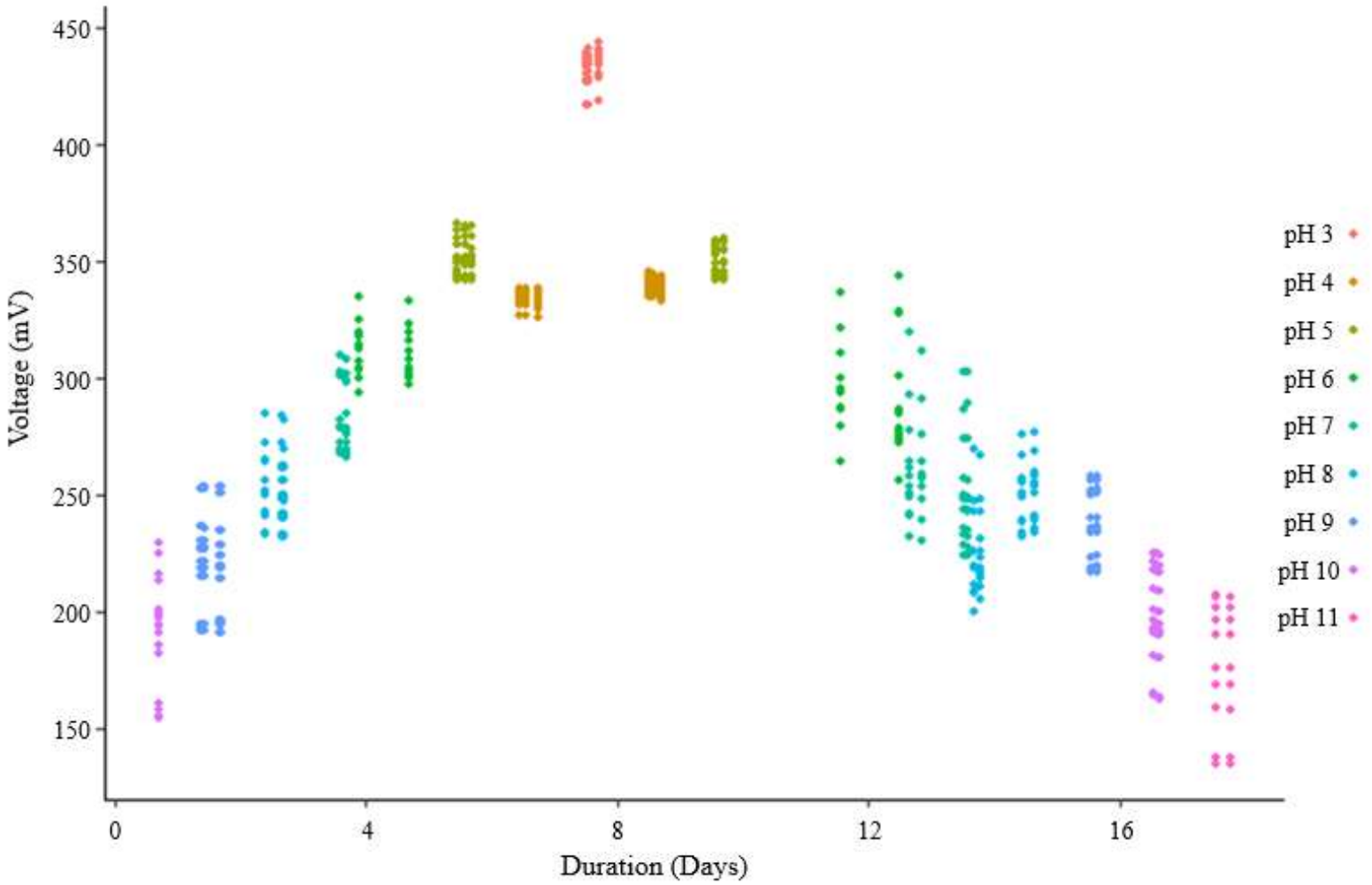

Figure 47. "Tails" of voltage responses of 12 sensors to the stepwise wide-range pH test measured with the HP34401A multimeter.

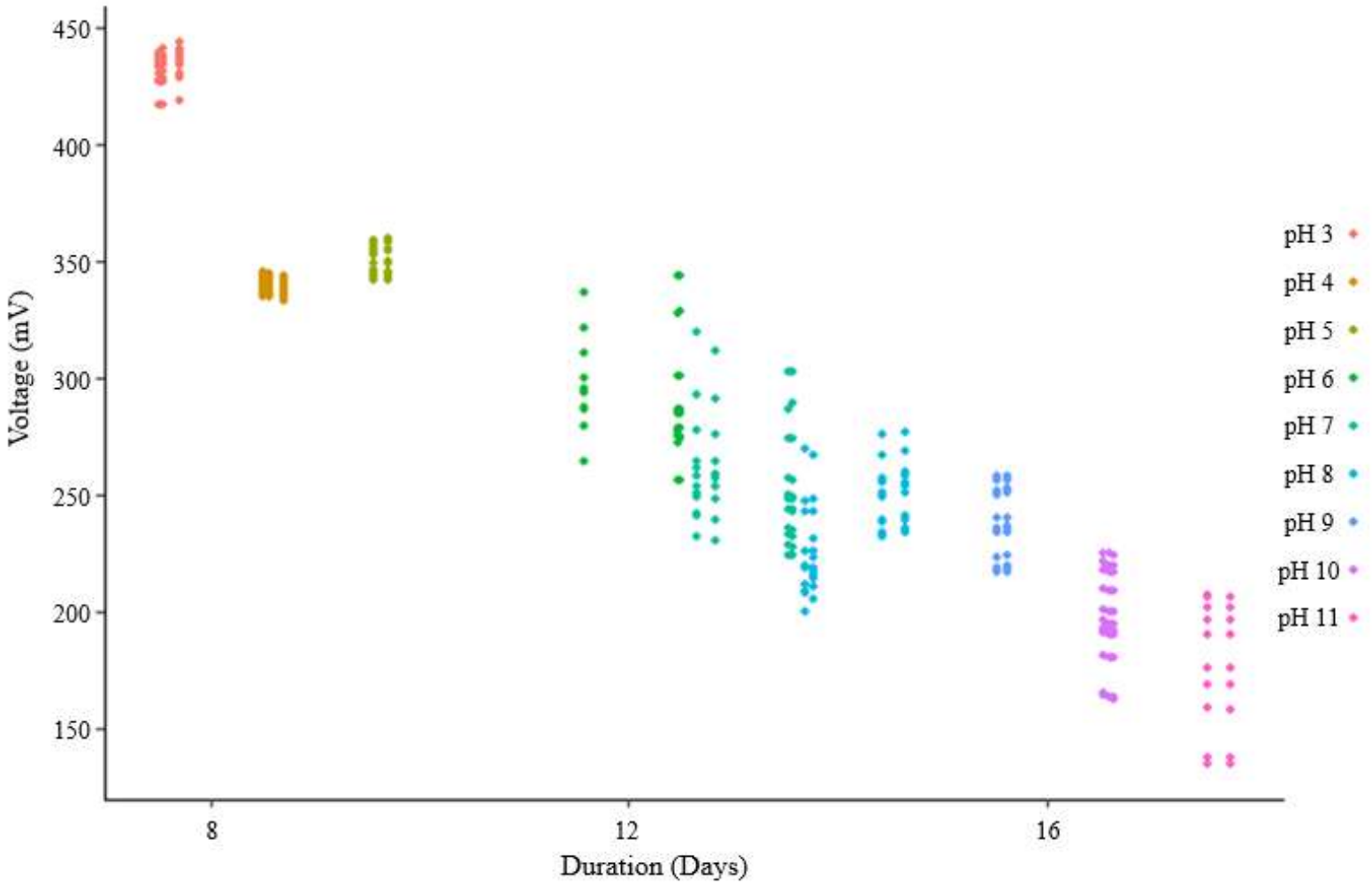

Figure 48. "Tails" of voltage responses of 12 sensors to a stepwise pH increase.

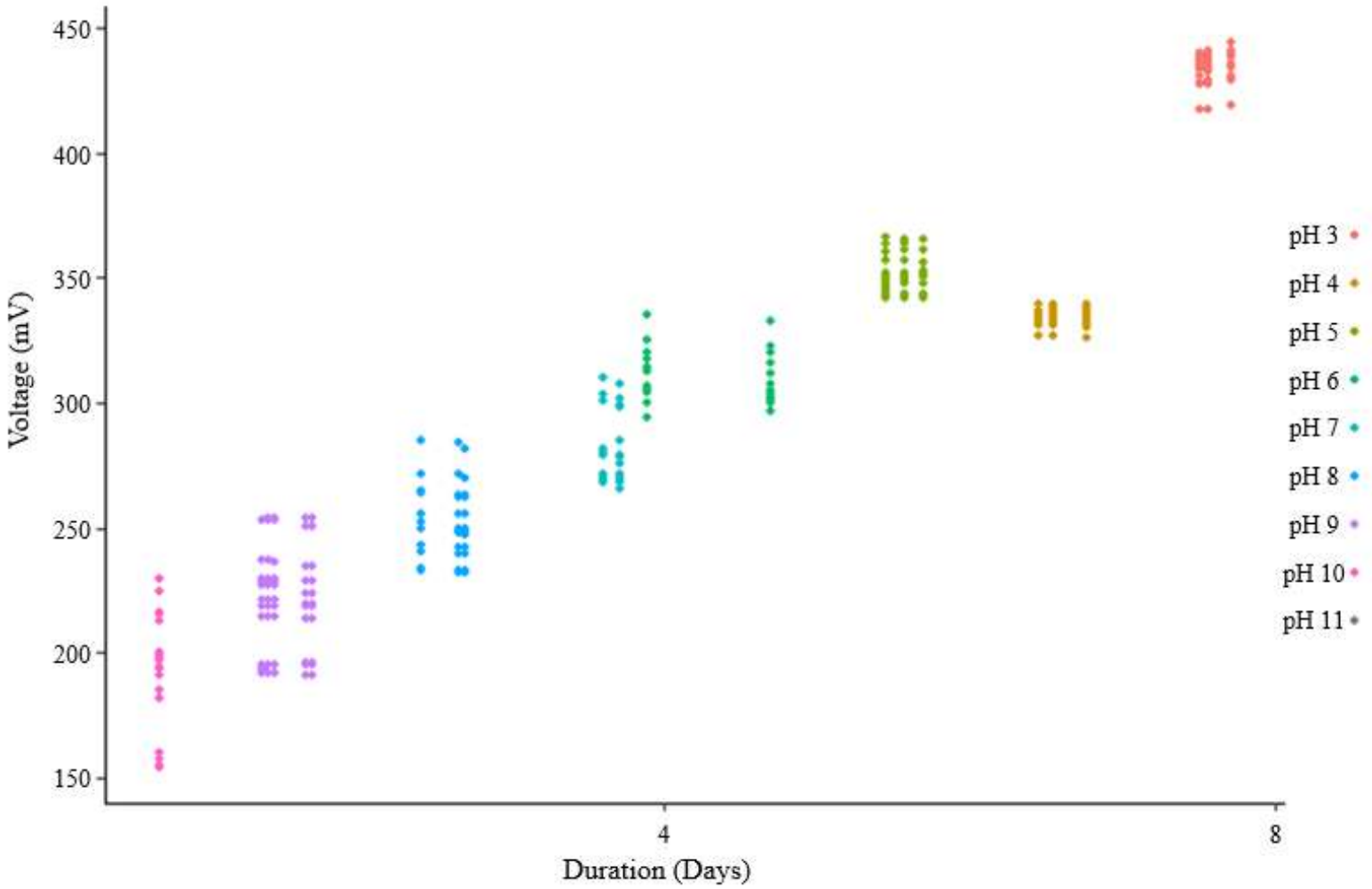

Figure 49. "Tails" of voltage responses of 12 sensors to a stepwise pH decrease.

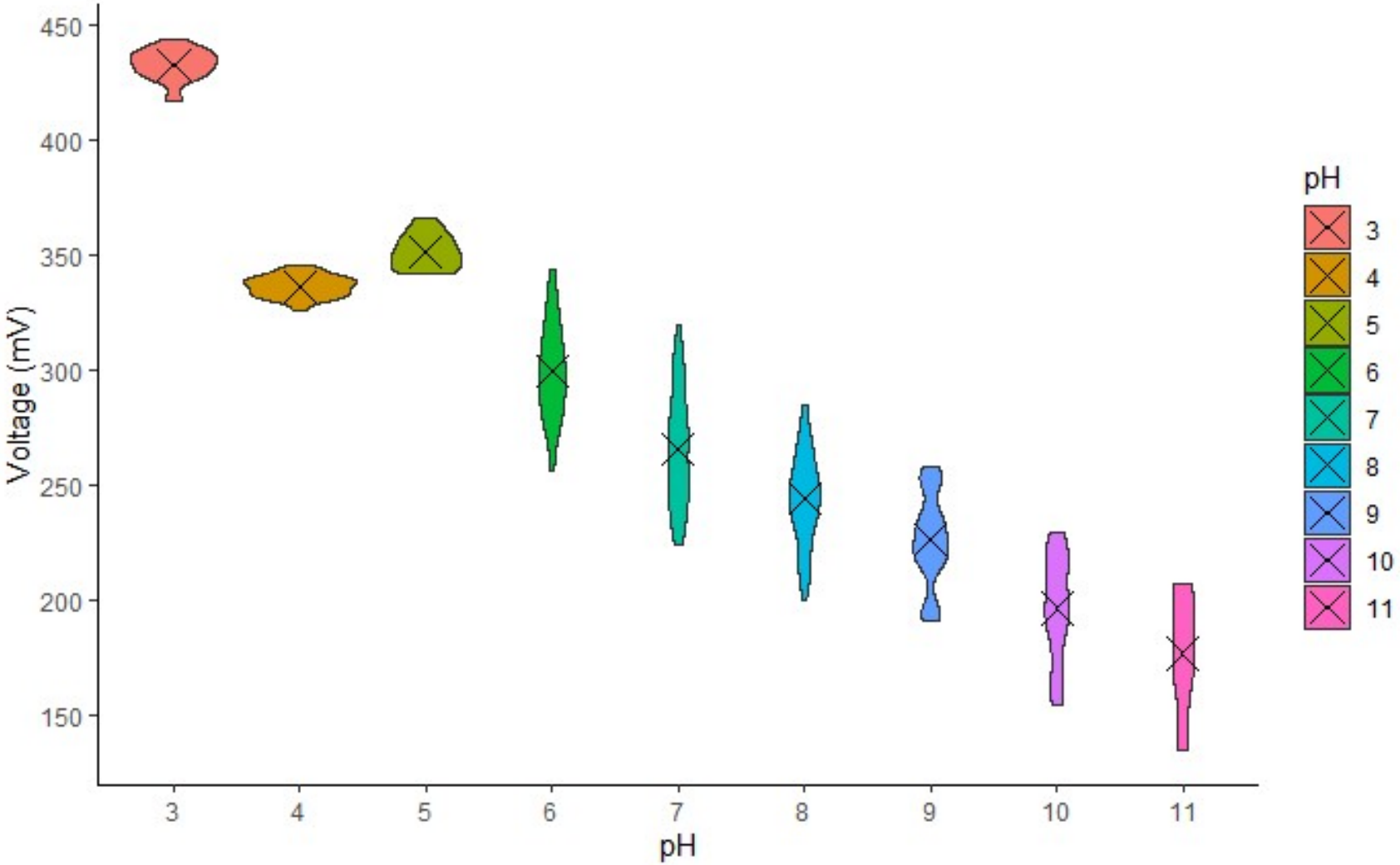

Figure 50. Violin plot (distribution) of voltage response "tails" during stepwise wide-range pH test measured on the HP34401A multimeter with each pH's mean voltage marked with "X."

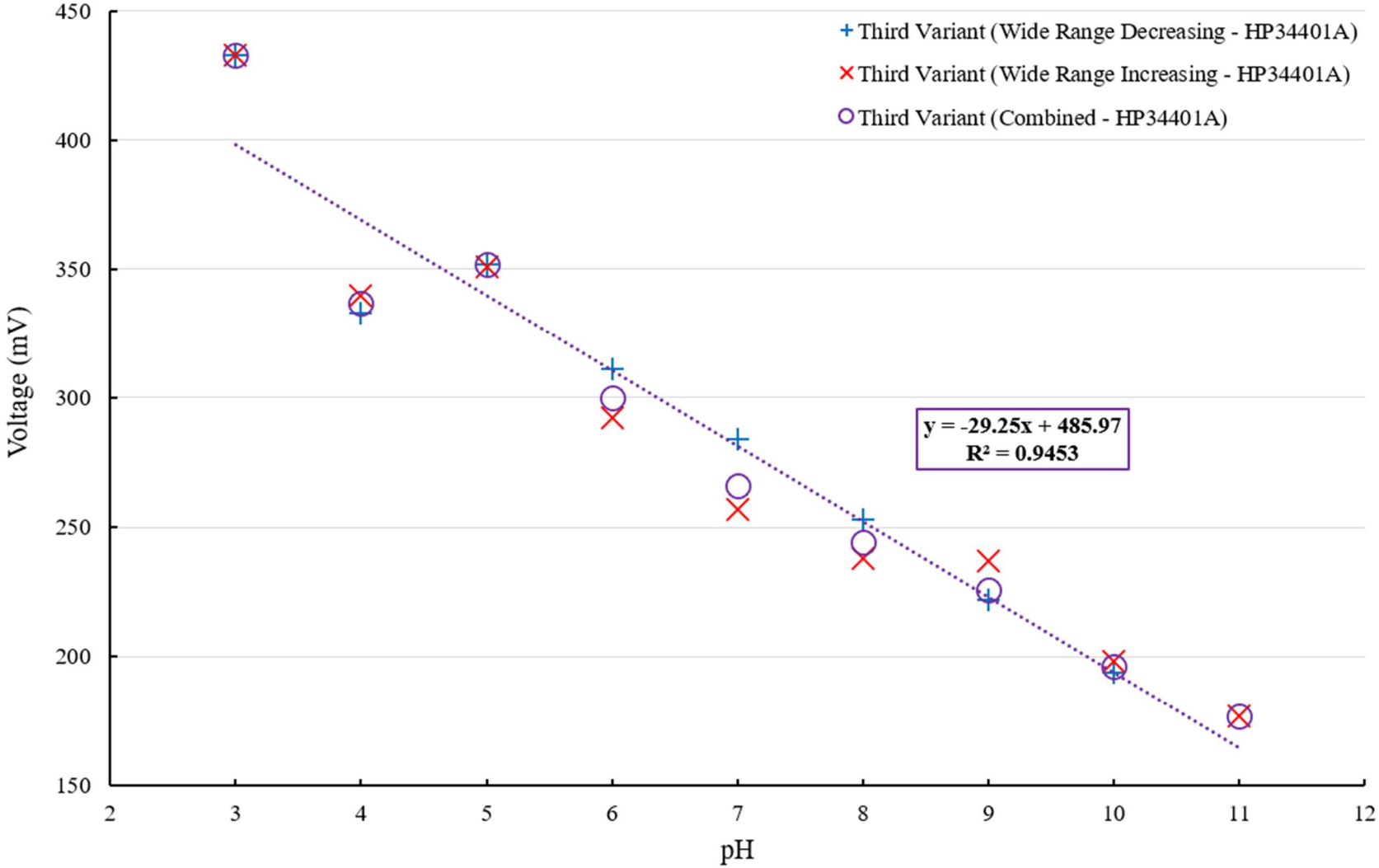

Figure 51. Third variant of the stepwise pH experiment shows very little hysteresis effect with increasing and decreasing pH.

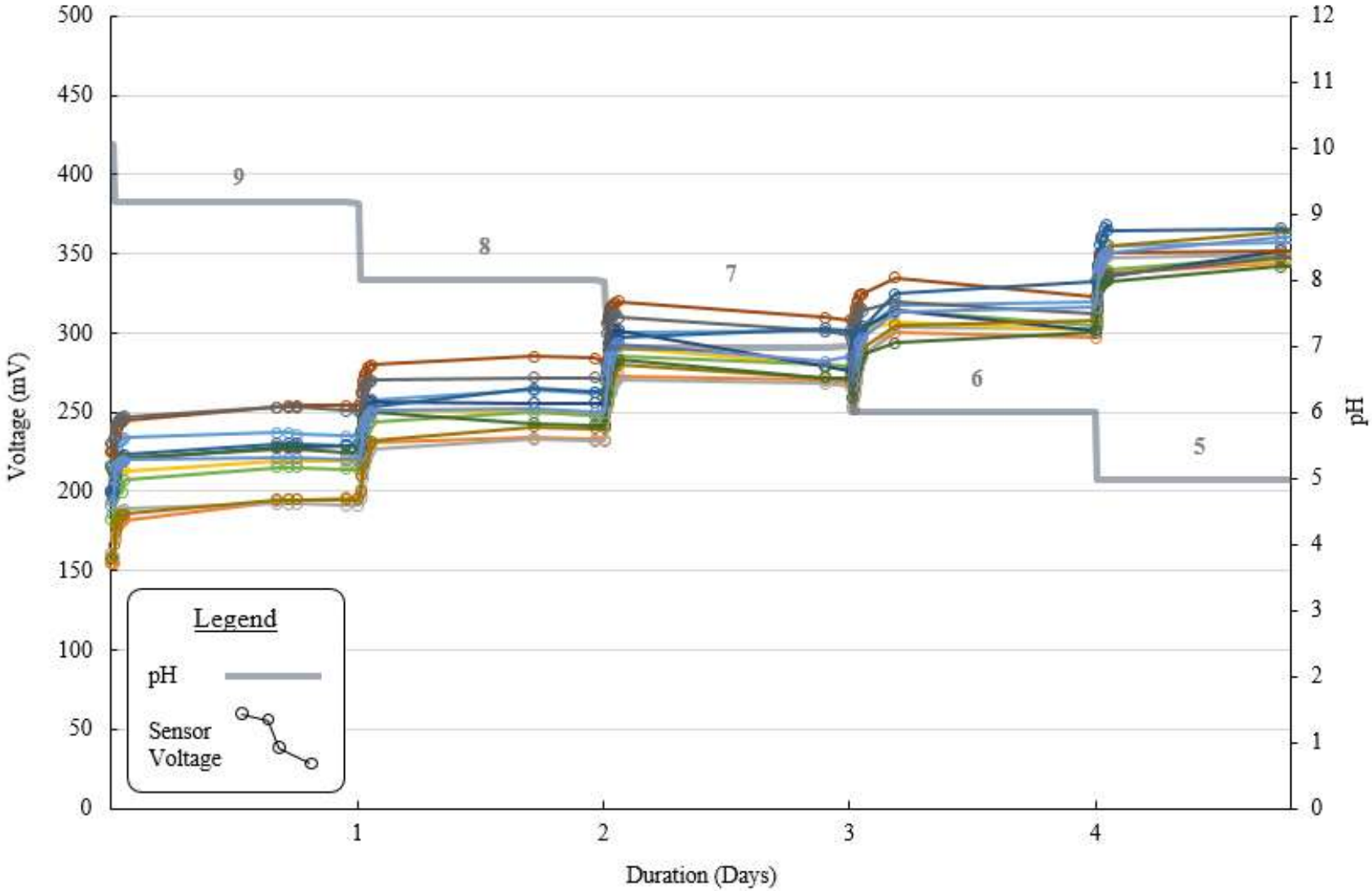

Figure 52. First five pH steps used to analyze response time.

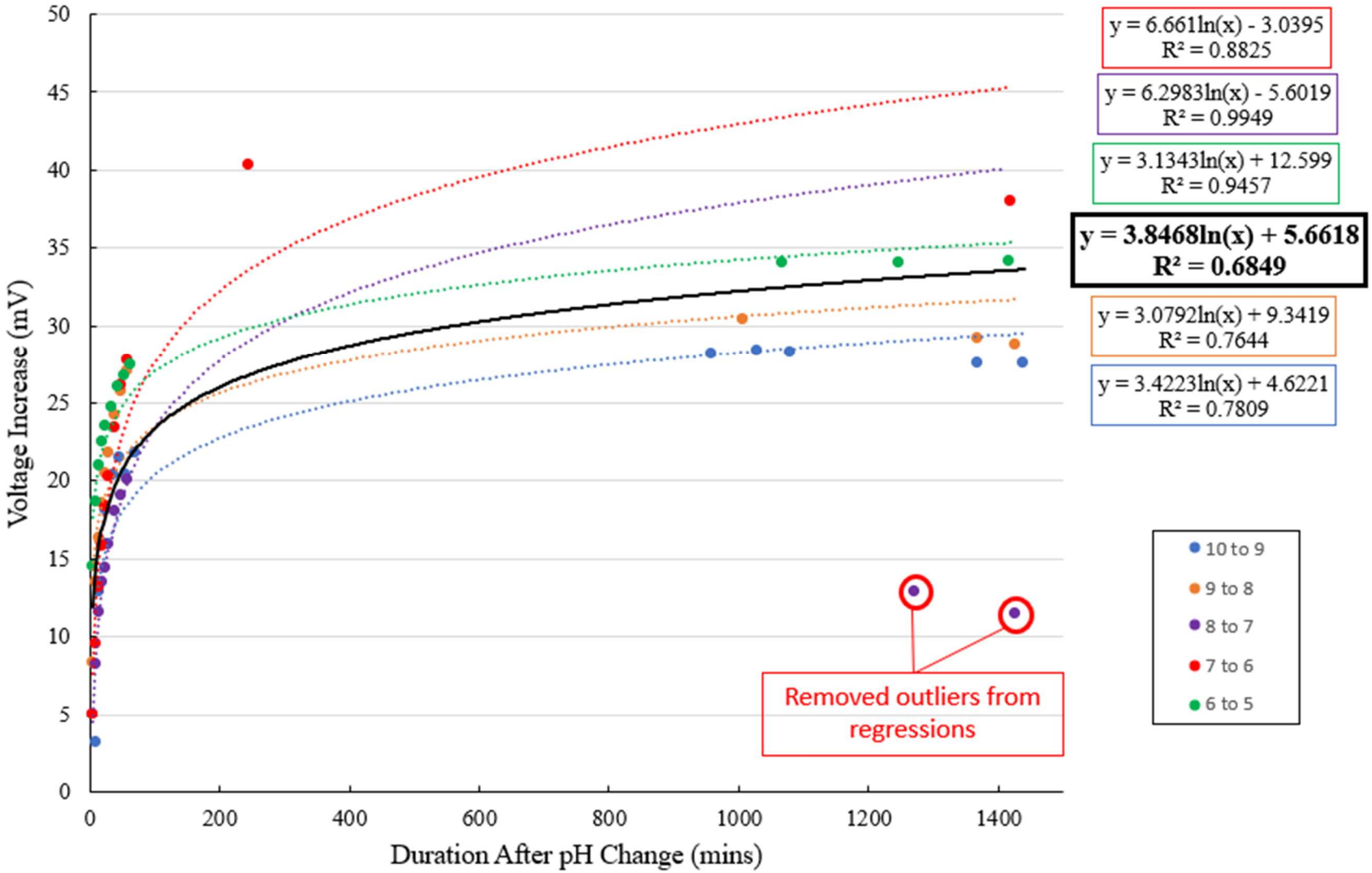

Figure 53. Regression analysis of sensor voltage responses to each of the five pH steps with time on normal scale.

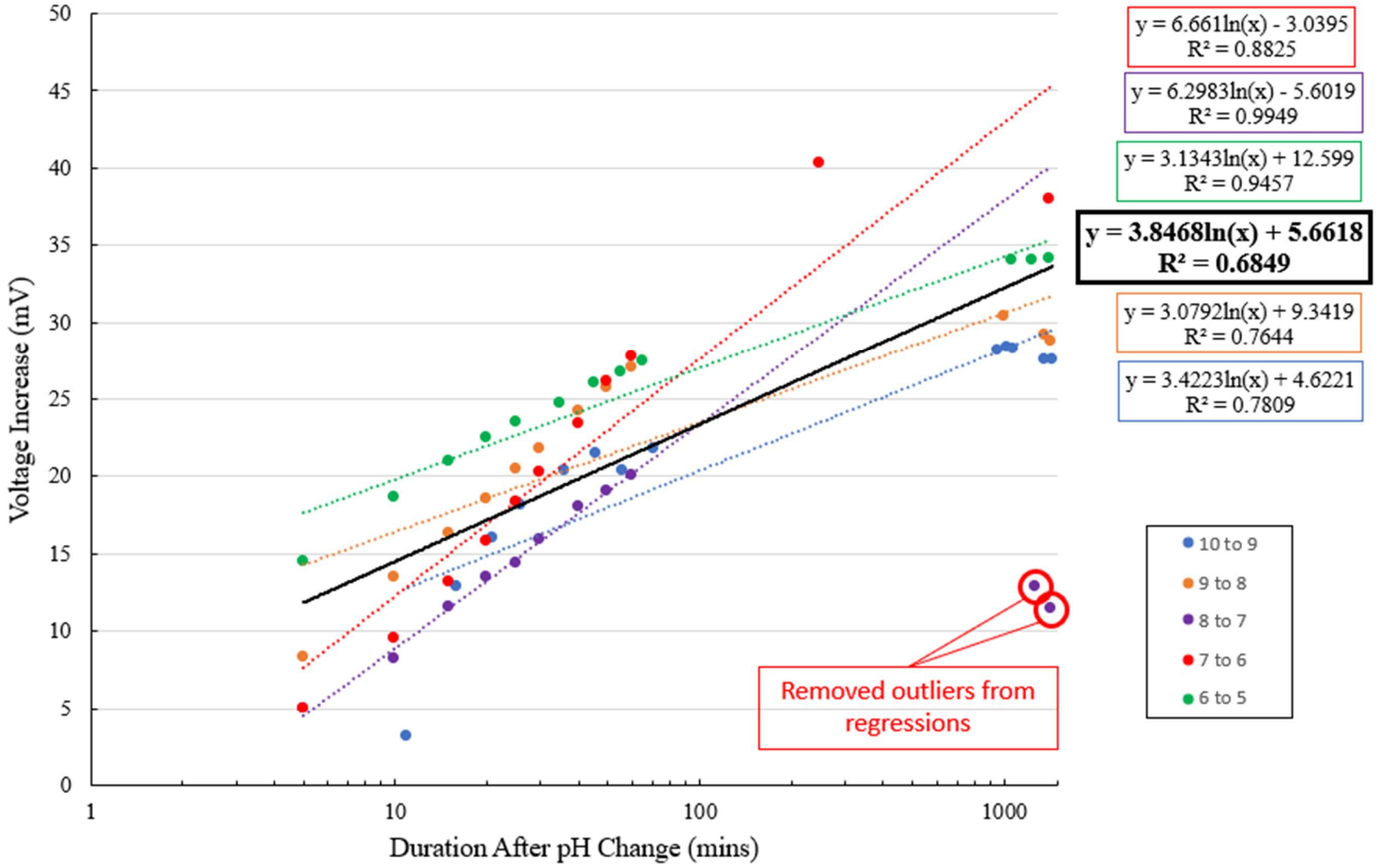

Figure 54. Regression analysis of sensors voltage responses to each of the five pH steps with time on logarithmic scale.

6.6 Sensor Durability Testing

Sensors were tested to determine if the sensors could withstand physical stresses associated with deep deployments in the subsurface up to 200 ft. By placing the sensors in an abrasive, coarse sand and compressing the sand and embedded sensors, the intent was to explore if the sand grains would damage the Nafion^{TM} coating or sensor body. The sensor voltage responses to pH changes were recorded before and after compression and a visual inspection was performed to determine if damage was readily apparent.

Table 11 shows the weights used with the soil oedometer to simulate the total stresses experienced at different depths with a soil dry unit weight of 20 kN/m^3. Sensor voltages were measured using the HP34401A multimeter and are shown in Figure 55 color-coded by simulated depth. Two sensors were used with each of the simulated depths besides the 200 ft (for which only one sensor was tested). One sensor showed abnormally low voltages before compression and was removed from the experiment.

Table 11. Weights Used to Simulate Depths up to 200 ft in the Soil Oedometer.

Simulated Depth (ft)	Simulated Depth (m)	Total Stress (kPa)	Force (N)	Moment-Arm-Applied Mass (kg)	Weights Added Mass (kg)
25	7.62	152	455	46.4	4.6
50	15.2	305	910	92.7	9.3
100	30.5	610	1819	185.4	18.5
150	45.7	914	2729	278.1	27.8
200	61.0	1219	3638	370.9	37.1

A second graph, Figure 56, shows the post-compression voltage plotted against the pre-compression voltage with the measurements grouped by circles indicating their pH. Based on the results of sensor durability tests, sensors appear to have been undamaged by stresses simulating

burial up to 200 ft. If failure occurred, the sensors placed under the highest stresses would show the most abnormal behavior, but the results do not indicate any of the sensors displaying abnormal behavior. Though the voltages after compression were somewhat different than those before compression, there is no trend showing progressive failure with depth. Significantly lower post-compression voltages were observed on all sensors in pH 10 matching behaviors seen in previous experiments where sensors take longer to achieve a steady state voltage in higher pHs. The increased variance in higher pHs matches the results from the third variant of the stepwise pH experiment. No apparent damage was discovered in the visual inspection.

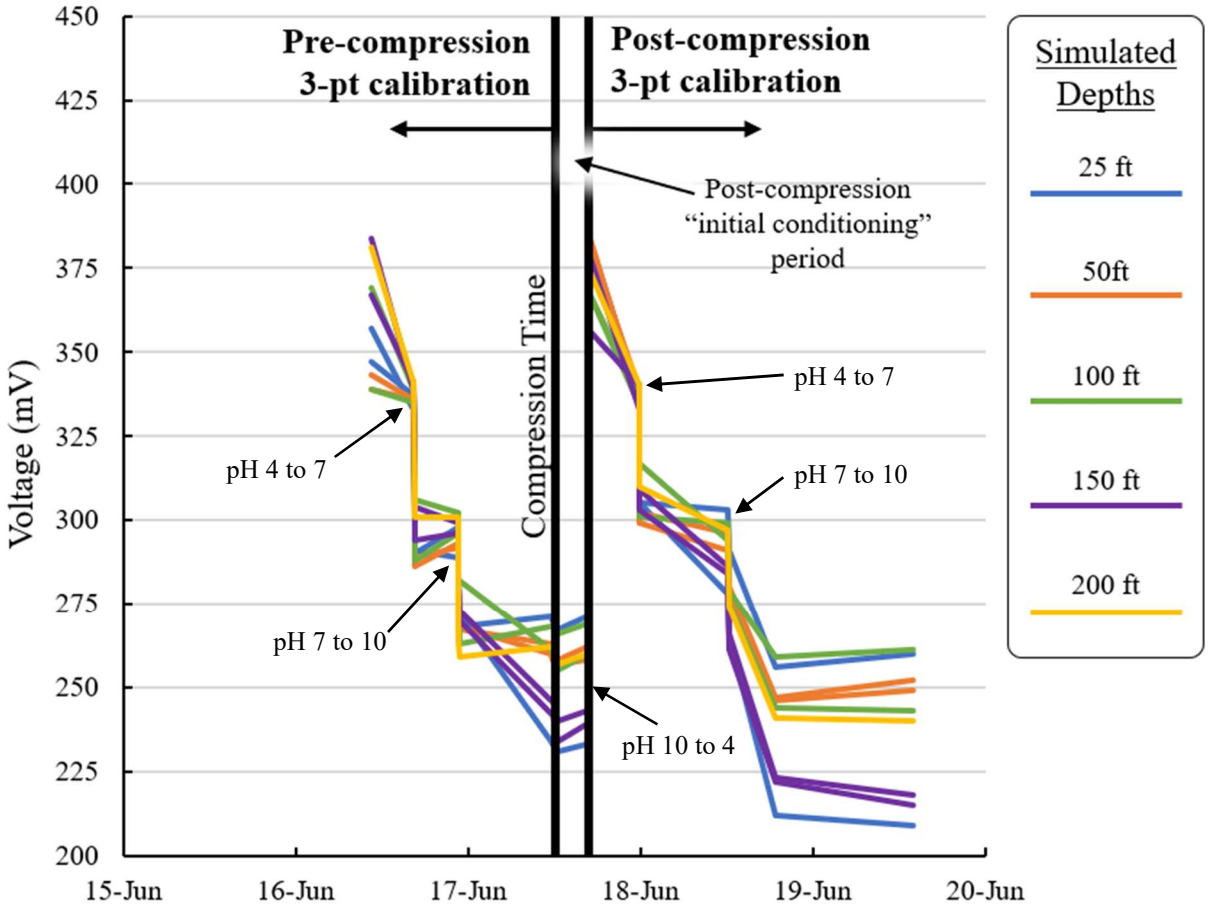

Figure 55. Pre-compression and post-compression sensor voltage responses in pH 4, 7, and 10 after applying normal stresses to simulate depths up to 200 ft.

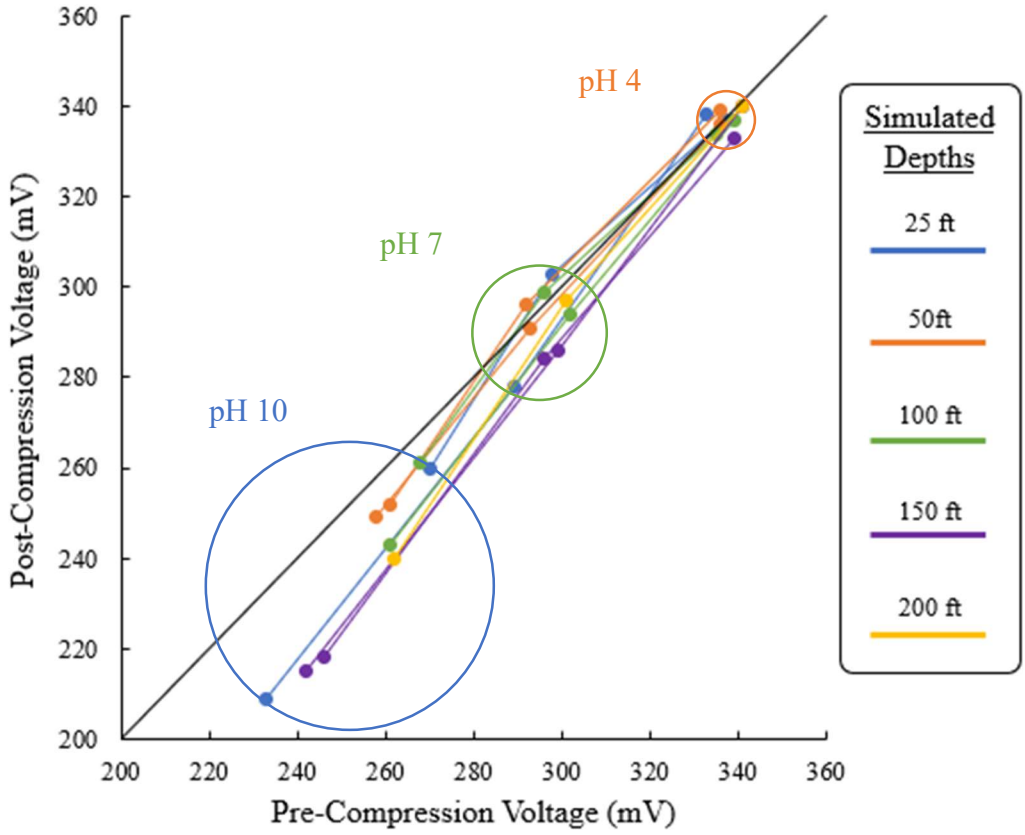

Figure 56. Post-compression voltage plotted against pre-compression voltage for each sensor color-coded by depth showing similar behavior among all simulated depths.

7. SUMMARY AND CONCLUSION

Two objectives were defined at the outset of this work:

1. Develop a robust, low-maintenance, solid-state sensor and IoT-based monitoring system for pH in soil and groundwater;
2. Perform laboratory experiments to characterize and test the pH sensor and monitoring system.

To satisfy Objective 1, a pH sensing electrode was designed and fabricated, shown in Figure 57; developments were made in designing and fabricating an IoT-based monitoring system where two versions of that system, the pH Meter V1.0 and V1.1 were created.

The pH sensor design combines a titanium mixed-metal-oxide electrode (TiMMO), solid epoxy body, and a proton-selective Nafion^{TM} ionomer coating to yield a durable solid-state sensor that is sensitive to aqueous proton activities. As the sensor is exposed to water, the diffusion of aqueous protons through the selective Nafion^{TM} coating causes an increase in voltage on the electrode as compared to a reference electrode. The Nafion^{TM} coating reduces the influence of other ions in the system, creating a proton selective sensor.

The IoT-based pH meters successfully collected voltages from multiple sensors on a set schedule and reported them to a cloud-based database where an online dashboard allowed the data to be viewed in real time. However, there were issues with the reliability of the developed pH meters that introduced uncertainty into the measurements made in these experiments. In hindsight co-development of the sensor and pH meter should have been conducted using high-fidelity measurements as a baseline to compare with. Still, the concept was proven that these sensors can be used in conjunction with an IoT-based system.

To satisfy Objective 2, multiple experiments were performed which have been documented here. As this work was intended to be a first approximation for studying this technology, multiple promising results and points of improvement were discovered, but still, more work must be done to continue advancing toward a field-ready pH sensor and monitoring system.

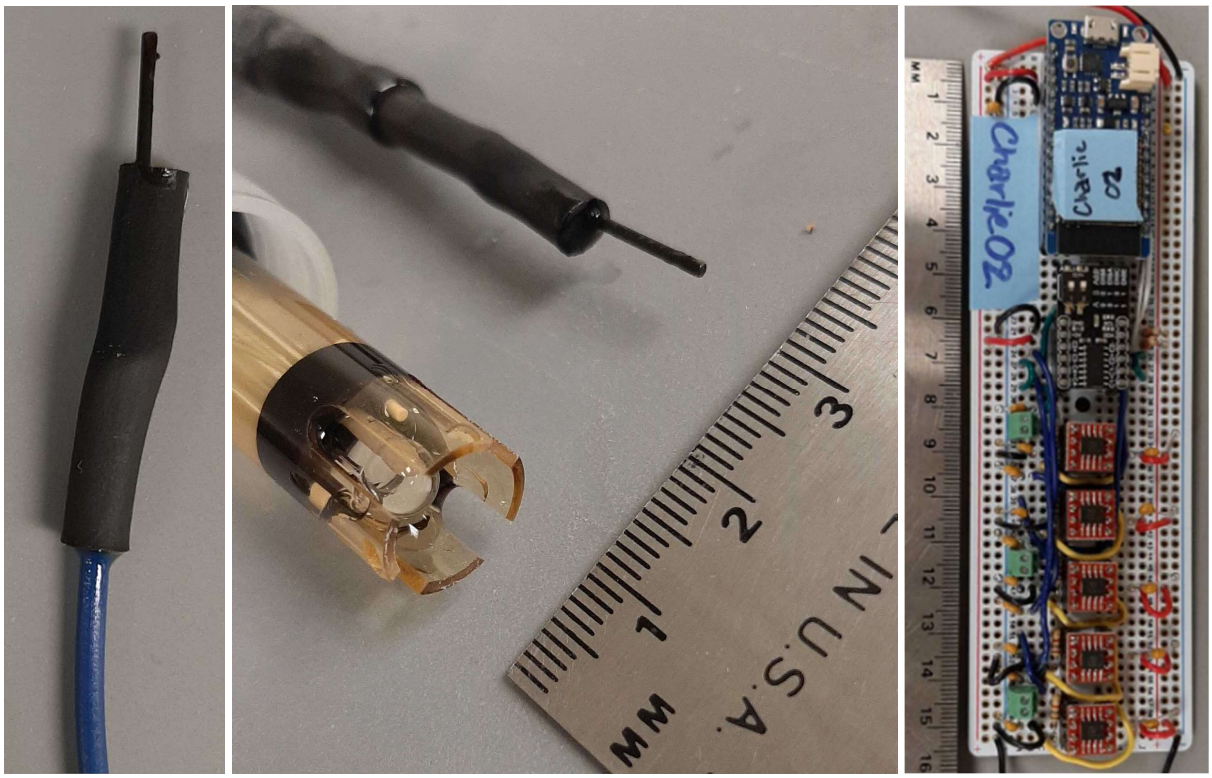

Figure 57. Left: Designed solid-state pH sensor; Middle: Sensor compared to standard glass pH probe; Right: IoT-based pH Meter V1.1

7.1 Data Summary

Using the sensors, different pH-voltage relationships were observed across multiple experiments, and this is most likely due to effects in the measuring system which must be removed or controlled if these sensors are to be used in their intended applications. The most consistent results were produced by the third variant of the stepwise pH experiment which used the HP34401A ultra-high impedance multimeter to take voltage measurements. Data from that

experiment is shown in Figure 58, where a direct pH-voltage relationship of -29 mV/pH was demonstrated across a pH range of 3 to 11. Though this trend was found, inconsistencies in the timing of measurements taken during experiments introduce uncertainty. These preliminary results do, however, give evidence that these sensors can report pH with an accuracy of at least one pH unit, demonstrated with the final stepwise experiment.

These sensors are shown to respond on the order of hours, a reasonable timeframe for groundwater monitoring. Improvements in the design may yield faster response times and improved accuracy. Though ultimate drift after long deployments is not clear, the sensors will show relative changes in pH. Change behavior during stepwise pH changes is approximately logarithmic (Δ_{volt}=3.85ln[t], where Δ_{volt} is the change in millivolts and t is time in minutes). This behavior may be related to the process of proton diffusion through the Nafion^{TM} membrane and adsorption to the electrode surface. Diffusion occurs more quickly at a high concentration gradient (upon a stepwise change) and slows down as the gradient lowers (during equilibration).

Preliminary physical stress tests on the sensors indicated no signs of damage after a simulated 60-m depth deployment in angular sand. Because of the durable solid-state construction, the sensor can likely be deployed in-situ in challenging environments such as in soils where common glass pH sensors are too fragile for use. These results support that this technology is promising for future work.

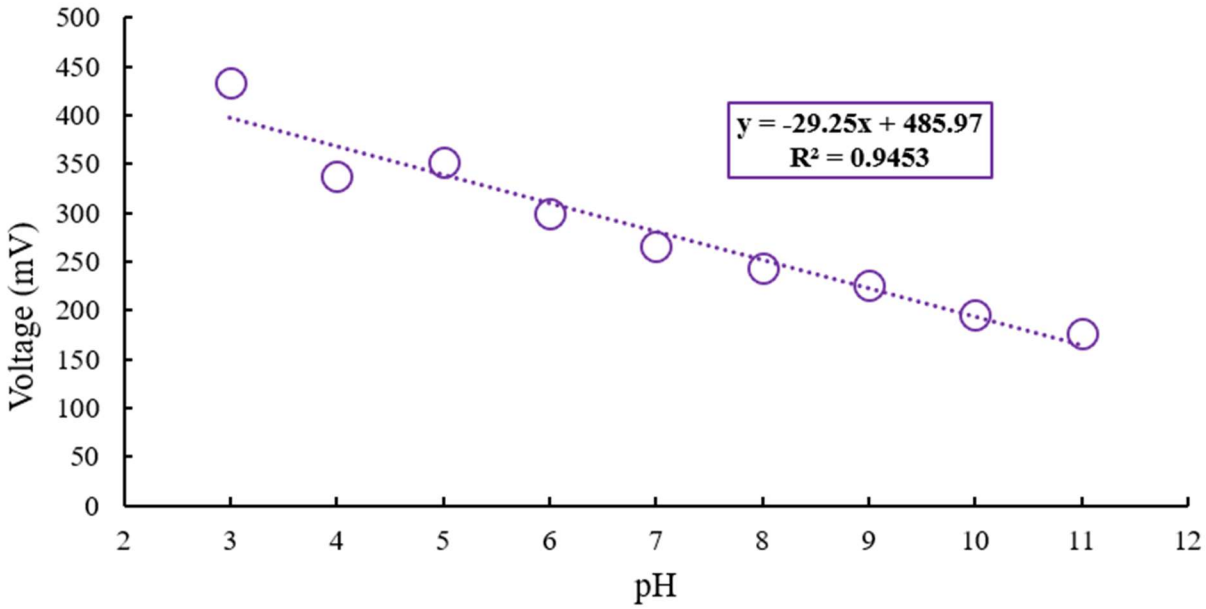

Figure 58. Best pH-voltage relationship demonstrated with TiMMON sensor.

Interestingly, the measured pH-voltage slope is approximately half of the theoretical Nernstian slope of 59 mV/pH. Though there is no conclusive explanation to the approximately half-Nerstian slope, this behavior may indicate that the pH-dependent redox reaction taking place at the electrode surface transfers two electrons for every proton. This is demonstrated in Equations 12 through 14 below for a generic pH-dependent redox reaction.

$$E = E^0 - \frac{2.303RT}{nF}\log_{10}[\mathrm{H}^+] \quad (12)$$

$$E = \text{constant} - \frac{0.059\mathrm{V}}{n}\mathrm{pH} \quad (13)$$

$$E = \frac{-0.059\mathrm{V}}{2}\mathrm{pH} = (-29.5\ \mathrm{mV})\mathrm{pH} \quad (14)$$

Identifying the process taking place at the electrode surface is critical for validating or disproving this idea, and may lead to significant improvements in the design. Some reasonable

processes would include the redox reactions involving iridium and ruthenium oxides, as they are the electrochemically active species coating the titanium substrate in the TiMMON electrode.

7.2 Future Work

Recommended future work includes:

- Develop a reliable and accurate IoT-based pH meter that can be used in the lab and field;
- Improve the fabrication process to improve quality of the Nafion^{TM} coating and ensure standardization between sensors;
- Evaluate more post-fabrication treatment processes that can improve the sensor responses to pH;
- Evaluate sensor responses to other ions, especially other cations;
- Evaluate sensor responses to dehydration and rehydration;
- Resolve the pH dependent redox processes occurring at the electrode surface responsible for the voltage response to pH;
- Evaluate long-term deployments and the need for maintenance or calibration;
- Install and monitor sensors in field settings;
- Evaluate cost-benefit analyses for multiple designs;
- Create analytics that incorporate pH (and pe) sensor data.

7.3 Conclusion

This work advances the pursuit of new biogeochemical monitoring strategies that leverage a high volume of discrete in-situ measurements for near-real-time continuous datastreams. This new strategy, powered by IoT systems, can integrate with smart networks of

multiple components and generate large amounts of data for use in artificial intelligence and machine learning systems while also providing insight into processes that occur at smaller spatial and temporal scales than those understood with current subsurface monitoring strategies. This will aid in the selection and realization of effective remedial strategies and offer better context to understand trends observed in chemical concentrations

pH is a master variable in aqueous and soil chemistry, both an indicator and controller of most chemical reactions and many physical processes that take place in soil and groundwater. pH is important for understanding chemical speciation, mobility, and stability in the soil, while also influencing soil physical properties like soil structure. pH is a parameter of interest to many industries and fields of study including, but not limited to, agriculture, mining, water resources, and engineering. For these reasons, the work presented here is an important contribution toward the future of reliable, high-resolution, insightful pH measurements which will improve the management of biogeochemical systems across multiple industries.

REFERENCES

Bates R. (1964). *Determination of pH: Theory and Practice.* New York: Wiley.

Beer H. (1965). *GB1147442A: Improvements in or relating to electrodes for electrolysis.* United Kingdom Intellectual Property Office.

Böttger W. (1897). "Die Anwendung des Elektrometers als Indikator beim Titrieren von Säuren und Basen." *Zeitschrift für Physikalische Chemie*, vol. 24U, no. 1, pp. 253-301. DOI:10.1515/zpch-1897-2414

Brown, LeMay, Busten, Murphy, and Woodward. (2022). *Chemistry – The Central Science.* Chemistry Libre Texts. https://chem.libretexts.org. Date accessed: 2022-07-08

Christensen T, Bjerg P, Banwart S, Jakobsen R, Heron G, and Albrechtsen HJ. (2000). "Characterization of Redox Conditions in Groundwater Contaminant Plumes." *Journal of Contaminant Hydrology*. 45. DOI:10.1016/S0169-7722(00)00109-1.

Cremer M. (1906). "Origin of electromotor properties of tissues and instructional contribution for polyphasic electrolyte chain." *Z. Biol (Munich)*. 47. 562.

Curtin D, Lousenberg R, Henry T, Tangeman P, and Tisack M. (2004). "Advanced Materials for Improved PEMFC Performance and Life." *J. Power Sources*. 131. DOI:10.1016/j.jpowsour.2004.01.023

Cushman, C. (2021). "Anatomy of pH Electrodes." *YSI.* https://www.ysi.com/ysi-blog/water-blogged-blog/2019/02/anatomy-of-ph-electrodes. Date accessed: 2022-10-27.

Czop M, Motyka J, Sracek O, and Szuwarzynski M. (2011). "Geochemistry of the Hyperalkaline Gorka Pit Lake (pH > 13) in the Chrzanow Region, Southern Poland." *Water, Air, & Soil Pollution*. 214. 423–434. DOI:10.1007/s11270-010-0433-x

Fan Y, Wang X, Funk T, Rashid I, Herman B, Bompoti N, Shaad Mahmud MD, Chrysochoou M, Yang M, Vadas TM, Lei Y, and Li B. (2022). "A Critical Review for Real-Time Continuous Soil Monitoring: Advantages, Challenges, and Perspectives." *Environmental Science & Technology*. 56 (19). 13546-13564. DOI:10.1021/acs.est.2c03562

Fernandez Bordín S, Andrada H, Carreras A, Castellano G, Oliveira R, and Galván Josa V. (2018). "Nafion membrane channel structure studied by small-angle X-ray scattering and Monte Carlo simulations." *Polymer*. 155. DOI:10.1016/j.polymer.2018.09.014.

Ferrie Z. (2020). *Real-Time Visualization of Advective Groundwater Flow*. ProQuest Dissertations Publishing.

Fetter C, Boving T, and Kreamer D. (2018). *Contaminant Hydrogeology 3rd ed.* Long Grove, IL: Waveland Press.

Gilbert D and Sale T. (2005). "Sequential Electrolytic Oxidation and Reduction of Aqueous Phase Energetic Compounds." *Environmental Science & Technology*. 39. DOI:10.1021/es051452k.

Grot W. (2011). *Fluorinated Ionomers 2nd ed.* Waltham, MA, USA: Elsevier.

Grunwald S, Vasques G, and Rivero R. (2015). "Chapter One - Fusion of Soil and Remote Sensing Data to Model Soil Properties." Ed: Sparks D. *Advances in Agronomy.* Academic Press. 131. 1-109. DOI:10.1016/bs.agron.2014.12.004.

Haber F. and Klemensiewicz Z. (1909). "Uber elektrische Phasengrenzkrafte." *Zeitschrift für Physikalische Chemie*, 67U(1). 385-431. DOI:10.1515/zpch-1909-6720.

Irianni Renno M, Akhbari D, Olson M, Byrne A, Lefevre E, Zimbron J, Lyverse M, Sale T, and De Long S. (2016). "Comparison of Bacterial and Archaeal Communities in Depth-Resolved Zones in an LNAPL Body." *Applied Microbiology and Biotechnology*. 100. DOI:10.1007/s00253-015-7106-z.

Karimi Askarani K and Sale T. (2019). "Thermal estimation of natural source zone depletion rates without background correction." *Water Research.* DOI:10.1016/j.watres.2019.115245

Kinlen P, Heider J, and Hubbard D. (1994). "A solid-state pH sensor based on a Nafion-coated iridium oxide indicator electrode and a polymer-based silver chloride reference electrode." *Sensors and Actuators B: Chemical.* 22. DOI:10.1016/0925-4005(94)01254-7

Kitanidis P, McCarty P, and Abriola L. (2012). *Delivery and Mixing in the Subsurface: Processes and Design Principles for In Situ Remediation*. New York: Springer.

Kreuer K, Paddison S, Spohr E, and Schuster M. (2004). "Transport in Proton Conductors for Fuel-Cell Applications: Simulations, Elementary Reactions, and Phenomenology." *Chemical Reviews.* 104. DOI:10.1021/cr020715f.

Kuwertz R, Kirstein C, Turek T, and Kunz U. (2016). "Influence of Acid Pretreatment on Ionic Conductivity of Nafion® Membranes". *Journal of Membrane Science*. 500. DOI:10.1016/j.memsci.2015.11.022.

Lemos S, Nogueira AR, Torre-Neto A, Parra A, and Alonso J. (2007). "Soil Calcium and pH Monitoring Sensor System." *Journal of Agricultural and Food Chemistry*. 55 (12), 4658-4663. DOI:10.1021/jf063746a

Lemos S, Nogueira AR, Torre-Neto A, Parra A, Artigas J, and Alonso J. "In-Soil Potassium Sensor System." (2004). *Journal of Agricultural and Food Chemistry*. 52 (19), 5810-5815. DOI:10.1021/jf0492924

Lindsay W. (1979). *Chemical Equilibria in Soils.* New York: Wiley Interscience.

Maher MH and Shahriari MR. (1993). "A Fiber Optic Chemical Sensor for Measurement of Groundwater pH." *J. Testing and Evaluation*. 21(5). 448–452. DOI:10.1520/JTE11789J

Martin-Hayden J and Robins G. (1997). "Plume Distortion and Apparent Attenuation Due to Concentration Averaging in Monitoring Wells." *Groundwater.* 35. DOI:10.1111/j.1745-6584.1997.tb00091.x

MATCOR. (2022). "MMO Anodes (Mixed Metal Oxide) for Cathodic Protection." https://www.matcor.com/mmo-anodes-mixed-metal-oxide/. Date accessed: 2022-07-08.

Mauritz K and Moore R. (2004). “State of Understanding of Nafion” *Chemical Reviews.* 104. DOI:10.1021/cr0207123.

McBride M. (1994) *Environmental Chemistry of Soils*. New York: Oxford University Press.

McConnell L, Karimi Askarani K, Cognac K, Mack E, Bartlett C, Ronayne M, and Blotevogel J. (2022). “Forecasting Groundwater Contaminant Plume Development Using Statistical and Machine Learning Methods.” *Groundwater Monitoring and Remediation.* DOI:10.1111/gwmr.12523

McHugh T, Kulkarni P, and Newell C. (2016). “Time Vs. Money: A Quantitative Evaluation of Monitoring Frequency vs. Monitoring Duration.” *Groundwater.* DOI: 10.1111/gwat.12407

Merino N, Aronson HS, Bojanova DP, Feyhl-Buska J, Wong ML, Zhang S, and Giovannelli D. (2019). “Living at the Extremes: Extremophiles and the Limits of Life in a Planetary Context.” *Frontiers of Microbiology.* 10. DOI:10.3389/fmicb.2019.00780

Microchip Technology. (2009). *MCP3422/3/4 18-bit, Multi-Channel Analog to Digital Converter with I2C Interface and On-Board Reference Data Sheet.* Microchip Technology.

Mitchell J and Soga K. (2005). *Funamentals of Soil Behavior 3rd ed.* Wiley.

National Research Council. (2013). *Alternatives for Managing the Nation's Complex Contaminated Groundwater Sites.* Washington, DC: The National Academies Press. DOI:10.17226/14668.

Nernst W. (1889). “Die elektromotorische Wirksamkeit der Jonen.” *Zeitschrift für Physikalische Chemie*, 4U(1), 129-181. DOI:10.1515/zpch-1889-0412

Nordstrom D, Alpers C, Ptacek C, and Blowes D. (2000). “Negative pH and Extremely Acidic Mine Waters from Iron Mountain, California.” *Environ. Sci. Technol.* 34. 254–258. DOI:10.1021/es990646v

Nordstrom D, Majzlan J, and Koenigsberger E. (2014). “Thermodynamic Properties for Arsenic Minerals and Aqueous Species.” *Reviews in Mineralogy and Geochemistry.* 79. DOI:10.2138/rmg.2014.79.4.

Overton E, Wetzel D, Wickliffe J, and Adhikari P. (2020). “Spilled Oil Composition and the Natural Carbon Cycle: The True Drivers of Environmental Fate and Effects of Oil Spills.” *Scenarios and Responses to Future Deep Oil Spills.* Editors Murawski S, Ainsworth C, Gilbert S, Hollander D, Paris C, Schluter M, and Wetzel D. Springer, Cham. DOI:10.1007/978-3-030-12963-7_3

Roelofsen H, van Bodegom P, Kooistra L, van Amerongen J, and Witte JP. (2015). “An evaluation of remote sensing derived soil pH and average spring groundwater table for ecological assessments.” *Int. J. Appl. Earth Observation and Geoinformation.* 43. 149-159. DOI:10.1016/j.jag.2015.05.005.

Sale T and Newell C. (2010). *The Dependence of Plumes On Source Zones, Chapter 7 In Situ Remediation Of Chlorinated Solvent Plumes*. Editors H. Ward and H. Stroo. Springer, New York, pp.85-117.

Sale T, Gallo S, Karimi Askarani K, Irriani Renno M, Lyverse M, Hopkins H, Blotevogel J, and Burge S. (2020). “Real-time soil and groundwater monitoring via spatial and temporal resolution of biogeochemical potentials.” *Journal of Hazardous Materials*. 408. DOI:10.1016/j.jhazmat.2020.124403.

Sale T, Hopkins H, and Kirkman A. (2018). *Managing Risk at LNAPL Sites.* American Petroleum Institute Soil and Groundwater Research Bulletin No 18. API.

Sale T and Olson M. (2010). *Field Demonstration/Validation of Electrolytic Reactive Barriers for Energetic Compounds at Pueblo Chemical Depot*. Environmental Security Technology Certification Program ER-200519. United States Department of Defense.

Sale T, Parker B, Newell C, and Devlin J. (2013). *State-of-the-Science-Review: Management of Contaminants Stored in Low Permeability Zones.* SERDP Project ER-1740. United States Department of Defense.

Scholz F. (2011). “From the Leiden jar to the discovery of the glass electrode by Max Cremer.” *J. Solid State Electrochem* 15, 5–14. DOI:10.1007/s10008-009-0962-7

Schwarzenbach R, Gschwend P, and Imboden D. (2016). *Environmental Organic Chemistry.* Hoboken, NJ: Wiley.

Sengupta S and Lyulin A. (2019). “Molecular Modeling of Structure and Dynamics of Nafion Protonation States.” *Journal of Physical Chemistry.* 122. DOI:10.1021/acs.jpcb.9b04534.

Sharma H and Reddy K. (2004). *Geoenvironmental Engineering: Site Remediation, Waste Containment, and Emerging Waste Technologies.* Hoboken, NJ: Wiley.

Sparks D. (2003). *Environmental Soil Chemistry.* Elsevier Science.

Stumm W and Morgan J. (1996). *Aquatic Chemistry: Chemical Equilibria and Rates in Natural Waters.* Wiley Interscience.

Texas Instruments. (2003). *CD74HC4067 16-Channel Analog Multiplexer/Demultiplexer Data Sheet*. Texas Instruments.

Texas Instruments. (2014). *LMP7721 3-Femptoampere Input Bias Current Precision Amplifier Data Sheet*. Texas Instruments.

Thorstenson, D. (1984). “The Concept of Electron Activity and Its Relation to Redox Potentials in Aqueous Geochemical Systems.” United States Geologic Survey. DOI:10.3133/OFR8472

USEPA. (2021). *2019 Toxic Release Inventory National Analysis Complete Report*. United States Environmental Protection Agency.

USEPA. (2022). *List of Lists.* United States Environmental Protection Agency.

USCFR (2022). “Protection of Environment.” *United States Code of Federal Regulations.* National Archives and Records Administration.

Viacheslav A, Morgan M, and Ess D. (2002). *US6356830B1: System and method for automated measurement of soil pH.* United States Patent and Trademark Office.

Viscarra Rossel R, Lobsey C, Sharman C, Flick P, and McLachlan G. (2017). “Novel Proximal Sensing for Monitoring Soil Organic C Stocks and Condition.” *Environmental Science & Technology*. 51 (10), 5630-5641. DOI:10.1021/acs.est.7b00889

Zhang Y and Angelidaki I. (2011). “Submersible microbial fuel cell sensor for monitoring microbial activity and BOD in groundwater: Focusing on impact of anodic biofilm on sensor applicability.” *Biotechnol. Bioeng.* 108. 2339-2347. DOI:10.1002/bit.23204

Hardware

pH Meter V1.0 Details:

This meter used the CD74HC4067 multiplexer for which some of the specs are shown, below. This component was found to have insufficient specs for this project and was removed from the V1.1 design. The MCP3424 Analog-to-Digital Converter was used for both designs and also has some specs listed below. More specs can be found in the datasheets for each component. Because this design was not used for the final research, the circuit design is not shown here.

CD74HC4067 Multiplexer Specs (Texas Instruments 2003):

DC Electrical Specifications

PARAMETER	SYMBOL	TEST CONDITIONS		V_{CC} (V)	25°C			-40°C TO 85°C		-55°C TO 125°C		UNITS
		V_I (V)	V_{IS} (V)		MIN	TYP	MAX	MIN	MAX	MIN	MAX	
HC TYPES												
High Level Input Voltage	V_{IH}	-	-	2	1.5	-	-	1.5	-	1.5	-	V
				4.5	3.15	-	-	3.15	-	3.15	-	V
				6	4.2	-	-	4.2	-	4.2	-	V
Low Level Input Voltage	V_{IL}	-	-	2	-	-	0.5	-	0.5	-	0.5	V
				4.5	-	-	1.35	-	1.35	-	1.35	V
				6	-	-	1.8	-	1.8	-	1.8	V
Maximum "ON" Resistance I_O = 1mA	R_{ON}	V_{CC} or GND	V_{CC} or GND	4.5	-	70	160	-	200	-	240	Ω
				6	-	60	140	-	175	-	210	Ω
		V_{CC} to GND	V_{CC} to GND	4.5	-	90	180	-	225	-	270	Ω
				6	-	80	160	-	200	-	240	Ω
Maximum "ON" Resistance Between Any Two Switches	ΔR_{ON}	-	-	4.5	-	10	-	-	-	-	-	Ω
				6	-	8.5	-	-	-	-	-	Ω
Switch "Off" Leakage Current 16 Channels	I_{IZ}	$\overline{E}$ = V_{CC}	V_{CC} or GND	6	-	-	±0.8	-	±8	-	±8	µA
Logic Input Leakage Current	I_I	V_{CC} or GND	-	6	-	-	±0.1	-	±1	-	±1	µA

Red highlighted specs indicate resistance (impedance) is too low and leakage current is too high for this application which requires resistance on the order of mega-ohm to giga-ohms and no leakage current between sensors.

MCP3424 Analog-to-Digital Converter Specs (Microchip Technology 2009):

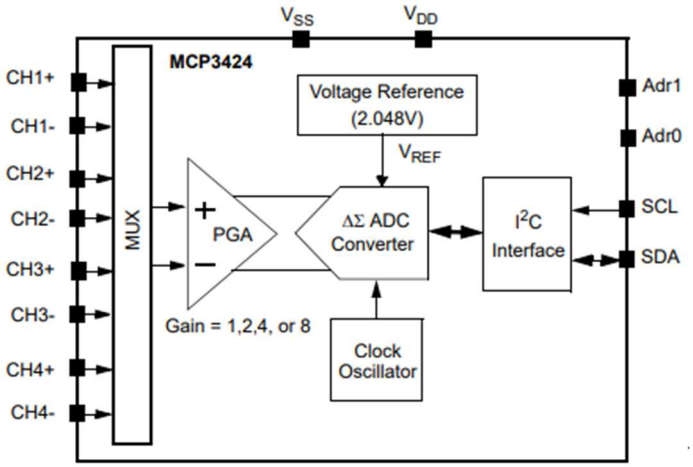

Figure 59. MCP3424 functional block diagram

Electrical Specifications: Unless otherwise specified, all parameters apply for T_A = -40°C to +85°C, V_{DD} = +5.0V, V_{SS} = 0V, CHn+ = CHn- = V_{REF}/2, V_{INCOM} = V_{REF} /2. All ppm units use 2*V_{REF} as differential full scale range.

Parameters	Sym	Min	Typ	Max	Units	Conditions
Analog Inputs						
Differential Full Scale Input Voltage Range	FSR	—	±2.048/PGA	—	V	V_{IN} = [CHn+ - CHn-]
Maximum Input Voltage Range		V_{SS}-0.3	—	V_{DD}+0.3	V	**(Note 1)**
Differential Input Impedance	Z_{IND} (f)	—	2.25/PGA	—	MΩ	During normal mode operation **(Note 2)**
Common Mode input Impedance	Z_{INC} (f)	—	25	—	MΩ	PGA = 1, 2, 4, 8
System Performance						
Resolution and No Missing Codes (Effective Number of Bits) **(Note 3)**		12	—	—	Bits	DR = 240 SPS
		14	—	—	Bits	DR = 60 SPS
		16	—	—	Bits	DR = 15 SPS
		18	—	—	Bits	DR = 3.75 SPS
Data Rate **(Note 4)**	DR	176	240	328	SPS	12 bits mode
		44	60	82	SPS	14 bits mode
		11	15	20.5	SPS	16 bits mode
		2.75	3.75	5.1	SPS	18 bits mode
Output Noise		—	1.5	—	μV_{RMS}	T_A = +25°C, DR = 3.75 SPS, PGA = 1, V_{IN}+ = V_{IN}- = GND
Integral Non-Linearity	INL	—	10	35	ppm of FSR	DR = 3.75 SPS, FSR = Full Scale Range **(Note 5)**
Internal Reference Voltage	V_{REF}	—	2.048	—	V	
Gain Error **(Note 6)**		—	0.05	0.35	%	PGA = 1, DR = 3.75 SPS

Red highlighted specs indicate impedance is too low without the op-amp (must exceed at least 10 Mohm), but the input voltage range is sufficient. The up-to 18-bit resolution allows for (2.048V x 2)/2^18 = 16 microvolt resolution.

pH Meter V1.1 Details:

This design, the final design of this work, was implemented on a Perma-Proto soldered breadboard. The circuit design for that board is shown on the following page. The multiplexer was removed from the circuit. The LMP7721 op-amp was included in this design, and some of the specs are shown below. More specs for this component can be found in the datasheet (Texas Instruments 2014).

LMP7721 3-Femptoampere Input Bias Current Precision Amplifier Specs (Texas Instruments 2014):

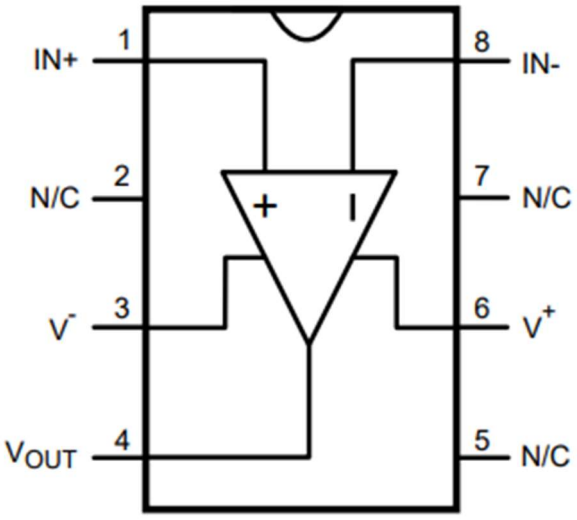

Figure 60. LMP7721 functional block diagram

Unless otherwise specified, all limits are specified for T_A = 25°C, V^+ = 2.5 V, V^- = 0 V, V_{CM} = (V^+ + V^-)/2.

PARAMETER		TEST CONDITIONS		MIN(1)	TYP(2)	MAX(1)	UNIT
V_{OS}	Input Offset Voltage			–180	±50	180	µV
		–40°C ≤ T_J ≤ 125°C		–480		480	
TC V_{OS}	Input Offset Voltage Drift (3)				–1.5	–4	µV/°C
I_{BIAS}	Input Bias Current	V_{CM} = 1 V(4) (5)	25°C	–20	±3	20	fA
			–40°C to 85°C	–900		900	
			–40°C to 125°C	–5		5	pA
I_{OS}	Input Offset Current	V_{CM} = 1 V(5)			±6	±40	fA
CMRR	Common-Mode Rejection Ratio	0 V ≤ V_{CM} ≤ 1.4 V		83	100		dB
		0 V ≤ V_{CM} ≤ 1.4 V, –40°C ≤ T_J ≤ 125°C		80			
PSRR	Power Supply Rejection Ratio	1.8 V ≤ V^+ ≤ 5.5 V, V^- = 0 V, V_{CM} = 0		84	92		dB
		1.8 V ≤ V^+ ≤ 5.5 V, V^- = 0 V, V_{CM} = 0, –40°C ≤ T_J ≤ 125°C		80			
CMVR	Input Common-Mode Voltage Range	CMRR ≥ 80 dB		−0.3		1.5	V
		CMRR ≥ 78 dB, –40°C ≤ T_J ≤ 125°C		–0.3		1.5	
A_{VOL}	Large Signal Voltage Gain	V_O = 0.15 V to 2.2 V, R_L = 2 kΩ to V^+/2		88	107		dB
		V_O = 0.15 V to 2.2 V, R_L = 2 kΩ to V^+/2, –40°C ≤ T_J ≤ 125°C		82			
		V_O = 0.15 V to 2.2 V, R_L = 10 kΩ to V^+/2		92	120		
		V_O = 0.15 V to 2.2 V, R_L = 10 kΩ to V^+/2, –40°C ≤ T_J ≤ 125°C		88			
V_O	Output Swing High	R_L = 2 kΩ to V^+/2		70	25		mV from V^+
		R_L = 2 kΩ to V^+/2, –40°C ≤ T_J ≤ 125°C		77			
		R_L = 10 kΩ to V^+/2		60	20		
		R_L = 10 kΩ to V^+/2, –40°C ≤ T_J ≤ 125°C		66			
	Output Swing Low	R_L = 2 kΩ to V^+/2			30	70	mV
		R_L = 2 kΩ to V^+/2, –40°C ≤ T_J ≤ 125°C				73	
		R_L = 10 kΩ to V^+/2			15	60	
		R_L = 10 kΩ to V^+/2, –40°C ≤ T_J ≤ 125°C				62	
I_O	Output Short Circuit Current	Sourcing to V^-, V_{IN} = 200 mV (6)		36	46		mA
		Sourcing to V^-, V_{IN} = 200 mV (6), –40°C ≤ T_J ≤ 125°C		30			
		Sinking to V^+, V_{IN} = −200 mV (6)		7.5	15		
		Sinking to V^+, V_{IN} = −200 mV (6), –40°C ≤ T_J ≤ 125°C		5.0			
I_S	Supply Current				1.1	1.5	mA
		–40°C ≤ T_J ≤ 125°C				1.75	
SR	Slew Rate	A_V = +1, Rising (10% to 90%)			9.3		V/µs
		A_V = +1, Falling (90% to 10%)			10.8		
GBW	Gain Bandwidth Product				15		MHz
e_n	Input-Referred Voltage Noise	f = 400 Hz			8		nV/√Hz
		f = 1 kHz			7		

Red highlighted specs indicate the input bias current, the current drawn from the sensors, is typically +/- 3 fA, the lowest in the industry. This is not enough current to drain the sensors and cause a voltage drop, meaning that this op-amp can be used to maintain the sensor voltage during measurements.

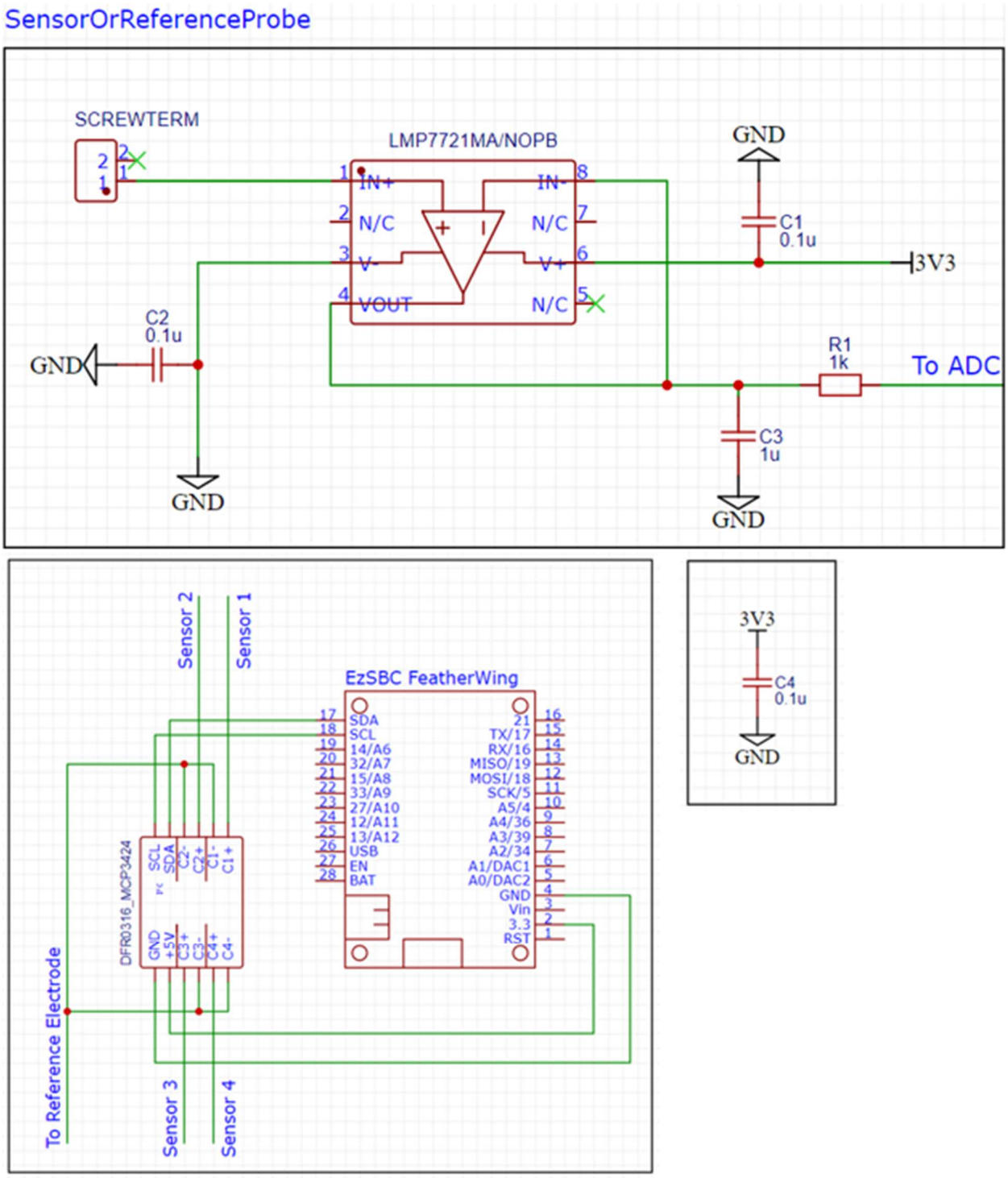

Figure 61. pH Meter V1.1 circuit design.

Proposed pH Meter V1.1 Printed Circuit Board Design:

A printed circuit board preliminary design was made for the pH Meter V1.1, shown in Figure 62 and Figure 63, but the PCB was never created. This is the same circuit design as the prototype version, but adds an SMA-adaptor for connecting a coaxial cable (if the sensor uses coaxial cable) and guard traces on the PCB for guarding the sensor input.

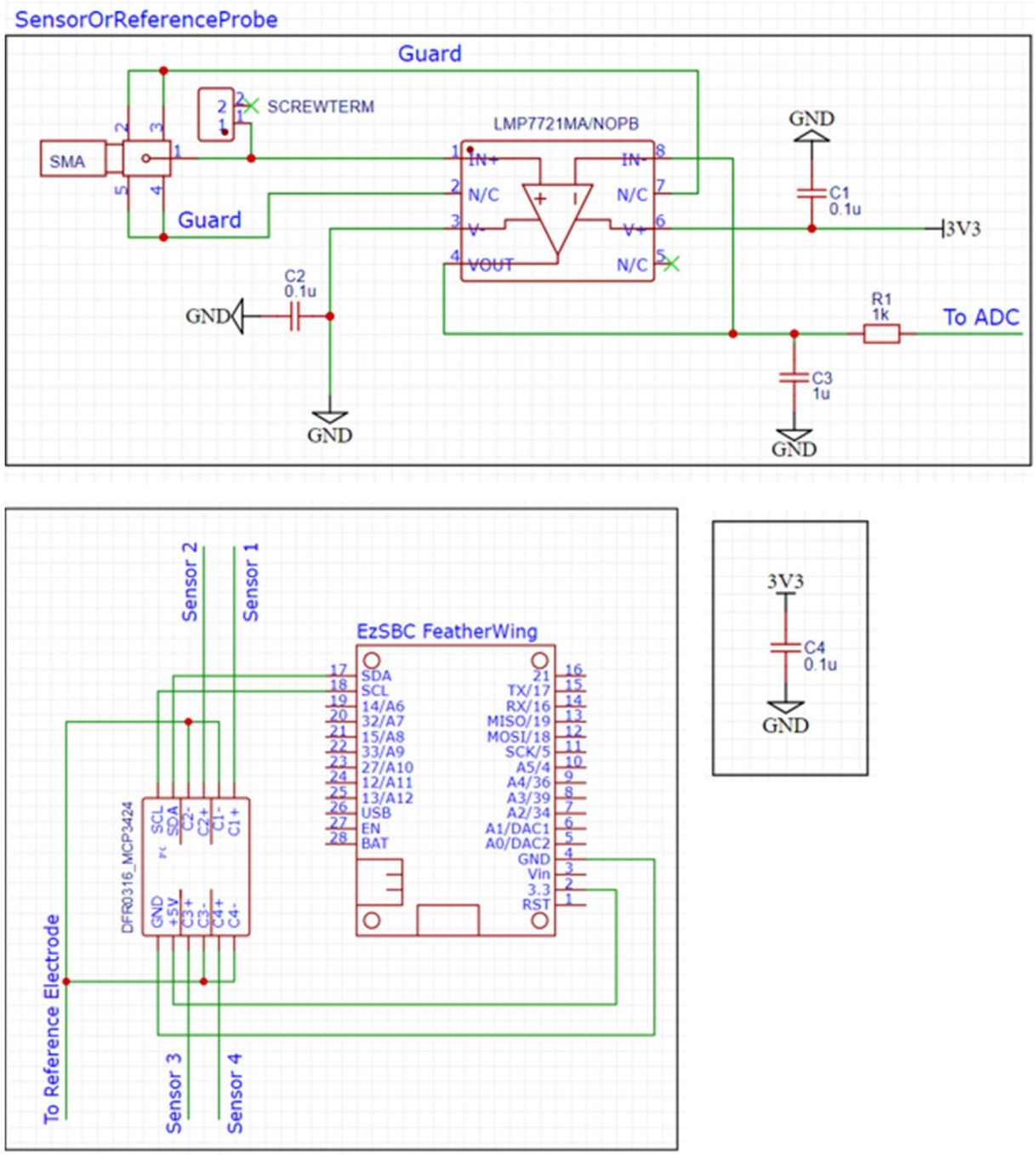

Figure 62. Proposed printed circuit board design for pH Meter V1.1

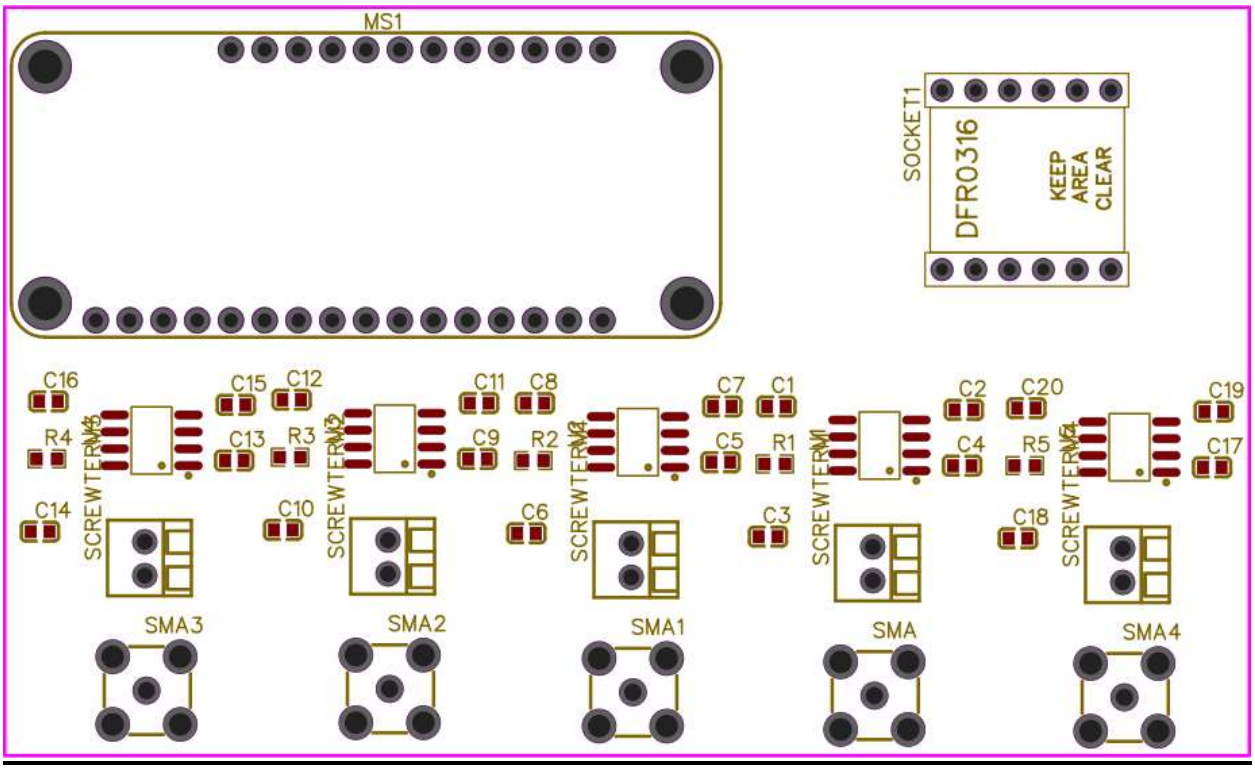

Figure 63. Proposed printed circuit board layout.

Firmware

Contact Charles VanTilburg for more information about this code.

Plain text of pH Meter V1.1 source code:

```
/* Title:   ESP32-MCP3424-Mux-Ubidots
 * Author:  Charles VanTilburg IV with assistance from Prof. Jay Ham (CSU)
 * Date:    Spring 2022
 * Purpose: Using EZSBC Feather ESP32 microcontroller board, take 5
samples of 4 voltages using 18-bit external analog-to-digital converter
(MCP3424).
 * Then, report the data to the serial comms and Ubidots. Intention is for
Charlie's pH sensor research. The hardware design incorporates 5 LMP7721
op-amps
 * between the sensor probe and the analog to digital converter. However,
they do not need to be programmed and are not mentioned in this code.
 * They are also not necessary for this code to be implemented without
them, but they are important for the pH sensor research hardware.
 * This code establishes an array for the storage of 4 values which are
reported to Ubidots. These 4 values are the result
 * of 5 samples per channel (4 channels), of which the 3 central values
are averaged. The 2 most-outlying values are discarded to help remove
noise.
 * This is accomplished with the RunningMedian library.
 */

/**************************************
 * Include Libraries
 **************************************/
#include <Wire.h>             //for I2C comms
#include <MCP342x.h>          //for MCP3424 ADC,
https://github.com/battosai30/MCP3424
#include <RunningMedian.h>    //for removing noise from sampling,
https://github.com/RobTillaart/RunningMedian
#include "UbidotsEsp32Mqtt.h" //for Ubidots connection
#include "secrets.h"          //header file stored in project folder for
credentials
#include <NTPClient.h>        //Network time protocol--gets the real time
from the network
#include <WiFiUdp.h>          //Wifi library

/* MCP3424 WIRING NOTES:
 * CH1+ --> First channel input, in this case LMP7721 output which is the
signal from pH sensor 1.
 * CH1- --> Comparative voltage, in this case LMP7721 output which is the
signal from reference electrode.
 * CH2+ --> Second channel input, in this case LMP7721 output which is the
signal from pH sensor 2.
 * CH2- --> Comparative voltage, in this case LMP7721 output which is the
signal from reference electrode.
```

```
 * CH3+ --> Third channel input, in this case LMP7721 output which is the
signal from pH sensor 3.
 * CH3- --> Comparative voltage, in this case LMP7721 output which is the
signal from reference electrode.
 * CH4+ --> Fourth channel input, in this case LMP7721 output which is the
signal from pH sensor 4.
 * CH4- --> Comparative voltage, in this case LMP7721 output which is the
signal from reference electrode.
 * SDA  --> SDA on ESP32
 * SCL  --> SCL on ESP32
 * GND  --> Grounded to board ground
 * 5V   --> 3.3V source on board, this board can work with up to 5V but
can use 3.3V as well.
 *
 * Both switches on DFR0316 MCP3424 should be set to "on" which selects
address 0x68.
 *
 * MCP3424 can only convert voltages up to 2.047 Volts!
 */

/**************************************
 * Define global variables, like inputs
 **************************************/
const unsigned int numChannels = 4;        //Number of channels using on
mux
const unsigned int numSamples = 5;          //Number of samples on each
channel for integration
float dataArray[numChannels];               //Array for storing average of
samples for each channel

const int PUBLISH_FREQUENCY = 5*60;         //Update rate in seconds
(desired min * 60 s/min)
const unsigned long TIMEOFFSET = 7;         //MST=7, MDT=6  time zone
offset (GMT-TIMEOFFSET)
unsigned long int previousMillis = 0;       //Facilitates timer
unsigned long int epoch=0;                  //creates time variable
int hours, minutes, seconds;                //creates time variables
int oldminutes = 99;                        //Facilitates timer
int oldhours = 99;                          //Facilitates timer
int oldseconds = 99;                        //Facilitates timer
unsigned long int secondsPrev=0;            //Facilitates timer and
published timestamp

/**************************************
 * Define Constants for Ubidots
 **************************************/
const char *UBIDOTS_TOKEN = SECRET_TOKEN_ERC;  // Put here your Ubidots
TOKEN
const char *WIFI_SSID = SECRET_SSID_WORK;      // Put here your Wi-Fi SSID
const char *WIFI_PASS = SECRET_PASS_WORK;      // Put here your Wi-Fi
password
const char *DEVICE_LABEL = "charlie03";    // Put here your Device label
to which data  will be published
```

```
const char *VARIABLE_LABEL_0 = "volt00";   // Put here your Variable label
to which data  will be published
const char *VARIABLE_LABEL_1 = "volt01";   // Put here your Variable label
to which data  will be published
const char *VARIABLE_LABEL_2 = "volt02";   // Put here your Variable label
to which data  will be published
const char *VARIABLE_LABEL_3 = "volt03";   // Put here your Variable label
to which data  will be published

/****************************************
 * Instancing
 ****************************************/
MCP342x MCP1(0x68);              //Declaration of MCP3424 with its I2C
address

Ubidots ubidots(UBIDOTS_TOKEN);  //Initialize Ubidots with Token for
target channel
WiFiUDP ntpUDP;
//NTPClient timeClient(ntpUDP, "us.pool.ntp.org",-3600*TIMEOFFSET, 5000);
// uncomment for off campus use
NTPClient timeClient(ntpUDP, "ntp.colostate.edu",-3600*TIMEOFFSET, 5000);
// uncomment for on csu campus,

/*
 *
*********************************************************************
*********************************
 /****************************************
 * User Defined/Auxiliary Functions
 ****************************************/
void Wifi_connected(WiFiEvent_t event, WiFiEventInfo_t info){ //Sets up
Wifi connected event
  Serial.println("Successfully connected to Access Point");
}

void Get_IPAddress(WiFiEvent_t event, WiFiEventInfo_t info){  //Sets up
Wifi IP Address event
  Serial.println("WIFI is connected!");
  Serial.println("IP address: ");
  Serial.println(WiFi.localIP());
}

void Wifi_disconnected(WiFiEvent_t event, WiFiEventInfo_t info){  //Sets
up Wifi disconnected event, will attempt reconnection--after 15 failed
attempts will restart device.
    int i = 1;
    while (WiFi.status() != WL_CONNECTED) {
      Serial.println("Disconnected from WIFI access point");
      Serial.print("WiFi lost connection. Reason: ");
      Serial.println(info.disconnected.reason);
      Serial.println("Reconnecting...");
      WiFi.begin(WIFI_SSID, WIFI_PASS);
      i++;
      delay(1000);
```

```
      if(i==15){
        ESP.restart();
      }
    }
}

void callback(char *topic, byte *payload, unsigned int length){ //Callback
function is used for the MQTT protocol in IoT. See Ubidots examples for
usage.
  Serial.print("Message arrived [");
  Serial.print(topic);
  Serial.print("] ");
  for (int i = 0; i < length; i++)
  {
    Serial.print((char)payload[i]);
  }
  Serial.println();
}


void CollectData(){ //Function created to loop 4 channels with 5 samples
per channel, average central 3 samples and discard 2 outliers, and store
data in dataArray.

   //construct variables and arrays
   float volt;
   RunningMedian voltAvg = RunningMedian(numSamples);  //creates a buffer
array for the RunningMedian library called voltAvg

//Channel 1
        ubidots.loop();
//VERY IMPORTANT: Keeps Ubidots connection from timing out while sampling
is occuring. Sends a ping to Ubidots to refresh.
        digitalWrite(LED_BUILTIN, HIGH);
//Turn the LED on (HIGH is the voltage level)

MCP1.setConfiguration(CH1,RESOLUTION_18_BITS,ONE_SHOT_MODE,PGA_X1);
//Channel 1, 18 bits resolution, one-shot mode, amplifier gain = 1x (no
gain)
        for(int k=0; k< numSamples; k++){
//Start sampling loop
            MCP1.newConversion();
//New analog to digital conversion is initiated
            volt = MCP1.measure()/1000000;
//Measure, note that the library waits for a complete conversion, output
is in millivolts (mV).
            voltAvg.add(volt);
//Add sample to buffer array for averaging
        digitalWrite(LED_BUILTIN, LOW);
//Turn the LED off by making the voltage LOW
        }
        dataArray[0] = voltAvg.getAverage(numSamples-2);
//Store the average of the 5 samples for channel [i], excluding 2
outliers, in an array called dataArray.
```

```
        voltAvg.clear();
//Clears the buffer array for next channel.


//Channel 2
        ubidots.loop();
//VERY IMPORTANT: Keeps Ubidots connection from timing out while sampling
is occuring. Sends a ping to Ubidots to refresh.
        digitalWrite(LED_BUILTIN, HIGH);
//Turn the LED on (HIGH is the voltage level)

MCP1.setConfiguration(CH2,RESOLUTION_18_BITS,ONE_SHOT_MODE,PGA_X1); //
Channel 2, 18 bits resolution, one-shot mode, amplifier gain = 1
        for(int k=0; k< numSamples; k++){   //Start sampling loop for
channel
            MCP1.newConversion();            //New analog to digital
conversion is initiated
            volt = MCP1.measure()/1000000;   //Measure, note that the
library waits for a complete conversion, output is in millivolts (mV).
            voltAvg.add(volt);              //Add sample to buffer array
for averaging
        digitalWrite(LED_BUILTIN, LOW);     //Turn the LED off by making
the voltage LOW
        }
        dataArray[1] = voltAvg.getAverage(numSamples-2);  //Store the
average of the 5 samples for channel [i], excluding 2 outliers, in an
array called dataArray.
        voltAvg.clear();                                  //Clears the
buffer array for next channel.


//Channel 3
        ubidots.loop();
//VERY IMPORTANT: Keeps Ubidots connection from timing out while sampling
is occuring. Sends a ping to Ubidots to refresh.
        digitalWrite(LED_BUILTIN, HIGH);
//Turn the LED on (HIGH is the voltage level)

MCP1.setConfiguration(CH3,RESOLUTION_18_BITS,ONE_SHOT_MODE,PGA_X1); //
Channel 3, 18 bits resolution, one-shot mode, amplifier gain = 1
        for(int k=0; k< numSamples; k++){   //Start sampling loop for
channel
            MCP1.newConversion();            //New analog to digital
conversion is initiated
            volt = MCP1.measure()/1000000;   //Measure, note that the
library waits for a complete conversion, output is in millivolts (mV).
            voltAvg.add(volt);              //Add sample to buffer array
for averaging
        digitalWrite(LED_BUILTIN, LOW);     //Turn the LED off by making
the voltage LOW
        }
        dataArray[2] = voltAvg.getAverage(numSamples-2);  //Store the
average of the 5 samples for channel [i], excluding 2 outliers, in an
array called dataArray.
```

```
        voltAvg.clear();                                    //Clears the
buffer array for next channel.


//Channel 4
        ubidots.loop();
//VERY IMPORTANT: Keeps Ubidots connection from timing out while sampling
is occuring. Sends a ping to Ubidots to refresh.
        digitalWrite(LED_BUILTIN, HIGH);
//Turn the LED on (HIGH is the voltage level)

MCP1.setConfiguration(CH4,RESOLUTION_18_BITS,ONE_SHOT_MODE,PGA_X1); //
Channel 4, 18 bits resolution, one-shot mode, amplifier gain = 1
        for(int k=0; k< numSamples; k++){   //Start sampling loop for
channel [i]
            MCP1.newConversion();            //New analog to digital
conversion is initiated
            volt = MCP1.measure()/1000000;   //Measure, note that the
library waits for a complete conversion, output is in millivolts (mV).
            voltAvg.add(volt);              //Add sample to buffer array
for averaging
        digitalWrite(LED_BUILTIN, LOW);     //Turn the LED off by making
the voltage LOW
        }
        dataArray[3] = voltAvg.getAverage(numSamples-2);  //Store the
average of the 5 samples for channel [i], excluding 2 outliers, in an
array called dataArray.
        voltAvg.clear();                                    //Clears the
buffer array for next channel.

}

void SendData(){ //Adds the data from dataArray for each channel and the
variable name, given at the top, to the JSON for Ubidots and then sends
the JSON.
      ubidots.add(VARIABLE_LABEL_0, dataArray[0]);
      ubidots.add(VARIABLE_LABEL_1, dataArray[1]);
      ubidots.add(VARIABLE_LABEL_2, dataArray[2]);
      ubidots.add(VARIABLE_LABEL_3, dataArray[3]);

      ubidots.publish(DEVICE_LABEL);                //Sends the variables
to Ubidots
      Serial.println("Sent data packet");
}

void PrintData(){  //Prints the data stored in dataArray for all channels
to the serial comm.
  for (int i = 0; i < numChannels; i++) {
        Serial.print("Voltage at channel "); //Prints to serial comms
        Serial.print(i);
        Serial.print(" is ");
        Serial.print(dataArray[i]);
        Serial.println(" mV.");
  }
```

```
}
/*
 *
**************************************************************************
**********************************
/**************************************
 * Main Functions
 *************************************/

void setup() { //Setup code that runs once when board is reset

    Serial.begin(115200);                          //initialize serial
comms
    pinMode(LED_BUILTIN, OUTPUT);                  //Sets builtin RED LED
to output mode
    WiFi.disconnect(true);                         //Erases old saved wifi
info
    delay(1000);

    WiFi.onEvent(Wifi_connected,SYSTEM_EVENT_STA_CONNECTED);        //Sets
up Wifi connected event
    WiFi.onEvent(Get_IPAddress, SYSTEM_EVENT_STA_GOT_IP);           //Sets
up Wifi IP address event
    WiFi.onEvent(Wifi_disconnected, SYSTEM_EVENT_STA_DISCONNECTED); //Sets
up Wifi disconnected event, will attempt wifi reconnection
    WiFi.begin(WIFI_SSID, WIFI_PASS);
//Connects to Wifi
    Serial.println("Waiting for WIFI network...");

    // start NTP time client
    timeClient.begin();
    timeClient.forceUpdate();
    delay(1000);

    //Start Ubidots connection
    ubidots.setDebug(true);                        //uncomment this line to
make debug messages available
    ubidots.setCallback(callback);                 //MQTT Wizardry
    ubidots.setup();                               //Ubidots wizardry
    ubidots.reconnect();                           //Ensures Ubidots
connection is established

    MCP1.begin(0);
//begin ADC

    Serial.println();
    Serial.print("Hi! I'm a device called: ");
    Serial.println(DEVICE_LABEL);
    Serial.println();
    Serial.print("Publish frequency set to: ");
    Serial.print(PUBLISH_FREQUENCY);
    Serial.print("seconds or ");
    Serial.print(PUBLISH_FREQUENCY/60);
    Serial.print("minutes.");
```

```
}
/*
 *
************************************************************************
**********************************
 */
void loop() { //Loop that is the lifeblood of the system. This calls the
previously defined functions and completes the intended process of
collecting, sending, and printing data.

      if(WiFi.status() == WL_CONNECTED){
        while(!timeClient.update()) {       // update NTP if needed
          timeClient.forceUpdate();
        }
      }

      if(WiFi.status() == WL_CONNECTED){
          if (!ubidots.connected()){ //Reconnects Ubidots MQTT broker
connection if signal interrupted.
          ubidots.reconnect();
          }
      }

      hours=timeClient.getHours();        // update time variables
      minutes=timeClient.getMinutes();
      seconds=timeClient.getSeconds();
      epoch=timeClient.getEpochTime();



      if ((epoch%PUBLISH_FREQUENCY==0) && (epoch!=secondsPrev)) {
//Triggers the routine based on the NTP time and set interval (Publish
Frequency).
          secondsPrev=epoch;

          Serial.println();
          Serial.print("Time: ");

Serial.print(hours);Serial.print(":");Serial.print(minutes);Serial.print("
:");Serial.println(seconds);
          Serial.println("COLLECTING DATA!");
          CollectData();                                  //Cycle
'numChannels' channels, sample each channel for 'numSamples' times, and
store the average of the samples in dataArray.
          Serial.println("SENDING DATA!");
          SendData();                                     //Send data from
dataArray to Ubidots
          PrintData();                                    //Print data from
dataArray to serial comm

          Serial.println("FINISHED LOOP!");               //Give a message
when finished
          Serial.println();
          Serial.print("Publish frequency set to: ");
```

```
            Serial.print(PUBLISH_FREQUENCY);
            Serial.print("seconds or ");
            Serial.print(PUBLISH_FREQUENCY/60);
            Serial.print("minutes.");
            Serial.println();
            Serial.print("Epoch Timestamp: ");
            Serial.println(epoch);
        }

        ubidots.loop();                                     //Ping Ubidots to
maintain connection
    }
```

Buffer Solution Recipes
Charles VanTilburg
pH Sensor Research - Spring 2022

Based on recipes found in:
Robinson, R and Stokes R. (1968)
"Electrolyte solutions"
2nd ed., rev. London, Butterworths.

Buffer Makeup (400 mL of buffer):

pH 1: 100 mL 0.2 M KCl + 268 mL of 0.2 M HCl + rest water (32 mL)

pH 2: 100 mL 0.2 M KCl + 26 mL of 0.2 M HCl + rest water (274 mL)

pH 3: 200 mL 0.1 M potassium hydrogen phthalate + 89.2 mL of 0.1 M HCl + rest water (110.8 mL)

pH 5: 200 mL 0.1 M potassium hydrogen phthalate + 90.4 mL of 0.1 M NaOH + rest water (109.6 mL)

pH 6: 200 mL 0.1 M potassium dihydrogen phosphate + 22.4 mL of 0.1 M NaOH + rest water (187.6 mL)

pH 8: 200 mL 0.025 M borax + 82 mL of 0.1 M HCl + rest water (118 mL)

pH 9: 200 mL 0.025 M borax + 18.4 mL of 0.1 M HCl + rest water (181.9 mL)

pH 11: 200 mL 0.05 M sodium bicarbonate + 90.8 mL of 0.1 M NaOH + rest water (109.2 mL)

pH 12: 100 mL 0.2 M KCl + 24.0 mL of 0.2 M NaOH + rest water (276 mL)

pH 13: 100 mL 0.2 M KCl + 264.0 mL of 0.2 M NaOH + rest water (36 mL)

(V_1) Required Solutions:

- 189.6 mL 0.1 M HCl
- 294.0 mL 0.2 M HCl
- 203.6 mL 0.1 M NaOH
- 288.0 mL 0.2 M NaOH
- 400.0 mL 0.2 M KCl
- 200 mL 0.1 M Potassium Dihydrogen Phosphate
- 400 mL 0.1 M Potassium Hydrogen Phthalate
- 400 mL 0.025 M Borax
- 200 mL 0.05 M Sodium Bicarbonate

(C_2) Lab Stock Solutions:

- 37% HCl = 12.2 M HCl

Lab Stock Salts:

- NaOH - 40.00 g/mol
- KCl - 75.00 g/mol
- Potassium Dihydrogen Phosphate - 135.93 g/mol
- Potassium Hydrogen Phthalate - 204.22 g/mol
- Borax - 381.37 g/mol
- Sodium Bicarbonate - 84.01 g/mol

Ingredient Makeup:

294 mL 0.2 M HCl

$C_1 \cdot V_1 = C_2 \cdot V_2$

$V_2 := 6.5\ mL$ of stock $C_2 := 12.2\ \frac{mol}{L}$ solution dilutes to desired concentration of

$C_1 := 0.2\ \frac{mol}{L}$ in $V_1 := \frac{C_2 \cdot V_2}{C_1} = 396.5\ mL$ solution.

Use 294 mL. $Left := V_1 - 294\ mL = 102.5\ mL$

189.6 mL 0.1 M HCl

Use remaining 0.2 M HCl solution to make 0.1 M HCl solution.

$C_1 \cdot V_1 = C_2 \cdot Left$

$Left = 102.5\ mL$ of stock $C_2 := 0.2\ \frac{mol}{L}$ solution dilutes to desired concentration of

$C_1 := 0.1\ \frac{mol}{L}$ in $V_1 := \frac{C_2 \cdot Left}{C_1} = 205\ mL$ solution.

Use 189.6 mL. $Left := V_1 - 189.6\ mL = 15.4\ mL$ waste.

288 mL 0.2 M NaOH

$C_1 := 0.2\ \frac{mol}{L}$ $V_1 := 288\ mL$ $M_1 := C_1 \cdot V_1 = 0.058\ mol$

$W_1 := M_1 \cdot 40.00\ \frac{gm}{mol} = 2.304\ gm$

Use 2.304 gm NaOH in 288 mL of water.

203.6 mL 0.1 M NaOH

$C_1 := 0.1\ \frac{mol}{L}$ $V_1 := 203.6\ mL$ $M_1 := C_1 \cdot V_1 = 0.02\ mol$

$W_1 := M_1 \cdot 40.00\ \frac{gm}{mol} = 0.814\ gm$

Use 0.814 gm NaOH in 203.6 mL of water.

400.0 mL 0.2 M KCl

$C_1 := 0.2 \frac{mol}{L}$ $V_1 := 400\ mL$ $M_1 := C_1 \cdot V_1 = 0.08\ mol$

$W_1 := M_1 \cdot 75.00 \frac{gm}{mol} = 6\ gm$

Use 6 gm KCl in 400 mL of water.

200 mL 0.1 M Potassium Dihydrogen Phosphate

$C_1 := 0.1 \frac{mol}{L}$ $V_1 := 200\ mL$ $M_1 := C_1 \cdot V_1 = 0.02\ mol$

$W_1 := M_1 \cdot 135.93 \frac{gm}{mol} = 2.719\ gm$

Use 2.719 gm potassium dihydrogen phosphate in 200 mL of water.

400 mL 0.1 M Potassium Hydrogen Phthalate

$C_1 := 0.1 \frac{mol}{L}$ $V_1 := 400\ mL$ $M_1 := C_1 \cdot V_1 = 0.04\ mol$

$W_1 := M_1 \cdot 204.22 \frac{gm}{mol} = 8.169\ gm$

Use 8.169 gm potassium hydrogen phthalate in 400 mL of water.

400 mL 0.025 M Borax

$C_1 := 0.025 \frac{mol}{L}$ $V_1 := 400\ mL$ $M_1 := C_1 \cdot V_1 = 0.01\ mol$

$W_1 := M_1 \cdot 381.37 \frac{gm}{mol} = 3.814\ gm$

Use 3.814 gm borax in 400 mL of water.

200 mL 0.05 M Sodium Bicarbonate

$C_1 := 0.05 \frac{mol}{L}$ $V_1 := 200\ mL$ $M_1 := C_1 \cdot V_1 = 0.01\ mol$

$W_1 := M_1 \cdot 84.01 \frac{gm}{mol} = 0.84\ gm$

Use 0.84 gm sodium bicarbonate in 200 mL of water.

Experiment-04-03-22-SensorCalibration

Charles VanTilburg

5/19/2022

The purpose of this script is to interpret sensor data from the calibration experiment in which 12 sensors were monitored using 3 pH meters (4 each) at 5-minute intervals.

Include libraries:

```
library(tidyverse)
```

```
## -- Attaching packages --------------------------------------- tidyverse 1.
3.1 --
```

```
## v ggplot2 3.3.6     v purrr   0.3.4
## v tibble  3.1.7     v dplyr   1.0.9
## v tidyr   1.2.0     v stringr 1.4.0
## v readr   2.1.2     v forcats 0.5.1
```

```
## -- Conflicts ------------------------------------------ tidyverse_conflict
s() --
## x dplyr::filter() masks stats::filter()
## x dplyr::lag()    masks stats::lag()
```

```
library(ggplot2)
library(RcppRoll)
```

Import data:

```
CalRaw <- read.csv("U:/GRAresearch/Software/DataAnalysis/SensorCalibration/Ex
periment-04-03-22-SensorCalibrationData.csv")

str(CalRaw)
```

```
## 'data.frame':    37238 obs. of  16 variables:
##  $ ï..Timestamp    : num  1.65e+12 1.65e+12 1.65e+12 1.65e+12 1.65e+12 ...
##  $ DateTime        : chr  "4/3/2022 17:30" "4/3/2022 17:30" "4/3/2022 17:3
0" "4/3/2022 17:55" ...
##  $ charlie01_volt00: chr  "111.333" "-" "-" "128.667" ...
##  $ charlie01_volt01: chr  "133.333" "-" "-" "126" ...
##  $ charlie01_volt02: chr  "87.6667" "-" "-" "140.333" ...
##  $ charlie01_volt03: chr  "126.333" "-" "-" "138.667" ...
##  $ charlie03_volt00: chr  "-" "260.667" "-" "-" ...
##  $ charlie03_volt01: chr  "-" "230.667" "-" "-" ...
##  $ charlie03_volt02: chr  "-" "120.333" "-" "-" ...
```

```
##  $ charlie03_volt03: chr  "-" "84.3333" "-" "-" ...
##  $ charlie04_volt00: chr  "-" "-" "165" "-" ...
##  $ charlie04_volt01: chr  "-" "-" "151.667" "-" ...
##  $ charlie04_volt02: chr  "-" "-" "153" "-" ...
##  $ charlie04_volt03: chr  "-" "-" "155" "-" ...
##  $ pH              : int  7 7 7 7 7 7 7 7 7 7 ...
##  $ Stage           : int  1 1 1 1 1 1 1 1 1 1 ...
```

Change to appropriate data types:

```
Cal <- CalRaw %>%
  mutate(DateTime = as.POSIXct(DateTime, format = "%m/%d/%Y %H:%M"),
         Sensor1.0 = as.numeric(charlie01_volt00),
         Sensor1.1 = as.numeric(charlie01_volt01),
         Sensor1.2 = as.numeric(charlie01_volt02),
         Sensor1.3 = as.numeric(charlie01_volt03),
         Sensor3.0 = as.numeric(charlie03_volt00),
         Sensor3.1 = as.numeric(charlie03_volt01),
         Sensor3.2 = as.numeric(charlie03_volt02),
         Sensor3.3 = as.numeric(charlie03_volt03),
         Sensor4.0 = as.numeric(charlie04_volt00),
         Sensor4.1 = as.numeric(charlie04_volt01),
         Sensor4.2 = as.numeric(charlie04_volt02),
         Sensor4.3 = as.numeric(charlie04_volt03),
                pH = as.factor(pH)) %>%
  select(DateTime, Sensor1.0, Sensor1.1, Sensor1.2, Sensor1.3, Sensor3.0, Sen
sor3.1, Sensor3.2, Sensor3.3, Sensor4.0,                    Sensor4.1, Sensor4
.2, Sensor4.3, pH, Stage) %>%
  fill(Sensor1.0, Sensor1.1, Sensor1.2, Sensor1.3) %>%
  fill(Sensor4.0, Sensor4.1, Sensor4.2, Sensor4.3, .direction = "up") %>%
  filter(!is.na(Sensor3.0))
```

```
## Warning in mask$eval_all_mutate(quo): NAs introduced by coercion

## Warning in mask$eval_all_mutate(quo): NAs introduced by coercion

## Warning in mask$eval_all_mutate(quo): NAs introduced by coercion

## Warning in mask$eval_all_mutate(quo): NAs introduced by coercion

## Warning in mask$eval_all_mutate(quo): NAs introduced by coercion

## Warning in mask$eval_all_mutate(quo): NAs introduced by coercion

## Warning in mask$eval_all_mutate(quo): NAs introduced by coercion

## Warning in mask$eval_all_mutate(quo): NAs introduced by coercion

## Warning in mask$eval_all_mutate(quo): NAs introduced by coercion
```

```
## Warning in mask$eval_all_mutate(quo): NAs introduced by coercion

## Warning in mask$eval_all_mutate(quo): NAs introduced by coercion

## Warning in mask$eval_all_mutate(quo): NAs introduced by coercion

rm(CalRaw)
```

Create moving average columns to reduce noise:

```
CalSmooth <- Cal %>%
  mutate(Sensor1.0s = roll_meanr(Sensor1.0, n = 12),
           Sensor1.1s = roll_meanr(Sensor1.1, n = 12),
           Sensor1.2s = roll_meanr(Sensor1.2, n = 12),
           Sensor1.3s = roll_meanr(Sensor1.3, n = 12),
           Sensor3.0s = roll_meanr(Sensor3.0, n = 12),
           Sensor3.1s = roll_meanr(Sensor3.1, n = 12),
           Sensor3.2s = roll_meanr(Sensor3.2, n = 12),
           Sensor3.3s = roll_meanr(Sensor3.3, n = 12),
           Sensor4.0s = roll_meanr(Sensor4.0, n = 12),
           Sensor4.1s = roll_meanr(Sensor4.1, n = 12),
           Sensor4.2s = roll_meanr(Sensor4.2, n = 12),
           Sensor4.3s = roll_meanr(Sensor4.3, n = 12),
           pHstage = str_c(pH,".", Stage)) %>%
  select(DateTime, pH, Stage, pHstage, ends_with("s"))
```

Gather Data into Long Form for a ggplot:

```
LongCal <- CalSmooth %>%
  gather(key = Sensor, value = Voltage, -pH, -Stage, -DateTime, -pHstage) %>%
  mutate(Meter = as.factor(str_sub(Sensor,7,7)))
```

Plot all data:

```
ggplot(LongCal, aes(x = DateTime, y = Voltage, color = pH)) +
  geom_point() +
  labs(x = "Date", y = "Voltage (mV)") +
  scale_x_datetime(breaks = as.POSIXct(c("2022-04-03", "2022-04-10", "2022-04
-17", "2022-04-24", "2022-05-01", "2022-05-08", "2022-05-15", "2022-05-22")))
+
  theme_classic()

## Warning: Removed 132 rows containing missing values (geom_point).
```

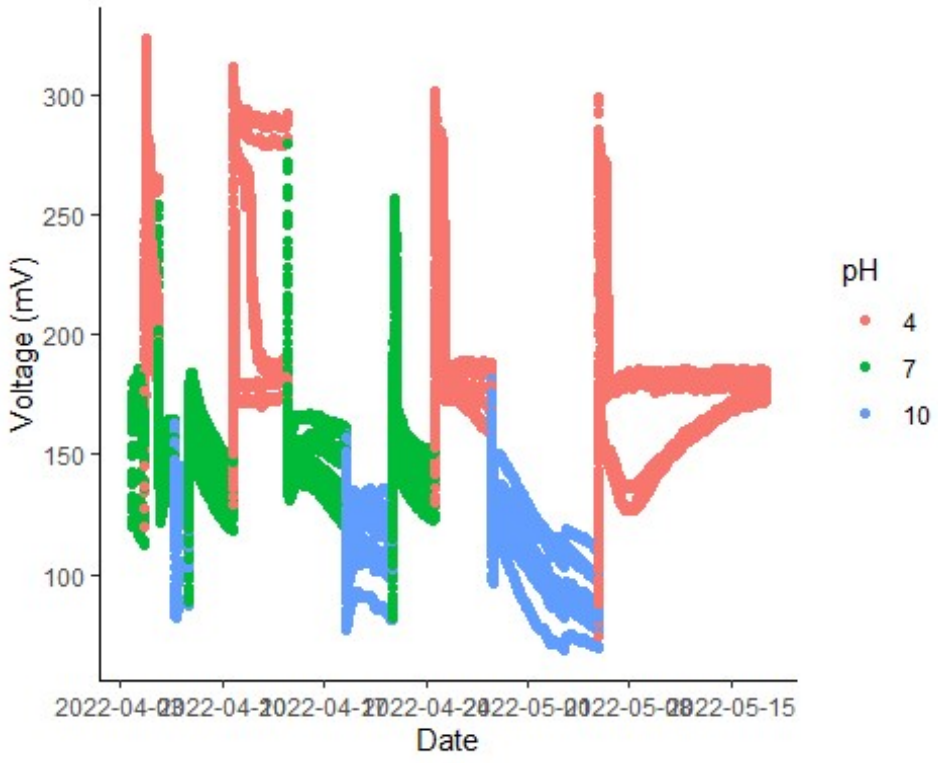

Create data frame for each pH and then each “stage”:

```
pH4 <- filter(CalSmooth, pH == 4)
pH7 <- filter(CalSmooth, pH == 7)
pH10 <- filter(CalSmooth, pH == 10)

pH4.1 <- filter(pH4, Stage == 1)
pH4.2 <- filter(pH4, Stage == 2)
pH4.3 <- filter(pH4, Stage == 3)
pH4.4 <- filter(pH4, Stage == 4)

pH7.1 <- filter(pH7, Stage == 1)
pH7.2 <- filter(pH7, Stage == 2)
pH7.3 <- filter(pH7, Stage == 3)
pH7.4 <- filter(pH7, Stage == 4)
pH7.5 <- filter(pH7, Stage == 5)

pH10.1 <- filter(pH10, Stage == 1)
pH10.2 <- filter(pH10, Stage == 2)
pH10.3 <- filter(pH10, Stage == 3)
```

Reduce each dataframe to just the final hour and then combine into one final frame, “Tails”:

```
pH4.1tail <- tail(pH4.1, n = 12)
pH4.2tail <- tail(pH4.2, n = 12)
pH4.3tail <- tail(pH4.3, n = 12)
pH4.4tail <- tail(pH4.4, n = 12)
```

```
pH7.1tail <- tail(pH7.1, n = 12)
pH7.2tail <- tail(pH7.2, n = 12)
pH7.3tail <- tail(pH7.3, n = 12)
pH7.4tail <- tail(pH7.4, n = 12)
pH7.5tail <- tail(pH7.5, n = 12)

pH10.1tail <- tail(pH10.1, n = 12)
pH10.2tail <- tail(pH10.2, n = 12)
pH10.3tail <- tail(pH10.3, n = 12)

Tails <- bind_rows(pH4.1tail,
                   pH4.2tail,
                   pH4.3tail,
                   pH4.4tail,
                   pH7.1tail,
                   pH7.2tail,
                   pH7.3tail,
                   pH7.4tail,
                   pH7.5tail,
                   pH10.1tail,
                   pH10.2tail,
                   pH10.3tail
                   ) %>%
  gather(key = Sensor, value = Voltage, -pH, -Stage, -pHstage, -DateTime) %>%
  mutate(Meter = as.factor(str_sub(Sensor,7,7)))

ggplot(Tails, aes(x=DateTime, y=Voltage, color = pH))+
  geom_point() +
  labs(x = "Date", y = "Voltage (mV)") +
  scale_x_datetime(breaks = as.POSIXct(c("2022-04-03", "2022-04-10", "2022-04
-17", "2022-04-24", "2022-05-01", "2022-05-08", "2022-05-15", "2022-05-22")))
+
  theme_classic()
```

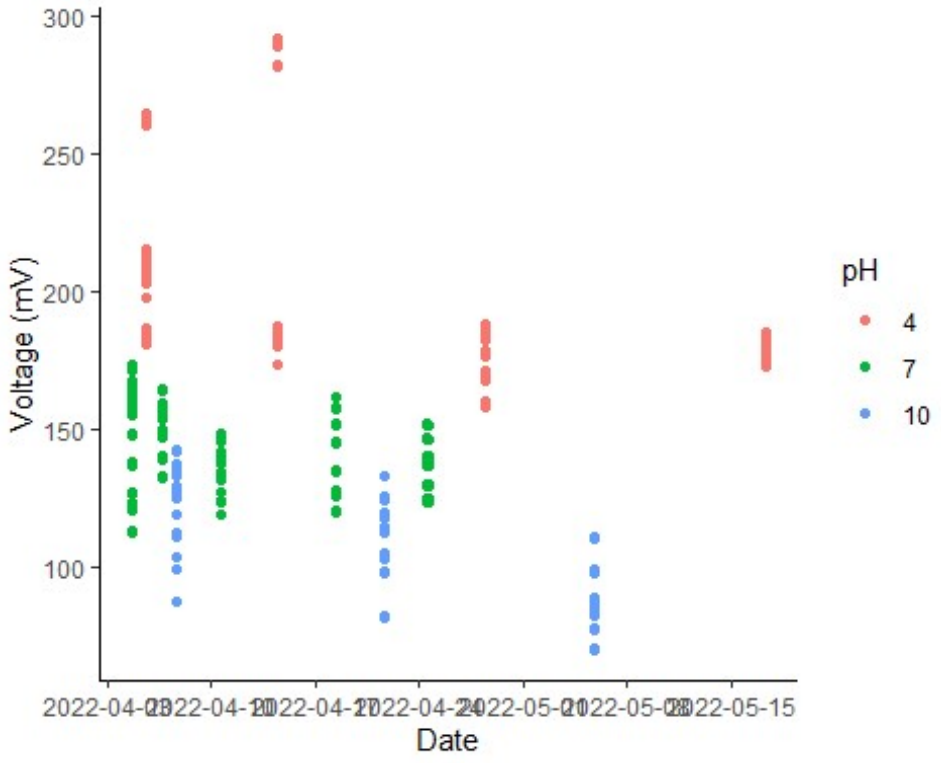

Compute stats:

```
pHStats <-  Tails %>%
  group_by(pH) %>%
  summarise(Mean = mean(Voltage),
            SD = sd(Voltage),
            Median = median(Voltage),
            n = n(),
            StdErr = SD*n()^(-1/2))
pHStats
```

```
## # A tibble: 3 x 6
##   pH     Mean    SD Median     n StdErr
##   <fct> <dbl> <dbl>  <dbl> <int>  <dbl>
## 1 4      197.  37.0   183.   576  1.54
## 2 7      142.  14.4   140.   720  0.535
## 3 10     107.  19.2   108.   432  0.925
```

```
MeterStats <-  Tails %>%
  group_by(pH, Meter) %>%
  summarise(Mean = mean(Voltage),
            SD = sd(Voltage),
            Median = median(Voltage))
```

```
## `summarise()` has grouped output by 'pH'. You can override using the `.gro
ups`
## argument.
```

```
MeterStats
```

```
## # A tibble: 9 x 5
## # Groups:   pH [3]
##   pH    Meter  Mean    SD Median
##   <fct> <fct> <dbl> <dbl>  <dbl>
## 1 4     1     203.   34.6  184.
## 2 4     3     202.   50.3  183.
## 3 4     4     186.   14.5  180.
## 4 7     1     135.   10.2  136.
## 5 7     3     145.   17.4  144.
## 6 7     4     146.   11.9  149.
## 7 10    1      93.9  13.1   98.0
## 8 10    3     114.   18.7  119.
## 9 10    4     115.   17.7  119.
```

Display boxplots and means for each pH:

```
ggplot(Tails, aes(x = pH, y = Voltage, fill = pH)) +
  geom_violin() +
  stat_summary(fun.y="mean",geom="point",pch=4,color="black", size = 5) +
  labs(x = "pH", y = "Voltage (mV)") +
  theme_classic()
```

```
## Warning: `fun.y` is deprecated. Use `fun` instead.
```

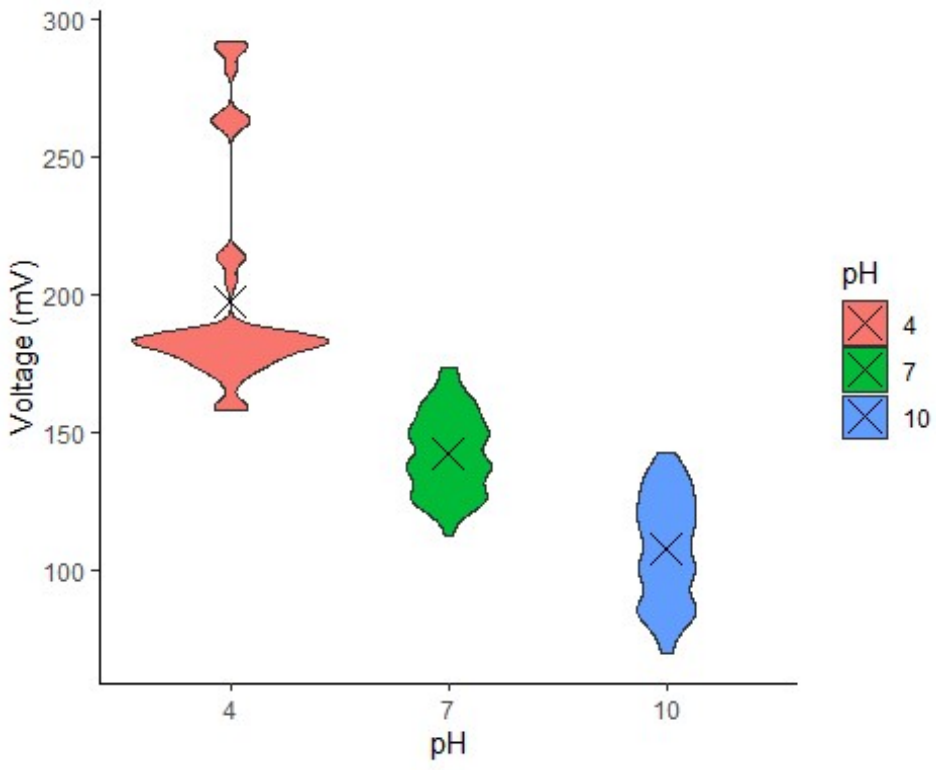

Experiment-05-17-22-StaticBufferTest

Charles VanTilburg

The purpose of this script is to interpret sensor data from the static buffer experiment in which 12 sensors were monitored using 3 pH meters (4 each) at 5-minute intervals.

Include libraries:

```
library(tidyverse)
```

```
## -- Attaching packages --------------------------------------- tidyverse 1.
3.1 --
```

```
## v ggplot2 3.3.6     v purrr   0.3.4
## v tibble  3.1.7     v dplyr   1.0.9
## v tidyr   1.2.0     v stringr 1.4.0
## v readr   2.1.2     v forcats 0.5.1
```

```
## -- Conflicts ------------------------------------------ tidyverse_conflict
s() --
## x dplyr::filter() masks stats::filter()
## x dplyr::lag()    masks stats::lag()
```

```
library(ggplot2)
library(RcppRoll)
```

Import data:

```
Raw <- read.csv("U:/GRAresearch/Software/DataAnalysis/StaticBufferTest/Experi
ment-05-17-22-FinalStaticBufferExperiment.csv")
```

```
str(Raw)
```

```
## 'data.frame':    6804 obs. of  15 variables:
##  $ ï..Column                          : int  0 0 0 0 0 0 0 0 0 0 ...
##  $ Human.readable.date..America.Denver.: chr  "5/23/2022 14:55" "5/23/2022
14:55" "5/23/2022 14:55" "5/23/2022 15:00" ...
##  $ charlie01_volt00                   : chr  "349.667" "-" "-" "389" ...
##  $ charlie01_volt01                   : chr  "355" "-" "-" "395" ...
##  $ charlie01_volt02                   : chr  "349.333" "-" "-" "387" ...
##  $ charlie01_volt03                   : chr  "358" "-" "-" "397.333" ...
##  $ charlie03_volt00                   : chr  "-" "443" "-" "-" ...
##  $ charlie03_volt01                   : chr  "-" "437" "-" "-" ...
##  $ charlie03_volt02                   : chr  "-" "438" "-" "-" ...
##  $ charlie03_volt03                   : chr  "-" "424" "-" "-" ...
##  $ charlie04_volt00                   : chr  "-" "-" "368" "-" ...
##  $ charlie04_volt01                   : chr  "-" "-" "375" "-" ...
##  $ charlie04_volt02                   : chr  "-" "-" "326.333" "-" ...
##  $ charlie04_volt03                   : chr  "-" "-" "369" "-" ...
##  $ pH                                 : int  3 3 3 3 3 3 3 3 3 3 ...
```

Change to appropriate data types:

```
Data <- Raw %>%
  mutate(DateTime = as.POSIXct(Human.readable.date..America.Denver., format =
"%m/%d/%Y %H:%M"),
         Sensor1.0 = as.numeric(charlie01_volt00),
         Sensor1.1 = as.numeric(charlie01_volt01),
         Sensor1.2 = as.numeric(charlie01_volt02),
         Sensor1.3 = as.numeric(charlie01_volt03),
         Sensor3.0 = as.numeric(charlie03_volt00),
         Sensor3.1 = as.numeric(charlie03_volt01),
         Sensor3.2 = as.numeric(charlie03_volt02),
         Sensor3.3 = as.numeric(charlie03_volt03),
         Sensor4.0 = as.numeric(charlie04_volt00),
         Sensor4.1 = as.numeric(charlie04_volt01),
         Sensor4.2 = as.numeric(charlie04_volt02),
         Sensor4.3 = as.numeric(charlie04_volt03),
                pH = as.factor(pH)) %>%
  select(DateTime, Sensor1.0, Sensor1.1, Sensor1.2, Sensor1.3, Sensor3.0, Sen
sor3.1, Sensor3.2, Sensor3.3, Sensor4.0,                   Sensor4.1, Sensor4
.2, Sensor4.3, pH) %>%
  fill(Sensor3.0, Sensor3.1, Sensor3.2, Sensor3.3) %>%
  fill(Sensor4.0, Sensor4.1, Sensor4.2, Sensor4.3, .direction = "up") %>%
  filter(!is.na(Sensor1.0))

## Warning in mask$eval_all_mutate(quo): NAs introduced by coercion

## Warning in mask$eval_all_mutate(quo): NAs introduced by coercion

## Warning in mask$eval_all_mutate(quo): NAs introduced by coercion

## Warning in mask$eval_all_mutate(quo): NAs introduced by coercion

## Warning in mask$eval_all_mutate(quo): NAs introduced by coercion

## Warning in mask$eval_all_mutate(quo): NAs introduced by coercion

## Warning in mask$eval_all_mutate(quo): NAs introduced by coercion

## Warning in mask$eval_all_mutate(quo): NAs introduced by coercion

## Warning in mask$eval_all_mutate(quo): NAs introduced by coercion

## Warning in mask$eval_all_mutate(quo): NAs introduced by coercion

## Warning in mask$eval_all_mutate(quo): NAs introduced by coercion

## Warning in mask$eval_all_mutate(quo): NAs introduced by coercion

rm(Raw)
```

Create moving average columns to reduce noise:

```
Smooth <- Data %>%
  mutate(Sensor1.0s = roll_meanr(Sensor1.0, n = 12),
           Sensor1.1s = roll_meanr(Sensor1.1, n = 12),
           Sensor1.2s = roll_meanr(Sensor1.2, n = 12),
           Sensor1.3s = roll_meanr(Sensor1.3, n = 12),
           Sensor3.0s = roll_meanr(Sensor3.0, n = 12),
           Sensor3.1s = roll_meanr(Sensor3.1, n = 12),
           Sensor3.2s = roll_meanr(Sensor3.2, n = 12),
           Sensor3.3s = roll_meanr(Sensor3.3, n = 12),
           Sensor4.0s = roll_meanr(Sensor4.0, n = 12),
           Sensor4.1s = roll_meanr(Sensor4.1, n = 12),
           Sensor4.2s = roll_meanr(Sensor4.2, n = 12),
           Sensor4.3s = roll_meanr(Sensor4.3, n = 12)) %>%
  select(DateTime, pH, ends_with("s"))
```

Gather Data into Long Form for a ggplot:

```
LongSmooth <- Smooth %>%
  gather(key = Sensor, value = Voltage, -pH, -DateTime) %>%
  mutate(Meter = as.factor(str_sub(Sensor,7,7)))
```

Plot all data:

```
ggplot(LongSmooth, aes(x = DateTime, y = Voltage, color = pH)) +
  geom_point(size = 1) +
  labs(x = "Date", y = "Voltage (mV)") +
  scale_x_datetime(breaks = as.POSIXct(c("2022-05-23", "2022-05-25", "2022-05
-27", "2022-05-29", "2022-05-31" ))) +
  scale_y_continuous(breaks = seq(0,450,50)) +
  theme_classic()

## Warning: Removed 136 rows containing missing values (geom_point).
```

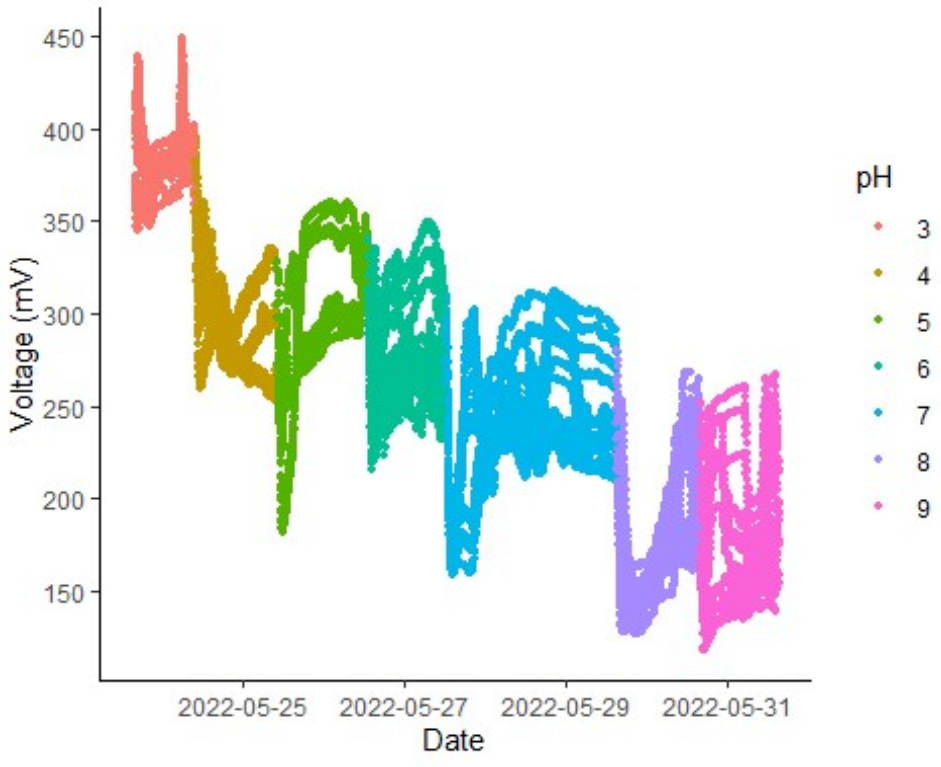

Create data frame for each pH and then each "stage":

```
pH3 <- filter(Smooth, pH == 3)
pH4 <- filter(Smooth, pH == 4)
pH5 <- filter(Smooth, pH == 5)
pH6 <- filter(Smooth, pH == 6)
pH7 <- filter(Smooth, pH == 7)
pH8 <- filter(Smooth, pH == 8)
pH9 <- filter(Smooth, pH == 9)

ggplot(LongSmooth, aes(x=DateTime, y=Voltage, color = Meter))+
geom_line() +
  facet_wrap(~pH)

## Warning: Removed 136 row(s) containing missing values (geom_path).
```

Compute stats:

```
pHStats <-  LongSmooth %>%
  group_by(pH) %>%
  summarise(Mean = mean(Voltage, na.rm = TRUE),
            SD = sd(Voltage, na.rm = TRUE),
            Median = median(Voltage, na.rm = TRUE),
            n = n(),
            StdErr = SD*n()^(-1/2))
pHStats

## # A tibble: 7 x 6
##   pH     Mean    SD Median     n StdErr
##   <fct> <dbl> <dbl>  <dbl> <int>  <dbl>
## 1 3      381.  14.8   381.  2688  0.286
## 2 4      295.  25.0   292.  3456  0.424
## 3 5      298.  36.2   296.  3804  0.586
## 4 6      283.  28.7   276.  3312  0.498
## 5 7      245.  33.5   240.  7284  0.393
## 6 8      175.  32.5   166.  3528  0.547
## 7 9      187.  39.8   179.  3372  0.686

MeterStats <-  LongSmooth %>%
  group_by(pH, Meter) %>%
  summarise(Mean = mean(Voltage, na.rm = TRUE),
            SD = sd(Voltage, na.rm = TRUE),
            Median = median(Voltage, na.rm = TRUE))
```

```
## `summarise()` has grouped output by 'pH'. You can override using the `.gro
ups`
## argument.

MeterStats

## # A tibble: 21 x 5
## # Groups:   pH [7]
##    pH    Meter  Mean    SD Median
##    <fct> <fct> <dbl> <dbl>  <dbl>
##  1 3     1      376.  7.27   377.
##  2 3     3      383. 15.0    379.
##  3 3     4      385. 18.3    386.
##  4 4     1      284. 28.0    273.
##  5 4     3      307. 20.9    308.
##  6 4     4      293. 19.6    290.
##  7 5     1      294. 16.9    294.
##  8 5     3      316. 52.2    340.
##  9 5     4      284. 19.5    286.
## 10 6     1      277. 16.0    274.
## # ... with 11 more rows
```

Display boxplots and means for each pH:

```
ggplot(LongSmooth, aes(x = pH, y = Voltage, fill = pH)) +
  geom_violin() +
  stat_summary(fun="mean",geom="point",pch=4,color="black", size = 5) +
  labs(x = "pH", y = "Voltage (mV)") +
  scale_y_continuous(breaks = seq(0,450,50)) +
  theme_classic()

## Warning: Removed 136 rows containing non-finite values (stat_ydensity).

## Warning: Removed 136 rows containing non-finite values (stat_summary).
```

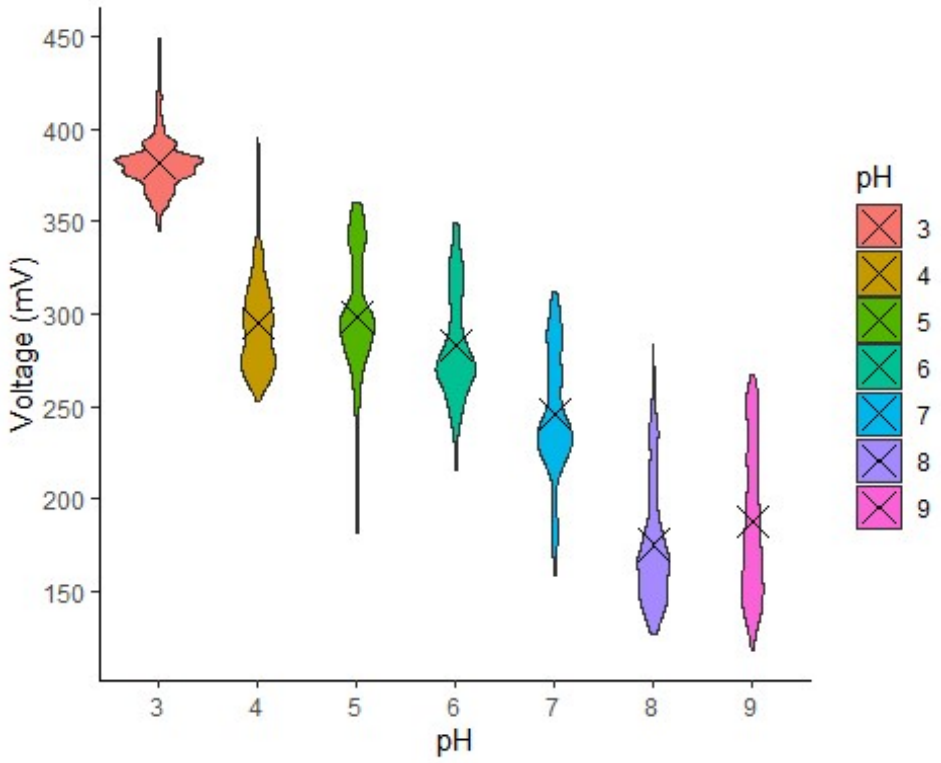
Voltage (mV)
450
400
350
300
250
200
150
3
4
5
6
7
8
9
pH
pH
3
4
5
6
7
8
9

Experiment-06-01-22-StaticBufferTest

Charles VanTilburg

6/29/2022

The purpose of this script is to interpret sensor data from the manually-collected, high impedance static buffer experiment in which 12 sensors were monitored using the HP34401a.

Include libraries:

```
library(dplyr)

##
## Attaching package: 'dplyr'

## The following objects are masked from 'package:stats':
##
##     filter, lag

## The following objects are masked from 'package:base':
##
##     intersect, setdiff, setequal, union

library(tidyr)
library(tidyverse)

## -- Attaching packages --------------------------------------- tidyverse 1.
3.1 --

## v ggplot2 3.3.6     v purrr   0.3.4
## v tibble  3.1.7     v stringr 1.4.0
## v readr   2.1.2     v forcats 0.5.1

## -- Conflicts ------------------------------------------ tidyverse_conflict
s() --
## x dplyr::filter() masks stats::filter()
## x dplyr::lag()    masks stats::lag()

library(ggplot2)
```

Import data:

```
Tails <- read.csv("U:/GRAresearch/Software/DataAnalysis/ManualStaticBufferTes
t/Experiment-06-01-22-HighImpedanceManualDataTails.csv")
Inc <- read.csv("U:/GRAresearch/Software/DataAnalysis/ManualStaticBufferTest/
Experiment-06-01-22-HighImpedanceManualDataInc.csv")
Dec <- read.csv("U:/GRAresearch/Software/DataAnalysis/ManualStaticBufferTest/
Experiment-06-01-22-HighImpedanceManualDataDec.csv")

str(Tails)
```

```
## 'data.frame':    46 obs. of  17 variables:
##  $ ï..Col   : int  0 0 0 0 0 0 0 0 0 0 ...
##  $ DateTime : chr  "6/1/2022 16:53" "6/1/2022 17:00" "6/2/2022 9:00" "6/2/
2022 10:10" ...
##  $ pH       : int  10 10 9 9 9 9 9 8 8 8 ...
##  $ Sensor1.0: num  155 155 194 195 195 ...
##  $ Sensor1.1: num  161 160 192 192 192 ...
##  $ Sensor1.2: num  194 194 219 219 219 ...
##  $ Sensor1.3: num  216 216 237 237 236 ...
##  $ Sensor3.0: num  182 185 215 215 215 ...
##  $ Sensor3.1: num  201 197 228 228 228 ...
##  $ Sensor3.2: num  225 225 253 254 254 ...
##  $ Sensor3.3: num  230 230 253 253 253 ...
##  $ Sensor4.0: num  158 158 195 195 195 ...
##  $ Sensor4.1: num  199 199 230 230 230 ...
##  $ Sensor4.2: num  216 213 227 227 227 ...
##  $ Sensor4.3: num  191 194 221 221 221 ...
##  $ Average  : num  194 194 222 222 221 ...
##  $ SD       : num  26 25.6 20.8 20.8 20.7 ...

str(Inc)

## 'data.frame':    26 obs. of  17 variables:
##  $ ï..Col   : int  0 0 0 0 0 0 0 0 0 0 ...
##  $ DateTime : chr  "6/8/2022 11:57" "6/8/2022 13:14" "6/8/2022 16:58" "6/9
/2022 11:53" ...
##  $ pH       : int  3 3 3 4 4 4 5 5 6 6 ...
##  $ Sensor1.0: int  431 432 434 340 339 338 347 349 294 285 ...
##  $ Sensor1.1: int  435 436 438 336 336 335 345 346 294 287 ...
##  $ Sensor1.2: int  427 427 429 335 335 333 342 344 264 256 ...
##  $ Sensor1.3: int  436 437 440 346 345 344 354 356 311 301 ...
##  $ Sensor3.0: int  431 432 434 337 336 336 343 345 280 272 ...
##  $ Sensor3.1: int  433 434 436 341 340 339 359 360 294 277 ...
##  $ Sensor3.2: int  428 429 431 340 340 339 355 358 300 287 ...
##  $ Sensor3.3: int  427 427 430 342 341 340 349 350 296 285 ...
##  $ Sensor4.0: int  438 439 441 341 341 340 357 359 288 275 ...
##  $ Sensor4.1: int  440 441 444 345 344 343 356 359 337 344 ...
##  $ Sensor4.2: int  417 417 419 339 338 338 342 342 287 279 ...
##  $ Sensor4.3: int  437 438 441 344 343 342 353 355 322 328 ...
##  $ Average  : num  432 432 435 340 340 ...
##  $ SD       : num  6.34 6.69 6.89 3.45 3.21 ...

str(Dec)

## 'data.frame':    46 obs. of  17 variables:
##  $ ï..Col   : int  0 0 0 0 0 0 0 0 0 0 ...
##  $ DateTime : chr  "6/1/2022 16:53" "6/1/2022 17:00" "6/2/2022 9:00" "6/2/
2022 10:10" ...
##  $ pH       : int  10 10 9 9 9 9 9 8 8 8 ...
##  $ Sensor1.0: num  155 155 194 195 195 ...
##  $ Sensor1.1: num  161 160 192 192 192 ...
```

```
##  $ Sensor1.2: num  194 194 219 219 219 ...
##  $ Sensor1.3: num  216 216 237 237 236 ...
##  $ Sensor3.0: num  182 185 215 215 215 ...
##  $ Sensor3.1: num  201 197 228 228 228 ...
##  $ Sensor3.2: num  225 225 253 254 254 ...
##  $ Sensor3.3: num  230 230 253 253 253 ...
##  $ Sensor4.0: num  158 158 195 195 195 ...
##  $ Sensor4.1: num  199 199 230 230 230 ...
##  $ Sensor4.2: num  216 213 227 227 227 ...
##  $ Sensor4.3: num  191 194 221 221 221 ...
##  $ Average  : num  194 194 222 222 221 ...
##  $ SD       : num  26 25.6 20.8 20.8 20.7 ...
```

Change to appropriate data types:

```
Tails <- Tails %>%
  mutate(DateTime = as.POSIXct(DateTime, format = "%m/%d/%Y %H:%M"),
                pH = as.factor(pH)) %>%
  select(DateTime, Sensor1.0, Sensor1.1, Sensor1.2, Sensor1.3, Sensor3.0, Sen
sor3.1, Sensor3.2, Sensor3.3, Sensor4.0,                    Sensor4.1, Sensor4
.2, Sensor4.3, pH)

Inc <- Inc %>%
  mutate(DateTime = as.POSIXct(DateTime, format = "%m/%d/%Y %H:%M"),
                pH = as.factor(pH)) %>%
  select(DateTime, Sensor1.0, Sensor1.1, Sensor1.2, Sensor1.3, Sensor3.0, Sen
sor3.1, Sensor3.2, Sensor3.3, Sensor4.0,                    Sensor4.1, Sensor4
.2, Sensor4.3, pH)

Dec <- Dec %>%
  mutate(DateTime = as.POSIXct(DateTime, format = "%m/%d/%Y %H:%M"),
                pH = as.factor(pH)) %>%
  select(DateTime, Sensor1.0, Sensor1.1, Sensor1.2, Sensor1.3, Sensor3.0, Sen
sor3.1, Sensor3.2, Sensor3.3, Sensor4.0,                    Sensor4.1, Sensor4
.2, Sensor4.3, pH)
```

Gather Data into Long Form for a ggplot:

```
LongTails <- Tails %>%
  gather(key = Sensor, value = Voltage, -pH, -DateTime)

LongInc <- Inc %>%
  gather(key = Sensor, value = Voltage, -pH, -DateTime)

LongDec <- Dec %>%
  gather(key = Sensor, value = Voltage, -pH, -DateTime)
```

Plot Data:

```
ggplot(LongTails, aes(x = DateTime, y = Voltage, color = pH)) +
  geom_point(size = 1) +
```

```
  labs(x = "Date", y = "Voltage (mV)") +
  scale_x_datetime(breaks = as.POSIXct(c("2022-06-01", "2022-06-05", "2022-06
-09", "2022-06-13", "2022-06-17"))) +
  scale_y_continuous(breaks = seq(0,450,50)) +
  theme_classic()
```

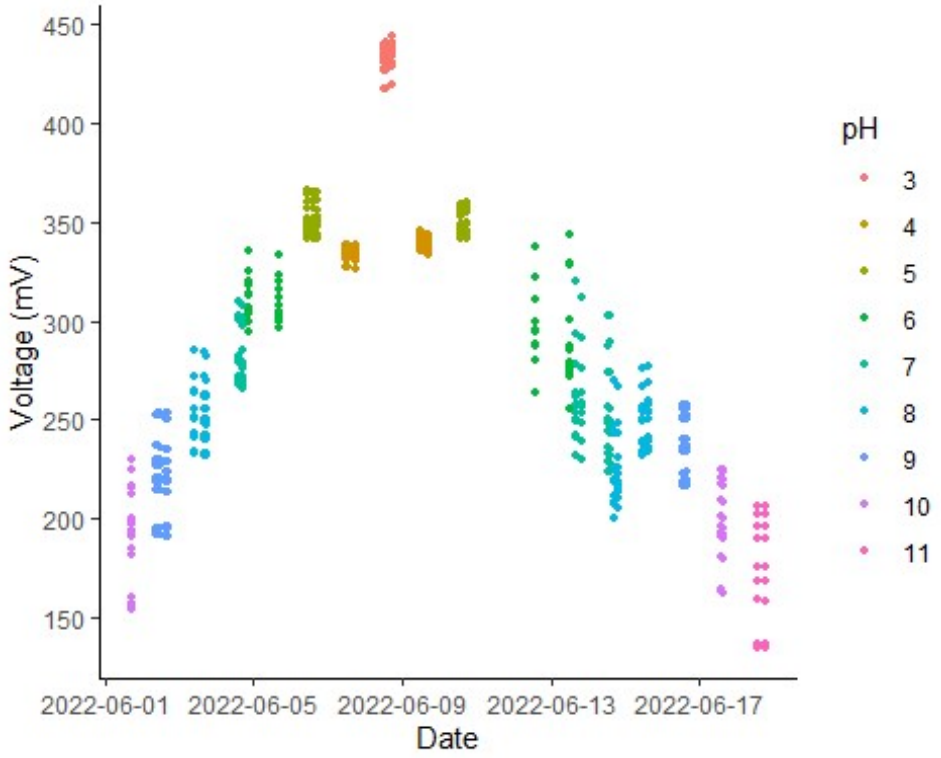


```
ggplot(LongInc, aes(x = DateTime, y = Voltage, color = pH)) +
  geom_point(size = 1) +
  labs(x = "Date", y = "Voltage (mV)") +
  scale_x_datetime(breaks = as.POSIXct(c("2022-06-01", "2022-06-05", "2022-06
-09", "2022-06-13", "2022-06-17"))) +
  scale_y_continuous(breaks = seq(0,450,50)) +
  theme_classic()
```

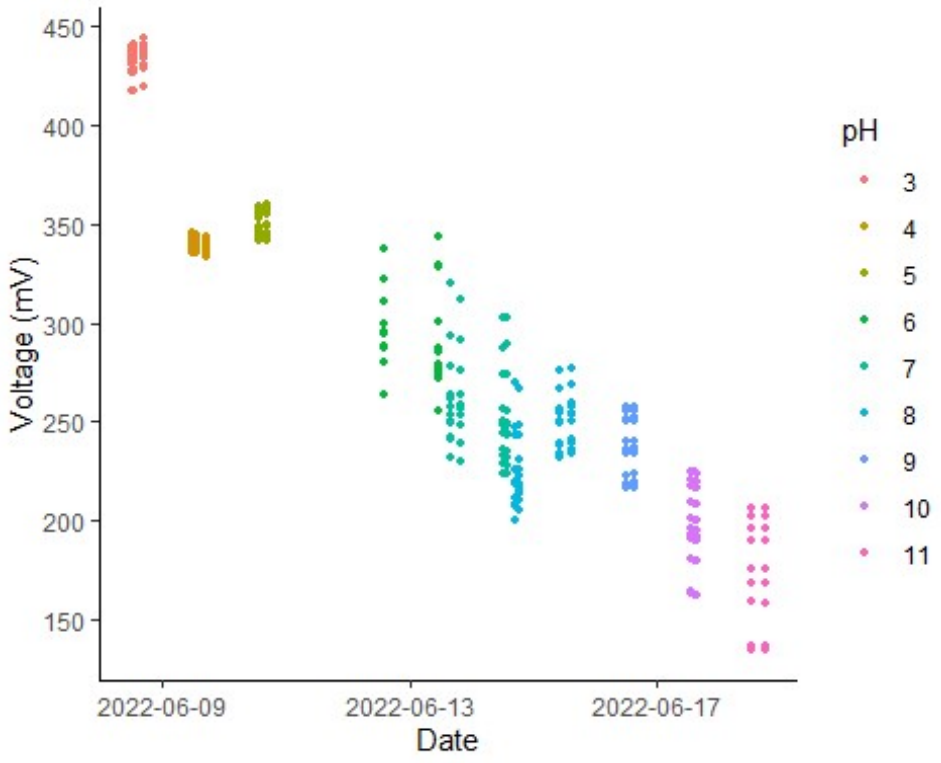


```
ggplot(LongDec, aes(x = DateTime, y = Voltage, color = pH)) +
  geom_point(size = 1) +
  labs(x = "Date", y = "Voltage (mV)") +
  scale_x_datetime(breaks = as.POSIXct(c("2022-06-01", "2022-06-05", "2022-06
-09", "2022-06-13", "2022-06-17"))) +
  scale_y_continuous(breaks = seq(0,450,50)) +
  theme_classic()

## Warning: Removed 276 rows containing missing values (geom_point).
```

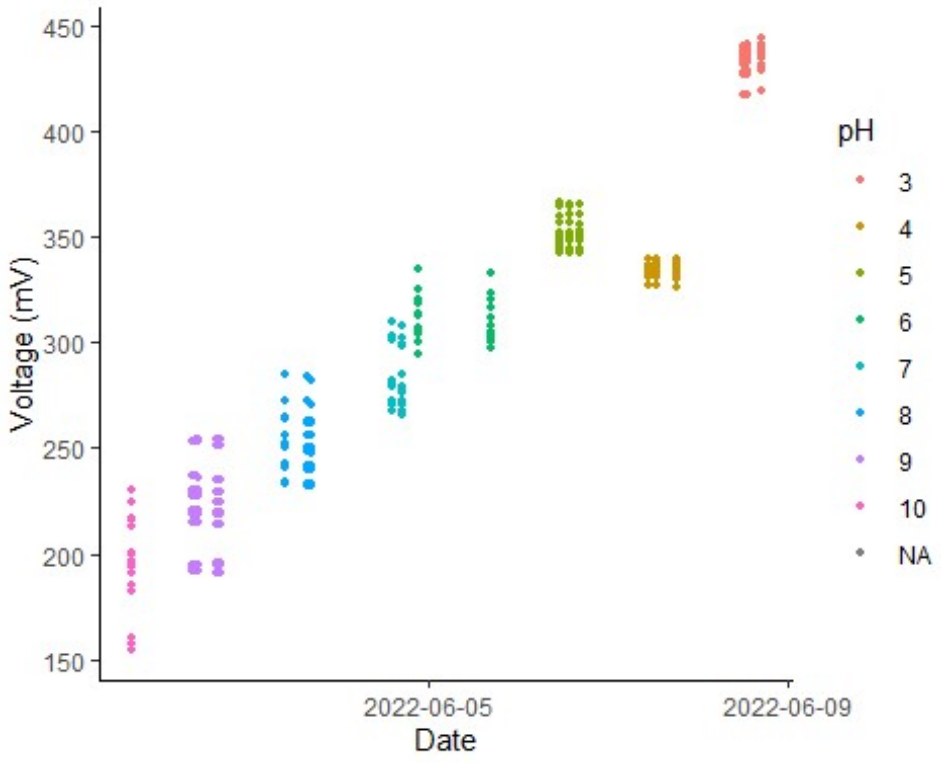

Compute stats:

```
TailsStats <-  LongTails %>%
  group_by(pH) %>%
  summarise(Mean = mean(Voltage, na.rm = TRUE),
            SD = sd(Voltage, na.rm = TRUE),
            Median = median(Voltage, na.rm = TRUE),
            n = n(),
            StdErr = SD*n()^(-1/2))
TailsStats
```

```
## # A tibble: 9 x 6
##   pH     Mean    SD Median     n StdErr
##   <fct> <dbl> <dbl>  <dbl> <int>  <dbl>
## 1 3      433.  6.59   434     36  1.10
## 2 4      337.  4.62   337     72  0.544
## 3 5      352.  7.13   351     60  0.920
## 4 6      300. 20.8    300     60  2.68
## 5 7      266. 24.8    265     72  2.92
## 6 8      244. 19.8    245     84  2.16
## 7 9      226. 19.7    227     84  2.15
## 8 10     196. 22.5    196.    60  2.91
## 9 11     177. 24.1    176     24  4.93
```

```
IncStats <-  LongInc %>%
  group_by(pH) %>%
  summarise(Mean = mean(Voltage, na.rm = TRUE),
```

```
            SD = sd(Voltage, na.rm = TRUE),
            Median = median(Voltage, na.rm = TRUE),
            n = n(),
            StdErr = SD*n()^(-1/2))
IncStats
```

```
## # A tibble: 9 x 6
##   pH     Mean    SD Median     n StdErr
##   <fct> <dbl> <dbl>  <dbl> <int>  <dbl>
## 1 3      433.  6.59   434     36  1.10
## 2 4      340.  3.27   340     36  0.545
## 3 5      351.  6.36   352.    24  1.30
## 4 6      292. 22.4    287     36  3.73
## 5 7      257. 23.9    250.    48  3.44
## 6 8      238. 20.5    239     48  2.95
## 7 9      237. 14.7    236.    24  3.00
## 8 10     198. 20.8    198     36  3.46
## 9 11     177. 24.1    176     24  4.93
```

```
DecStats <-  LongDec %>%
  group_by(pH) %>%
  summarise(Mean = mean(Voltage, na.rm = TRUE),
            SD = sd(Voltage, na.rm = TRUE),
            Median = median(Voltage, na.rm = TRUE),
            n = n(),
            StdErr = SD*n()^(-1/2))
DecStats
```

```
## # A tibble: 9 x 6
##   pH     Mean    SD Median     n StdErr
##   <fct> <dbl> <dbl>  <dbl> <int>  <dbl>
## 1 3      433.  6.59   434     36  1.10
## 2 4      333.  3.46   333     36  0.576
## 3 5      352.  7.63   351     36  1.27
## 4 6      311. 10.9    310     24  2.23
## 5 7      284. 14.4    280.    24  2.94
## 6 8      253. 15.0    250     36  2.50
## 7 9      222. 19.9    222.    60  2.57
## 8 10     194. 25.2    196.    24  5.15
## 9 <NA>   NaN  NA       NA    276 NA
```

Display boxplots and means for each pH:

```
ggplot(LongTails, aes(x = pH, y = Voltage, fill = pH)) +
  geom_violin() +
  stat_summary(fun="mean",geom="point",pch=4,color="black", size = 5) +
  labs(x = "pH", y = "Voltage (mV)") +
  scale_y_continuous(breaks = seq(0,450,50)) +
  theme_classic()
```

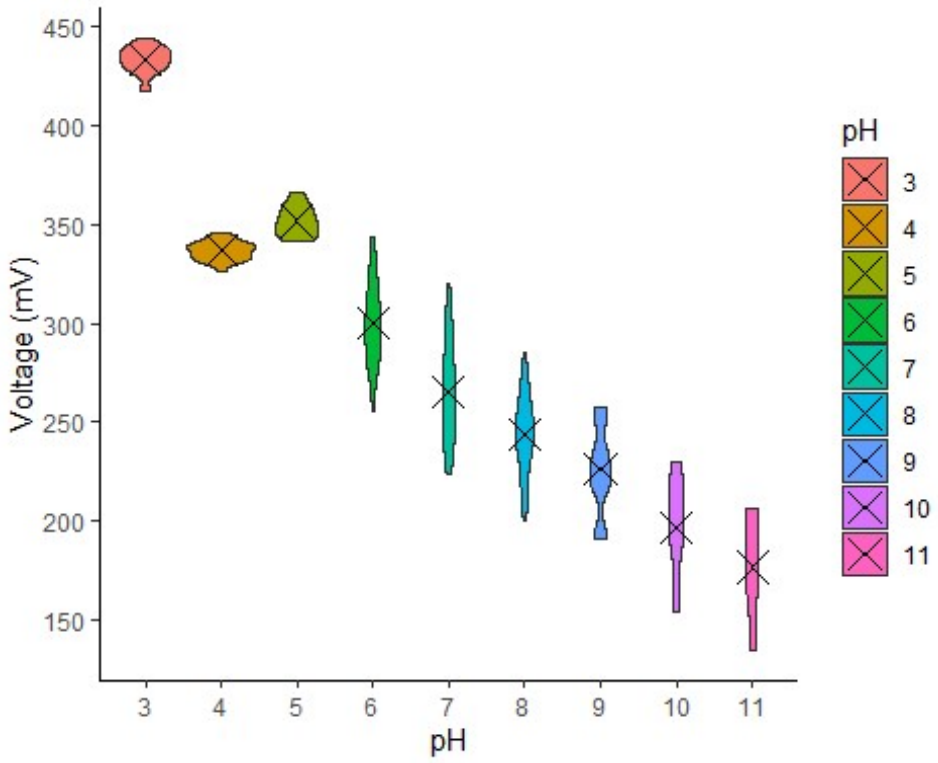


```
ggplot(LongInc, aes(x = pH, y = Voltage, fill = pH)) +
  geom_violin() +
  stat_summary(fun="mean",geom="point",pch=4,color="black", size = 5) +
  labs(x = "pH", y = "Voltage (mV)") +
  theme_classic()
```

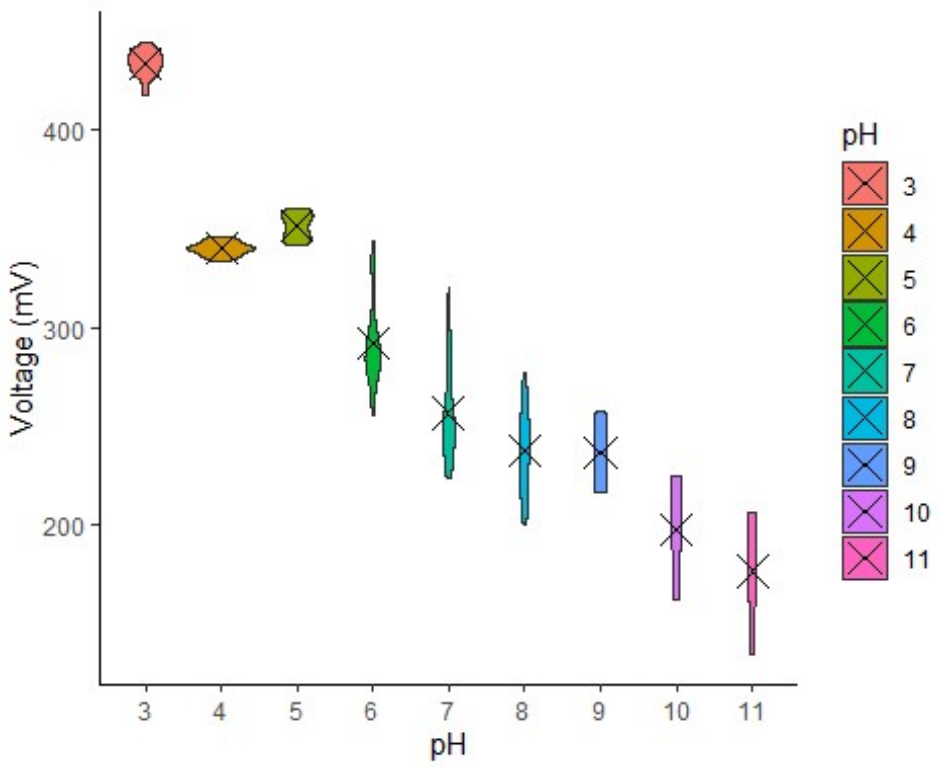


```
ggplot(LongDec, aes(x = pH, y = Voltage, fill = pH)) +
  geom_violin() +
  stat_summary(fun="mean",geom="point",pch=4,color="black", size = 5) +
  labs(x = "pH", y = "Voltage (mV)") +
  theme_classic()
```

```
## Warning: Removed 276 rows containing non-finite values (stat_ydensity).
```

```
## Warning: Removed 276 rows containing non-finite values (stat_summary).
```

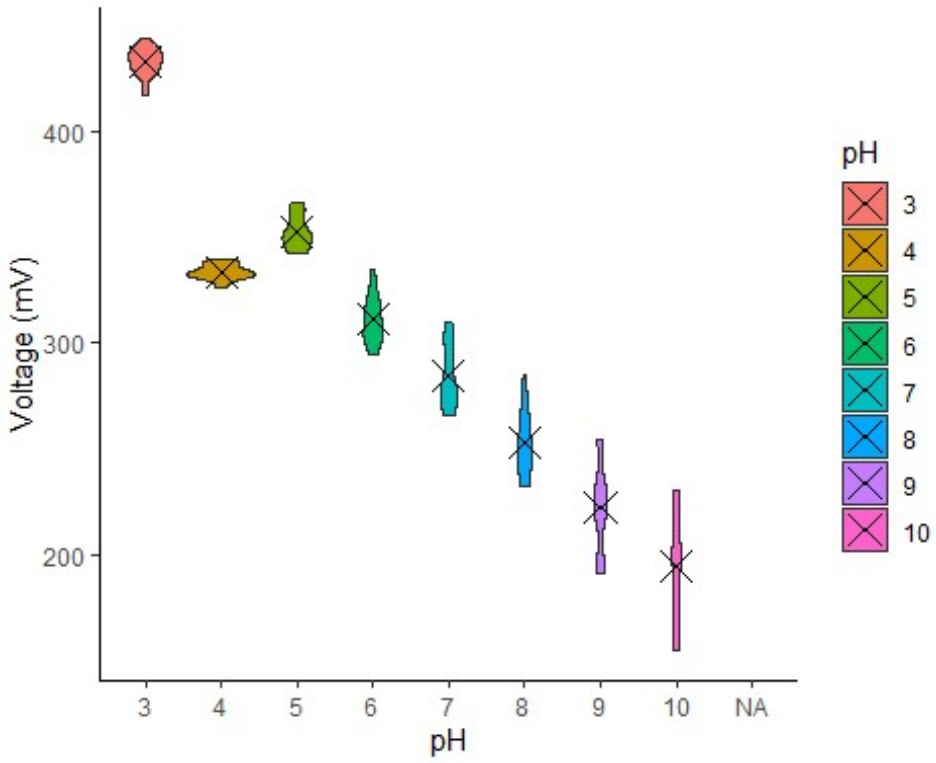

Create linear model for pH and voltage relationship:

```
ContTails <- LongTails %>%
  mutate(pH = as.numeric(pH))

VoltLM <- lm(Voltage~pH, data = ContTails)
summary(VoltLM)

##
## Call:
## lm(formula = Voltage ~ pH, data = ContTails)
##
## Residuals:
##     Min      1Q  Median      3Q     Max
## -53.604 -23.354   0.396  18.969  53.250
##
## Coefficients:
##             Estimate Std. Error t value Pr(>|t|)
## (Intercept) 419.0368     2.5246  165.98   <2e-16 ***
## pH          -28.2865     0.4611  -61.35   <2e-16 ***
## ---
## Signif. codes:  0 '***' 0.001 '**' 0.01 '*' 0.05 '.' 0.1 ' ' 1
##
## Residual standard error: 24.69 on 550 degrees of freedom
## Multiple R-squared:  0.8725, Adjusted R-squared:  0.8723
## F-statistic:  3763 on 1 and 550 DF,  p-value: < 2.2e-16
```